Een onderzoek naar de spektra van een argon boogontlading met holle kathode

EEN ONDERZOEK NAAR DE SPEKTRA VAN EEN ARGON BOOGONTLADING MET HOLLE KATHODE

B. van der Sijde

Dit proefschrift is goedgekeurd door de promotor
Prof. Dr. A.A.Kruithof

EEN ONDERZOEK NAAR DE SPEKTRA VAN EEN
ARGON BOOGONTLADING MET HOLLE KATHODE

(with summary in English)

PROEFSCHRIFT

TER VERKRIJGING VAN DE GRAAD VAN DOCTOR IN DE TECHNISCHE
WETENSCHAPPEN AAN DE TECHNISCHE HOGESCHOOL TE EINDHOVEN,
OP GEZAG VAN DE RECTOR MAGNIFICUS, PROF.Dr.Ir. G. VOSSERS,
VOOR EEN COMMISSIE AANGEWEZEN DOOR HET COLLEGE VAN DEKANEN
IN HET OPENBAAR TE VERDEDIGEN
OP DINSDAG 14 DECEMBER 1971 DES NAMIDDAGS TE 4 UUR

door

BASTIAAN VAN DER SIJDE

geboren te Soest

INHOUDSOPGAVE   PAG.

Aan Gerda
    Arjen
    Mariete

ALGEMENE INLEIDING

De holle kathode boogontlading met een lage achtergronddruk en bij-
eengehouden door een axiaal magneetveld, is een ontladingstype waarvan
de eerste uitgebreide gegevens in 1962 door Lidsky e.a. [1] zijn
gepubliceerd. Gelijksoortige opstellingen waren reeds geïntroduceerd
door Luce [2], en Gibbons en Mackin Jr. [3]. Doel van de opstelling
van Lidsky e.a. was een hoog geïoniseerde stationaire plasmabron
te kreëren om daarmede een mogelijke bijdrage tot het thermonucleaire
onderzoek te kunnen leveren.

De ontlading is in hoofdzaak te beschrijven door de volgende ken-
merken:
De kathode wordt gevormd door een hol pijpje van hittebestendig
materiaal, bij voorbeeld tantaal, wolfram of boronnitride, met een in-
wendige diameter van 1 tot 20 mm. Door de kathode stroomt gas, bij
voorbeeld met een debiet van ongeveer 10^{-3} torr $m^3 s^{-1}$ wanneer de dia-
meter van de kathode enige mm's is. In het kathodepijpje heerst dan
een druk van 0 tot 80 torr wanneer de ontlading ontstoken is. In de
ruimte tussen kathode en anode is de achtergronddruk zeer laag met
als uiterste waarden 10^{-4} en 10^{-2} torr. Het instromende gas wordt af-
gevoerd door één of meer hoogvakuümpompen met voldoend grote kapaci-
teit (pompsnelheid ongeveer 1 $m^3 s^{-1}$).
Wanneer de ontlading brandt, is de kathode tot ongeveer 2500 K
verhit door een ionenbombardement, zodat een grote thermische elek-
tronenemissie optreedt. Het gas wordt optimaal geïoniseerd in het
kathodepijpje doordat de energie van straling, ionen, metastabielen en
elektronen zeer goed benut wordt. Het "pendelen" van elektronen onge-
veer loodrecht op de as van het pijpje geeft waarschijnlijk een grote
bijdrage tot de ionisatie[4]. De stroomgeleiding vindt plaats tussen
de kathode en een plaat- of cilindervormige anode die tot op afstanden
van 1.5 m van de kathode verwijderd kan zijn of tussen de kathode en
een ringvormige anode die meestal zeer dichtbij de kathode is geplaatst.
Wanneer beide vormen aanwezig zijn, is één van beide anodes verbonden
met een voedingsapparaat, de andere wordt zwevend gehouden. De stromen,
variëren van ongeveer 10 tot 200 A.

Een axiaal gericht magneetveld zorgt, tezamen met de holle kathode, voor de typische verschijningsvorm van deze ontlading, namelijk een lichtende plasmakolom met een diameter van 10 à 20 mm. Deze begint in de kathode en volgt de gezamenlijke symmetrieas van het kathodepijpje en het magneetveld. De ontlading heeft deze vorm, ongeacht de anode-vorm, die gebruikt wordt. Bij een ringvormige anode met grote diameter is de diameter van de plasmakolom veel kleiner dan die van de ring. De beschreven vorm treedt reeds op bij velden van 3×10^{-2} tot 5×10^{-2}T. Boven deze waarden treedt soms nog zeer geleidelijk een verdergaande kontraktie op. Beneden genoemde waarden verbreedt de kolom zich zeer duidelijk. Bovendien verandert de spektrale verdeling van de door het plasma uitgezonden straling merkbaar. Bij argon bij voorbeeld wordt bij grote magneetvelden het zichtbare licht beheerst door het blauwe licht van het argon-ion (argon II) spektrum. Bij kleine magneetvelden daaren-tegen ziet men paarsachtig licht, voornamelijk afkomstig van het argon spektrum van neutrale deeltjes (argon I).

We geven enige waarden van temperaturen en dichtheden van het plasma der ontlading die gelden voor stromen van 10 tot 100 A, magneetvelden van 3×10^{-2} tot 15×10^{-2}T en gasdrukken van 1×10^{-3} tot 1.5×10^{-3} torr:

de elektronentemperatuur T_e : 30×10^3 tot 50×10^3K;
de ionentemperatuur T_i : 3×10^3 tot 40×10^3K;
de temperatuur van de neutrale deeltjes T_n : 500 tot 15×10^3K;
de elektronen- en ionendichtheid n_e : 1×10^{19} tot 3×10^{19}m^{-3};
de dichtheid van de neutrale deeltjes n_a : 5×10^{18} tot 4×10^{19}m^{-3}.

Men beschouwe deze getallen als zeer globale informatie. Voor waarden van de ontladingsstroom, het magneetveld en de gasdruk die buiten de aangegeven grenzen liggen, kunnen kleinere en grotere waarden voorkomen.

De bovengenoemde waarden van de elektronentemperatuur en in het bij-zonder die van de elektronendichtheid houden in dat een plasma met grote ruimtelijke uitgebreidheid met deze parameters zich in zogenaamd "Corona evenwicht" (C.E.) bevindt[5]. We gaan hier niet verder in op de extra verliezen aan geladen deeltjes aan de grenzen van het laboratoriumplasma tengevolge van de beperktheid van het volume van het plasma.

Zonder diep op het mechanisme van het C.E. in te gaan, worden toch enkele bijzonderheden ervan genoemd. Exciterende en ioniserende verschijnselen vinden plaats door botsingen met energierijke elektronen. Deëxcitatie vindt plaats door spontane emissie van straling, recombinatie gaat samen met emissie van een stralingskwant van onbepaalde energie of gebeurt door omlading bij een botsing met een neutraal deeltje. Deze beschrijving staat in tegenstelling met die voor atmosferische bogen, die min of meer door Locaal Thermisch Evenwicht (L.T.E.) beheerst worden. Dit evenwicht wordt bijna geheel door botsingen geregeerd en de uitgezonden straling kan opgevat worden als een kleine verstoring van het evenwicht. In C.E. is de relatieve bezetting van de aangeslagen niveaus ten opzichte van het grondniveau voor gelijke elektronentemperatuur slechts een fraktie van die van L.T.E.

De holle kathode boogontlading is sedert 1962 onderzocht door verscheidene groepen, waaronder die van Lidsky en Rose [1 en 6-9], die zich vooral bezig hield met de ionisatiegraad van het plasma en het temperatuurevenwicht tussen elektronen, ionen en neutrale deeltjes [1,7 en 8]. Ook zijn bijdragen geleverd op het gebied van Thomson verstrooiing van laserlicht [6] en van de diffusie van het plasma in radiele richting [9].

De groep van Delcroix heeft in de eerste plaats het onderzoek naar de processen in de holle kathode opgevat [10-13], hetgeen onder andere resulteerde in een model voor het veldsterkteverloop tussen het inwendige van de kathode en de anode [11 en 12]. Voorts is voor de kathode een "multichannel" ontwerp voorgesteld, bestaande uit een aantal parallel opgestelde holle kathode pijpjes [13].

Kretschmer, Boeschoten en Demeter [14 en 15] en ook Morse [16 en 17] en van der Sijde en Tielemans [18] waren vooral geïnteresseerd in de rotatieverschijnselen van het plasma, een gevolg van een loodrecht op elkaar staand radiëel elektrisch veld en drukgradiënt enerzijds en een axiaal magneetveld anderzijds.

We vermelden volledigheidshalve nog het spektroscopisch werk van Shipp en Tidwell [19 en 20], Leonard [21], van der Sijde [22] en Bleekrode en van Benthem [23].

Het onderzoek aan de boogontlading dat in de drie hierna volgende

delen beschreven wordt, omvat hoofdzakelijk een onderzoek naar het
argon II en het argon I spektrum, zowel wat betreft lijnintensiteiten,
waaruit de elektronentemperatuur berekend is, als lijnverbredingen,
waaruit de temperaturen van de ionen en de neutrale deeltjes berekend
zijn (Doppler verbreding). De elektronendichtheid is berekend uit de
faseverschuiving van met het plasma in interaktie gebrachte 4 mm mikro-
golven. De drie delen zijn tevens bedoeld als publikaties. Als afslui-
ting volgt nog een algemene slotbeschouwing over de resultaten van het
werk.

Het eerste deel houdt zich bezig met het onderzoek naar een mogelijk
optreden van wat in de literatuur aangegeven wordt met thermalisatie
van aangeslagen iontoestanden door zware deeltjes. We bedoelen hiermede
een verschijnsel waarbij aangeslagen iontoestanden, voordat binnen
ongeveer 10^{-8}s spontane emissie optreedt, nog overgaan in toestanden
op kleine energieafstanden van 0.05 tot 0.2 eV van de oorspronkelijke
verwijderd onder invloed van botsingen met neutrale deeltjes of ionen.
De temperatuur van deze deeltjes zal dan terug te vinden zijn in de
bezettingsgraad van de aangeslagen toestanden. Miller e.a. [24] en
Lejeune [25] nemen aan dat dit verschijnsel optreedt bij plasma's met
lage gasdruk. Het probleem vertoont enige verwantschap met een door
Drawin [26] berekende invloed van de neutrale deeltjes op de bezettings-
graad van toestanden met grote hoofdkwantumgetallen. De experimentele
verifikatie ervan was echter door gebrek aan nauwkeurigheid niet
goed mogelijk [27].

Als grondslag van de beschouwingen in deel 1 is een nauwkeurige
analyse van de in de literatuur gegeven overgangswaarschijnlijkheden
van een deel van het argon II spektrum verricht (Appendix bij deel 1).

In het tweede deel worden beschreven de metingen van de intensiteit
van een aantal lijnen van het argon I en II spektrum als funktie van
de hoogte in de plasmakolom. Door een Abel transformatie worden de
stralingsprofielen als funktie van de afstand r tot de as van de ont-
lading verkregen. Uit de verschillen die optreden wordt met behulp
van formules van het Coronamodel informatie verkregen over het radiële
verloop van de temperatuur en dichtheid van de elektronen ten opzichte
van de waarden van de as.

In het derde deel is deze informatie gebruikt om uit de absolute

waarden van de intensiteiten van de lijnen van de argon I en II spektra
en uit de faseverschuivingen van de mikrogolven de waarden van de
temperatuur en dichtheid van de elektronen op de as te bepalen. Tevens
wordt berekend hoeveel de afzonderlijke bijdrage is van de verschillende
mogelijkheden om een 4p niveau van het argon II spektrum te bevolken.

REFERENTIES

1 . L.M.Lidsky, G.D.Rothleder, D.J.Rose, S. Yoshikawa, C.Michelson en
   R.J. Mackin Jr., J.Appl.Phys. 33, 2490 (1962).

2 . J.S. Luce, Proc. 2th Un.Nations Conf. Peaceful Uses At.Energy,
   Genève, p. 305 (1958).

3 . R.A, Gibbons en R.J.Mackin Jr., Proc.5th Int.Conf.Ionization Phen.,
   München, (1961).

4 . D.J.Sturges en H.J.Oskam, Physica 37, 457 (1967).

5 . B.Wilner, Acta Polyt.Scand., Physics and Nucleonics 41, 1 (1966).

6 . E.T.Gerry en D.J.Rose, J.Appl.Phys. 37, 2715 (1966).

7 . E.T.Gerry en D.J.Rose, J.Appl.Phys. 37, 2725 (1966).

8 . M.Hudis, K.Chung en D.J.Rose, J.Appl.Phys. 39, 3297 (1968).

9 . D.L.Flannery en S.C.Brown, Phys. Fluids 13, 1066 (1970).

10. H.Minoo en A.R.Trindade, Proc. 8th Intern.Conf.Ionized Gases,
   Vienna,p. 97 (1967).

11. J.L.Delcroix, H. Minoo en A.R. Trindade, J.Physique 29, 605 (1968).

12. J.L.Delcroix, H.Minoo en A.R.Trindade, Rev.Roum.Phys. 13, 401 (1968).

13. J.L.Delcroix, H.Minoo en A.R.Trindade, Proc. 9th Intern.Conf.
   Ionized Gases,Bucharest,p. 169 (1969).

14. C.B.Kretschmer, F.Boeschoten en L.J.Demeter, Phys. Fluids 11, 1050
   (1968).

15. F.Boeschoten en L.J.Demeter, Plasma Physics 10, 391 (1968).

16. D.L.Morse, Phys. Fluids 8, 516 (1965).

17. D.L.Morse, Phys. Fluids 8, 1339 (1965).

18. B. van der Sijde en P.A.W.Tielemans, Proc.10th Intern.Conf.Ionized
   Gases, Oxford,p. 192 (1971).

19. J.I.Shipp en E.D.Tidwell, J.Opt.Soc. Am. 57, 1061 (1967).

20. E.D.Tidwell en J.I.Shipp, Proc. 8th Intern.Conf.Ionized Gases,
   Vienna, p. 453 (1967).

21. S.L.Leonard, Proc. 9th Intern.Conf.Ionized Gases,Bucharest,p. 170
    (1969).
22. B. van der Sijde, Proc. 9th Intern.Conf.Ionized Gases,Bucharest,
    p. 639 (1969).
23. R.Bleekrode en W. van Benthem, J.Appl.Phys. 40, 5274 (1969).
24. R.C.Miller, E.F. Labuda en C.E.Webb, Bell System. Techn.J. 46,
    281 (1967).
25. C.Lejeune, Proc. 9th Intern.Conf.Ionized Gases,Bucharest,p. 170
    (1969).
26. H.W.Drawin, Z.Phys. 228, 99 (1969).
27. H.W.Drawin, F.Klan en H.Ringler, Z.Naturforsch. 26a, 186 (1971).

CONFIGURATION TEMPERATURES IN A HOLLOW CATHODE ARGON ARC AND TRANSITION
PROBABILITIES OF THE ARGON II SPECTRUM

B. van der Sijde

Department of Technical Physics, University of Technology, Eindhoven,
Netherlands.

Summary- A comparison has been made between some kinds of configuration
temperatures of the argon II spectrum and the temperatures of the atoms,
ions and electrons for a hollow cathode, low-pressure, magnetically-
confined, argon arc discharge in the 10 to 80 A current region. We found
that thermalization by heavy particle collisions does not occur within
the 4p group of the argon II spectrum (excitation energies 19.22 to 19.97
eV), and that relative line-intensity measurements over a large spectral
range of 19 to 25 eV give hardly any relevant information on the
electron temperature. Our conclusion is that the population densities of
the excited levels are mainly determined by the excitation cross-section
functions for the levels concerned. Furthermore, we have compared
published transition probabilities (to 1970) for the argon II 4p group
transitions. The mean values were obtained for 31 transitions with
uncertainties (with two exceptions) between 1% and 20%.

I   INTRODUCTION

Several authors have calculated population densities of excited levels
and configuration temperatures from line-intensity measurements of the
argon II spectrum. The configuration temperature is derived from the
slope of the line determined by the magnetic sublevel densities
(population density divided by the statistical weight of the level)
plotted against the value of the excitation energy of the level in a
semilogarithmic plot.

Some of the references, MILLER et al[1] and RUDKO and TANG[2] deal
with argon$^+$ laser experiments with gas pressures of about 0.5 mm of Hg.
Other references, of which we mention SHIPP and TIDWELL[3], SHIPP[4],
LEONARD[5] and VAN DER SIJDE[6], report on hollow cathode, magnetically-

confined argon arc discharges with a working pressure of 10^{-4} to 10^{-3} mm of Hg. Finally, LEJEUNE[7] presented measurements of the duoplasmatron experiment with a pressure of 10^{-2} mm of Hg.

We are interested in the significance of configuration temperatures with respect to the temperatures of the various particles in the plasma. One of the most important problems is, whether or not the values of the configuration temperatures of spectral groups with small energy differences between the levels can be understood from a thermalization within a spectral group. Thermalization means a process of transitions between the various levels of the spectral group induced by collisions with particles by which the configuration temperature of the group is changed in that of the particles concerned. MILLER et al[1] and LEJEUNE[7] suggest such a thermalization by atoms, RUDKO and TANG[2] have arguments to deny the phenomenon.

Also the configuration temperature over a wider spectral range with excitation energies from 19 to 25 eV is of some interest. The comparison of this parameter with the electron temperature T_e can give information on the question whether or not this configuation temperature is equal to T_e. KRETSCHMER et al[8] determined T_e values from relative line-intensity measurements.

We made an investigation of a low-pressure, hollow cathode argon arc discharge, trying to solve these problems. We determined ion temperatures T_i and atom temperatures T_n by Doppler broadening measurements with the aid of a Fabry-Perot interferometer, and electron and configuration temperatures from line-intensity measurements. We compared the results with each other to find out if there are clear agreements or differences between the temperature of a certain kind of particle and a configuration temperature.

II   DEFINITION OF CONFIGURATION TEMPERATURE

The radiant flux ϕ_{mj} per unit volume of a transition $m \to j$ in the absence of absorption is given by

$$\phi_{mj} = h\nu \, A_{mj} \, n_m \, , \tag{1}$$

where n_m is the density of the population of the excited level m; A_{mj} is
the transition probability of the transition $m \rightarrow j$; h is Planck's
constant; ν is the frequency of the radiation.

n_m can be written as follows:

$$n_m = n_1 \, g_m/g_1 \, \exp(-E_m/kT), \tag{2}$$

where n_1 is the density of the ion ground level; g_i is the statistical
weight of level i; E_m is the excitation energy of the level m; k is
Boltzmann's constant.

One can explain the parameter T as a kind of temperature, without
knowing at the moment the physical sense. For L.T.E. circumstances the
parameter T can only be T_e, whose value for completely established
L.T.E. has to be the same as that of the heavy particle temperatures.
For Corona Equilibrium (C.E.) , the sense of the parameter T is less
clear and may be the object of investigation.

One can try to get information on a T from relative intensity
measurements of two or more lines and defined by the expression

$$T = \frac{E_m - E_p}{k \ln (\phi_{pq} A_{mj} g_m \nu_{mj}/\phi_{mj} A_{pq} g_p \nu_{pq})} , \tag{3}$$

which is equivalent to the formulation in the previous section.

If it is assumed that only inaccuracies in the quotients of the ϕ-
values and transition probability values (A-values) contribute to the
relative error in T, we find

$$\frac{\Delta T}{T} = \frac{kT}{|E_m - E_p|} \left\{ \frac{\Delta(A_{mj}/A_{pq})}{(A_{mj}/A_{pq})} + \frac{\Delta(\phi_{mj}/\phi_{pq})}{(\phi_{mj}/\phi_{pq})} \right\} . \tag{4}$$

From relation (4) we can see that the error $\Delta T/T$ strongly depends on
the ratio of the difference between E_m and E_p and the value of kT.

In the following we shall call a temperature determined by expression
(3), a configuration temperature. This expression is also used in the
survey of the literature, given in the following section, even when in
the reference itself the expression excitation temperature is used for

this parameter. We shall introduce an intra configuration temperature T_{4p} for the 4p group and also an inter configuration temperature T_{ic} for a spectral range between ~19 eV and ~25 eV.

III LITERATURE SURVEY

In this section we shall give a review of the literature, which may be of interest to the problems, formulated in the Introduction.

MILLER et al[1] reported on measurements with an argon$^+$ laser tube. The diameter of the tube was 2 mm, the pressure of the argon gas 0.6 mm of Hg and the discharge current 5A. They found that T_{4p} is 5.3×10^3 ^{o}K (0.46 eV) from line-intensity measurements and T_e is 30×10^3 ^{o}K (2.5 eV). An estimation of an inter configuration temperature T_{ic}, based on Fig. 1 of [1], gives a value of 12×10^3 ^{o}K. MILLER et al proposed a thermalization within a spectral group, based on the discrepancy between T_{4p} and T_e. For this explanation, transitions between the levels of the 4p group should take place within the radiation decay time of 5×10^{-9}s, leading to a rearrangement of the population densities of the levels involved. The particles, causing this rearrangement, must have a kinetic energy $\geq$ 0.2 eV, the largest energy gap in the group being 0.19 eV. Electrons are excluded from discussion, whereas the excitation from lower levels to the levels of the 4p group is caused by electrons with a mean energy of 2.5 eV. This large value in comparison with a T_{4p} of 0.46 eV just presents the problem. Ions are excluded by MILLER et al for reasons which are not perfectly clear, but based on arguments about direct excitation of the 4p levels from the ion ground level. They propose that neutral particles cause the thermalization, perhaps via short lived molecular ions.

In an extensive investigation of the argon$^+$ laser (tube diameter 2mm; pressure 0.3 mm of Hg; discharge current 5 A) RUDKO and TANG[2] found straight lines for each of the 4p, 4p', 5s, 5s', 4d and 4d' groups (E_m = 19 eV to 25 eV) in a semilogarithmic plot as discussed in the Introduction. They do not derive a temperature from the slopes of the lines. Our own calculations, based on Fig. 1 of ref.[2] give for T_{4p} a value of 7.4×10^3 ^{o}K and for T_{ic} a value of about 12×10^3 ^{o}K. The

T_{ic} includes the spectral region between 19 and 25 eV, i.e. all spectral groups mentioned above.

Moreover, RUDKO and TANG[2] performed an experiment, in which the radiation of the 4880 Å line of the argon$^+$ laser was modulated at a frequency of 800 cps. The other lines, originating from the $4p^2D_{5/2}$ state showed a modulation of 6 to 7% with the same frequency. Lines originating from the neighbouring levels only showed a modulation of $\leq$ 0.1%. They concluded that these experiments do not give an indication for a thermalization process.

In a hollow cathode, low-pressure, magnetically-confined argon arc discharge experiment SHIPP and TIDWELL[3] and SHIPP[4] determined a T_{ic} based on intensity measurements of lines, originating from levels of the 4p, 4p' and 5s group. They found values between 20×10^3 °K and 26×10^3 °K. These high values are mainly caused by the use of an A-value for the 3588 Å line (^3P 4d $^4F_{9/2} \rightarrow {}^3P$ 4p $^4D_{3/2}$ transition), which appears to be wrong by a factor of 4.5 (see reference [9] for comparison). Calculations with the improved A-value give T_{ic} values of 14×10^3 °K to 17×10^3 °K.

In an argon fed hollow cathode discharge, related to the device of SHIPP and TIDWELL but with another type of anode, LEONARD[5] calculated a T_{ic} in the 19 to 24 eV region with a value of 9.3×10^3 °K (0.8 eV) from line-intensity measurements, and determined T_e to be 30×10^3 °K (2.7 eV). The value of T_{ic} is lower than in the previous references, perhaps caused by the A-values used by LEONARD.

VAN DER SIJDE[6] determined a T_{ic} for the 4p and 4p' group for a hollow cathode argon discharge, similar to that of LEONARD. The value of 17×10^3 °K is nearly constant over a wide range of magnetic induction values. T_e was estimated to be 70×10^3 °K. The value of T_{ic} is rather high in comparison with the T_{ic} values of the authors, mentioned before. The reason of this fact is the selection of the levels, by which T_{ic} is determined.

LEJEUNE[7] reported on a low pressure, hot cathode, "duoplasmatron" discharge, with a T_{4p} of the order of 6.5×10^3 °K (0.55 eV) and a T_{ic} between 12×10^3 °K and 20×10^3 °K (1.0 to 1.7 eV). The value of T_{4p}

is in good agreement with other references. The range of T_{ic} values is rather wide; the maximum of 20×10^3 °K is larger than in any other reference. LEJEUNE also suggests a thermalization within spectral groups of the argon II spectrum, caused by heavy particle collisions .

Reviewing this part of the survey , we can conclude that contradictory ideas have been published about the question of thermalization within a spectral group. The values of T_{4p} range from 5.3×10^3 °K to 7.4×10^3 °K. Apart from the differences in the physical conditions of the discharges, the variation of the value of T_{4p} can be partly caused by differences in the A-values, used in the calculations.

The range of values of T_{ic} is rather wide, 9.3×10^3 °K to $20 \times 10^{3 \cdot}$°K. The variation in the values of this parameter can be caused by the following reasons: 1) the use of various combinations of spectral groups and lines ; 2) differences in the A-values used, which may have a rather large effect, due to the great uncertainty of these values for transitions, originating from other groups than the 4p group ; 3) the influence of the physical conditions of the discharge on T_{ic}. This question will be discussed further in a following section.

We finally want to discuss the theoretical work of JOHNSON[10], which is of interest to the subject of this paper. JOHNSON presented calculations on simultaneous charge transfer and fine structure transitions for argon neutral and argon ion excited particles. The transfer

$$ar({}^1S_0) + ar^+({}^2P_{1/2}) \rightarrow ar^+({}^2P_{3/2}) + ar({}^1S_0)$$
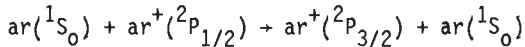
has a collision cross-section of 2×10^{-20} m^2 for 5 eV ions and of negligibly small values for ion energies smaller than 3 eV. The reverse transition has about twice smaller values. These cross-section values are too small to be able to influence quantitatively the population density of the excited levels for the energy region of the ions in the experiments, already mentioned. This example gives arguments to assume that charge transfer processes generally have too small cross-sections to induce thermalization effects.

IV EXPERIMENTAL

1. Discharge device

In[6], a short description of the discharge device was already given. We shall extend the description now (see Fig.1a). The discharge took place in a pyrex tube (4) having a length of 1.4 m and a diameter of
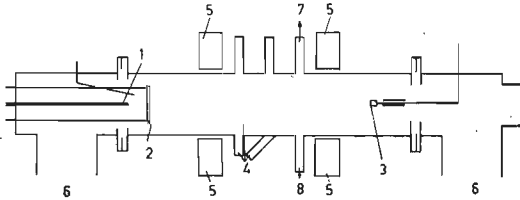
Fig. 1a Simplified design of the discharge device. 1 is a hollow cathode; 2 is a ring-shaped anode; 3 is an end-anode; 4 is a pyrex tube with small side tubes; 5 are magnetic coils; 6 are diffusion pumps with baffles; 7 is a tube and window for spectral measurements; 8 is a tube and window for line profile measurements.
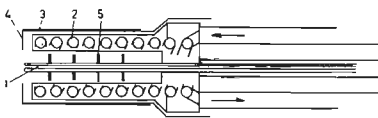
Fig.1b Detailed design of the water-cooled cathode. 1 is a tantalum pipe, inner diameter = 2.5 mm; 2 is a water-cooled cylinder; 3 is a fused silica cylinder; 4 is a tantalum sheet, at floating potential; 5 are tantalum fins (some-times not present).
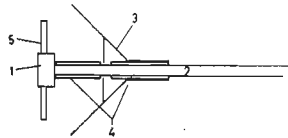
Fig.1c Detailed design of the end-anode. 1 is a tungsten cylinder; 2 is a tungsten rod; 3 is a tantalum conical surface, at floating potential; 4 are electrical insulators; 5 is a tantalum disc.

0.3 m. The argon gas with impurity concentrations smaller than 40 p.p.m., streamed through a hollow cathode pipe (1) into the large pyrex tube and was pumped away by two mercury diffusion pumps (6) each with a baffled pumping speed of 0.8 $m^3 s^{-1}$.

The cathode pipe of tantalum or tungsten containing 3% ThO_2(1), had an inner diameter of 2.5 mm and a length of 50 to 100 mm. The cathode was situated at one end of the axis of the pyrex tube (Fig.1b). Two different anodes could be used, the first being a ring-shaped one of tungsten (2), having an inner diameter of 120 mm. The axis of the ring coincided with the tube axis. The ring surrounded the discharge at a distance of 50 to 80 mm from the end of the cathode. The second anode was a cylindrical tungsten end-anode (3) with a tantalum disc (Fig.1c). The outer diameter of the disc of this anode was 50 mm. The axis of the anode also coincided with the tube axis.

When the discharge was running, one of both anodes was connected with the current supply, the other being at floating potential. The cathode was always at earth potential. The working pressure of the discharge was 1×10^{-3} to 2.5×10^{-3} mm of Hg, measured by an ionization gauge at some distance (0.5 m) from the discharge. The residual gas pressure of the system was 1×10^{-6} to 3×10^{-6} mm of Hg.

The discharge was confined around the axis of the pyrex tube by an axial magnetic field. Two magnetic coils (5) gave a bottle-shaped magnetic field (Fig.2), with continuously variable magnetic induction values between 0.01 T and 0.2 T for the two maxima in Fig. 2. In the following sections we shall use the values of the magnetic induction B_w , at a position marked w in Fig. 2.

The discharge current range for the ring-shaped anode was 10 to 100 A and for the end anode 10 to 50 A. The upper limits were imposed by the maximum heat dissipation of the anodes.

The neutral gas, streaming through the cathode pipe was highly ionized in the cathode itself. The ions formed in the cathode pipe caused a bombardment on the inner side of the cathode wall, resulting in a temperature of 2000 to 3000°K for the hottest spot of the cathode. The electrons delivered by the thermal electron emission ionized the flowing neutral gas and carry the current between anode and cathode. When the discharge was running, the voltage between cathode and anode

was of the order of 30 to 200 V. The discharge was started by a low
current 1000 V supply.
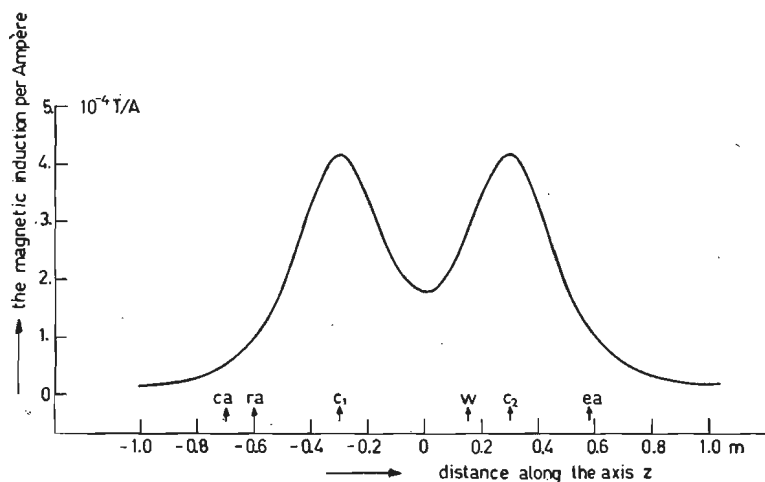
*Fig.2 The value of the magnetic induction per Ampère current through
the coils on the axis of the pyrex tube as a function of the distance
z along the axis. The point of symmetry has been chosen as z = 0.
The arrows and symbols denote the following objects: ca is the cathode;
ra is the ring-shaped anode; ea is the end-anode; c_1 and c_2 are magnetic
coils; w are windows for spectral measurements.*

Near the axis of the tube, the blue radiation of the argon II spectrum
could be seen. The radiating column had a diameter of 4 to 15 mm,
depending on the position along the axis and on the discharge conditions.
The argon I spectrum in the 4000 to 5000 Å region (5p → 4s transitions)
was very weak, partly due to the small A-values of the lines concerned.
Only a few lines could be detected. The argon I spectrum in the 7000
to 8000 Å region (4p → 4s transitions) was a factor 20 stronger, due
to the greater A-values, but still a factor 10 weaker than the strongest
lines of the argon II spectrum (4p → 4s and 4p → 3d transitions). The

same qualitative light phenomena were detected with the two anodes.
No radiation could be seen from the discharge region along the first
2 to 5 cm from the end of the cathode. This fact was perhaps caused
by the intense radiation of the cathode itself.

2.   *Line-intensity measurements*

The line-intensity measurements were performed with a 0.5 m Jarrell Ash
grating monochromator (Fig.3a and 3b). The radiation of the plasma
column (1) passed through a cylindrical glass tube perpendicular to the
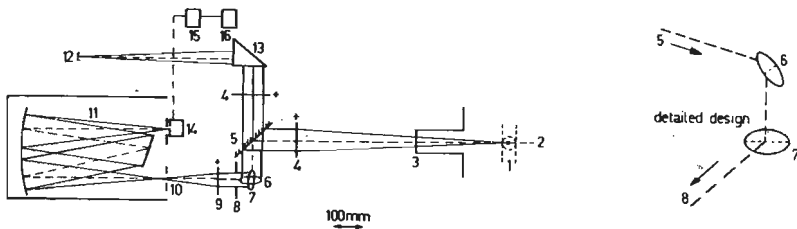
*Fig.3a   Design of the device for line-intensity measurements;
perpendicular to the optical axis not to scale. 1 is the plasma column;
2 is the optical axis; 3 is a fused silica window; 4 is a lens,
vertically movable; 5 is a large mirror, removable for tungsten ribbon
lamp measurements; 6 is a mirror, vertically movable (see Fig.3b);
7 is a mirror; 8 is a diaphragm; 9 is a lens; 10 is the monochromator
entrance slit; 11 is a grating monochromator; 12 is a tungsten ribbon
lamp; 13 is a 45° prism; 14 is a photomultiplier RCA IP 28; 15 is a
Keithley electrometer; 16 is a Moseley recorder.*

*Fig.3b   Detailed design of the position of the mirrors 6 and 7. The
rotation axes make angles of 45° with the optical axis of the system.*

pyrex tube. This small tube had a length of 150 mm and a diameter of
45 mm. After that, the radiation passed through a fused silica window
(3), sealing off the glass tube. This construction enabled us to do

side-on measurements. An optical system consisting of two fused silica lenses (4,9) and three mirrors (5,6,7) made it possible to focus on the vertical entrance slit (10) of the monochromator (size 100μ x 2.3 mm) a rectangular section having a length of 5 mm and a height of 230μ and situated in the vertical plane through the tube axis. As the entrance angle of the detection system was rather small (0.04 rad), the solution of the system was not seriously decreased at the edges of the plasma column. At a radius of 10 mm the rectangular section was 5.5 mm x 700μ.

One lens and one mirror were vertically movable to displace the optical axis of the system, enabling us to scan the radiation profile of the plasma column. A calibrated tungsten ribbon lamp, placed at a position, which was optically equivalent to the discharge position, made it possible to perform absolute line-intensity measurements.

The breadth of the entrance slit enabled us to measure the total radiation intensity of one line. The equivalent dispersion width of the 100μ slit is 1.6 A, in comparison with line profile widths of the order of 10 to 100 mÅ. The total radiation of one line was compared with the continuous radiation of a bandwidth of 1.6 Å.

In order to be able to compare the volume radiation of the plasma with the surface radiation of the tungsten ribbon lamp (12), the breadth of the radiation profile of the plasma was also measured in the vertical direction. By assuming cylindrical symmetry this measurement made it possible to calculate the absolute line radiation flux per unit volume. The radiation was detected by means of an RCA IP28 photomultiplier (S-5 response) (14) while a part of the information on the argon I spectrum was detected with an EMI 9698 B photomultiplier (S-20 response). The signals were measured with a Keithley 602 electrometer (15) and registered by a Mosely recorder (16).

3. The Fabry-Perot interferometer

The heavy particle temperatures were determined with the aid of a Fabry-Perot order-scanning-type interferometer (Fig.4)[11]. The interferometer provided the line profiles enabling us to derive the temperatures from calculations of the Doppler broadening of the spectral lines. A lens system (1,2) gave an image of the plasma column near the

axis of the pyrex tube on the vertical slit of a prism monochromator
(Hilger and Watts) (6) giving a bandwidth of 10 to 15 Å of the spectrum.
Another lens system (3,4) and the interferometer (7) itself gave an
image of the ring pattern, which was scanned by a 600μ x 50μ movable
slit (8). The ring pattern corresponded with a real image of the plasma
column, so that by scanning the various rings and by moving the optical
axis through the plasma column, a good impression could be obtained of
the temperature distribution in a vertical direction. The radiation was
detected by an EMI 6256 S photomultiplier (9),measured with a Keithley
409 picoammeter (10) and registered by a Mosely recorder (11).
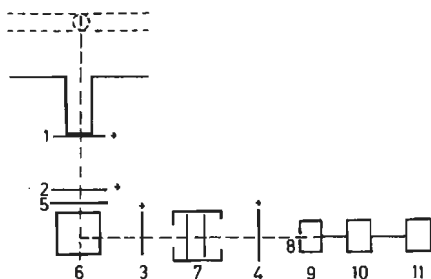
*Fig.4 Device for line profile measurements. 1,2,3 and 4 are lenses;
5 is a polaroid filter; 6 is a prism monochromator; 7 is a Fabry-Perot
interferometer; 8 is a movable slit; 9 is a photomultiplier EMI 6256 S;
10 is a Keithley picoammeter; 11 is a Moseley recorder.*

The magnetic field is responsible for a Zeeman splitting of the
spectral lines, which for most discharge conditions could not be
neglected in comparison with the Doppler broadening. In order to derive
an easily interpretable signal, only the linearly polarized component
($\Delta m = 0$) was measured, the two circularly polarized components ($\Delta m = \pm 1$)
being eliminated with a polaroid filter (5). The apparatus broadening
was known from calibration with the Cd 4800 and 5086 Å lines, giving
25 mÅ as a result. The Voigt profiles, directly measured, were
deconvoluted in order to derive the pure Doppler broadening.

4. Microwave interferometer

For a part of the measurements, presented in the following section, estimations of the electron densities n_e were made from phase shift measurements with a 4 mm microwave interferometer. These phase shift measurements were performed for discharge conditions, very similar to those of the presented measurements. The n_e values were of the order of 10^{18} m^{-3} for small values of the magnetic induction B_w and 10^{19} m^{-3} for large B_w values.

V   RESULTS

Ion temperatures T_i have been calculated from the Doppler broadened
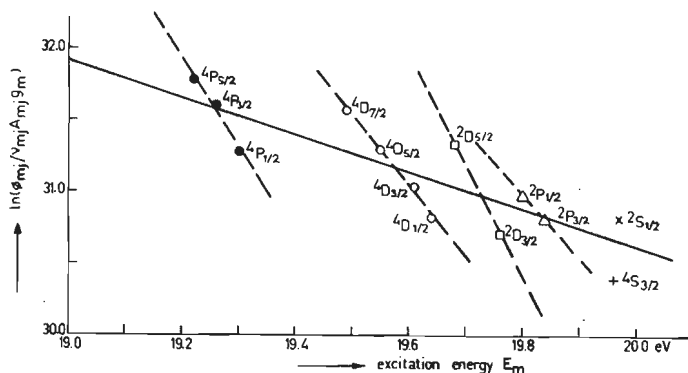
Fig.5 Example of the determination of the 4p group configuration temperature T_{4p} and the multiplet configuration temperatures T_{4P}, T_{4D}, T_{2D} and T_{2P}. $ln(\phi_{mj}/\nu_{mj}A_{mj}g_m)$ is plotted on a scale with an arbitrary zero point against the excitation energy E_m. Discharge parameters: discharge current $I_D = 24$ A; magnetic induction $B_w = 9 \times 10^{-2}$ T; pressure $= 1.5 \times 10^{-3}$ mm of Hg; end-anode used. $T_{4p} = 8.9 \times 10^3 \pm 250^O K$; $T_{4P} = 1.9 \times 10^3 \pm 200^O K$; $T_{4D} = 2.4 \times 10^3 \pm 200^O K$. $T_{2D} = 1.5 \times 10^3 \pm 200^O K$; $T_{2P} = 2.6 \times 10^3 \pm 200^O K$.

profile of the argon II 4806 Å line, having a normal Zeeman splitting. For the calculation of the temperature of the neutral atoms T_n the profiles of the argon I 4198 Å line ($3p_5 \rightarrow 1s_4$ transition) and 4201 Å line ($3p_9 \rightarrow 1s_5$ transition) have been measured. For the determination of T_{4p} one transition from each upper level was chosen. These transitions have been listed in Table 6 of the Appendix. The averaging procedure to find the A-values is explained in the Appendix. The value of the parameter $\ln(\phi_{mj}/\nu_{mj}A_{mj}g_m)$ for each line plotted against the excitation energy E_m of the upper level of the transition gives a straight line, from the slope of which T_{4p} is derived.

Figure 5 shows an example of this type of plot. The line was determined with the aid of the least-squares method. Only deviations in the ordinate have been taken into account, since the excitation energies are well-known. The uncertainty in T_{4p} is 600^oK for T_{4p} between 7×10^3 and 8×10^3 ^oK. The error in T_{4p} is estimated to be about 250^oK from the random deviations in the curves of Figs. 9 and 12. Systematic deviations must cause the other part ($\sim 350^oK$) of the total uncertainty. This assumption agrees well with the fact that the deviations from the line in Fig.5 apply to all measurements, exluding only those for very low magnetic inductions. We estimate that the errors in the A-values given in Table 6 of the Appendix, contribute only about 100^oK to these systematic deviations. This estimate is based on a comparison with calculations using other A-values. These values differed significantly from those presented in Table 6 of the Appendix and caused a difference of 300 ^oK in T_{4p}. The residual of the systematic deviations, i.e. about 250^oK, are attributed to details in the excitation phenomena in the spectrum of argon II.

The large scale of Fig.5 enables us to draw lines through the points of every separate multiplet (^4P triplet, ^4D quartet, ^2D doublet and ^2P doublet). These lines have steeper slopes than that for the 4p group. It may be remarked, that for the ^4P triplet and ^4D quartet these lines agree much better with the measured points than for the 4p group. In a similar way as for the 4p group we can determine multiplet configuration temperatures. For the example of Fig.5 the values of these temperatures for the four multiplets have been indicated in the legend of the Fig.. In the following figures we shall give the ^4D multiplet configuration

temperature T_{4p}, being the example based on the largest number of measured points.
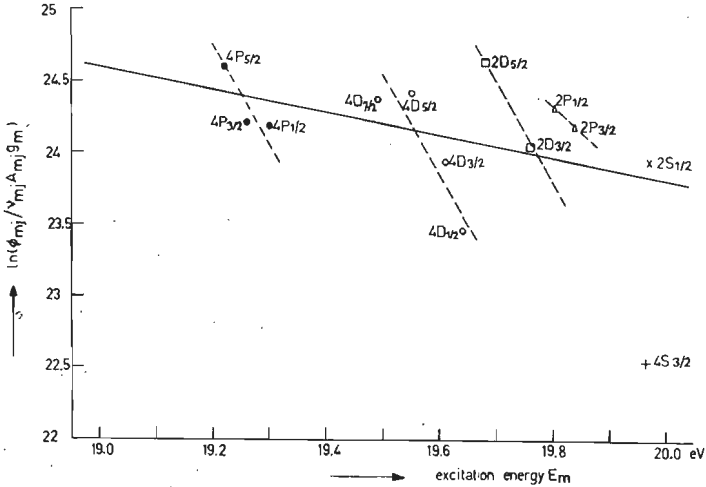
Fig.6 Example of the determination of T_{4p} and of the relative population densities of the 4p levels for $B_w = 9 \times 10^{-3}$ T; the other discharge parameters are similar to those of Fig. 5. $T_{4p} = 14.4 \times 10^3 \, {}^o K$.

We shall give here also the results of the line-intensity measurements for very low values of B_w. For $B_w = 2 \times 10^{-2}$T small deviations from the picture of Fig.5 could be seen. The deviations are much larger for $B_w = 9 \times 10^{-3}$T, the smallest value of B_w for which measurements have been performed. The results for this value are presented in Fig.6. We see that the lines, drawn through the points of the ^{4}P triplet and ^{4}D quartet now show larger deviations from these points in comparison with the situation in Fig.5. Also the doublet and singlet points have positions, which are changed with respect to the line, drawn through the points of the 4p group as a whole, in comparison with the picture of Fig. 5.
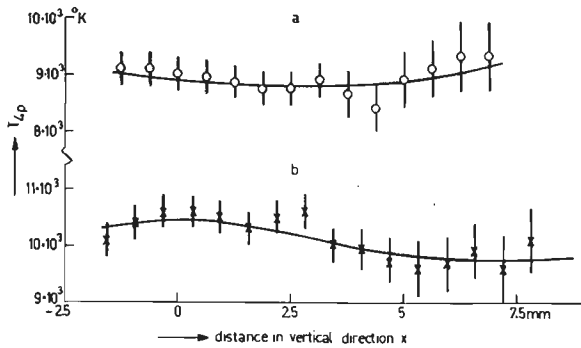
Fig.7 Configuration temperature T_{4p} for two discharge conditions as a function of the vertical scanning distance x from the axis of the discharge. x = 0 denotes the position of maximum radiation intensity. o ring-shaped anode; discharge current I_D = 25A; magnetic induction B_w = 2.25 x $10^{-2}T$; pressure = 2.0 x 10^{-3} mm of Hg. x ring-shaped anode; discharge current I_D = 25 A; magnetic induction B_w = 7.5 x $10^{-2}T$; pressure = 2.0 x 10^{-3} mm of Hg. The error bars give the random error of the values.

Neither the measurements of line-intensities nor those of line profiles have been subjected to an Abel transformation. This simplification can be justified with the help of the results given in the Figs. 7 and 8. Figure 7 shows the values of T_{4p} for two different discharge conditions described in the legend of the figure and for side-on measurements scanned in a vertical direction. We conclude that the differences in T_{4p} are only 10% of the mean value, and do not depend in a systematic way on the vertical position. Other measurements show the same behaviour.

Figure 8 shows the T_i-values, derived from side-on measurements, also scanned in a vertical direction. The deviations are again not larger than about 10%. From these facts we conclude that the Abel transformation will not give a significant improvement of the presented results.
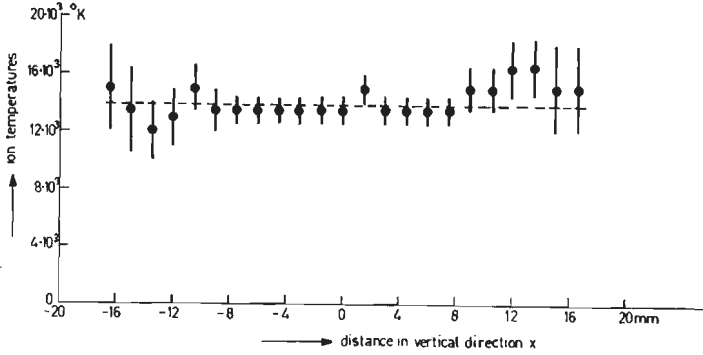
Fig.8 *The ion temperature T_i as a function of the vertical scanning distance x from the axis of the discharge. Discharge conditions: ring-shaped anode; discharge current $I_D = 50$ A; magnetic induction $B_w = 6 \times 10^{-2}$ T; pressure = 1.8×10^{-3} mm of Hg. The error bars give the random error of the values.*
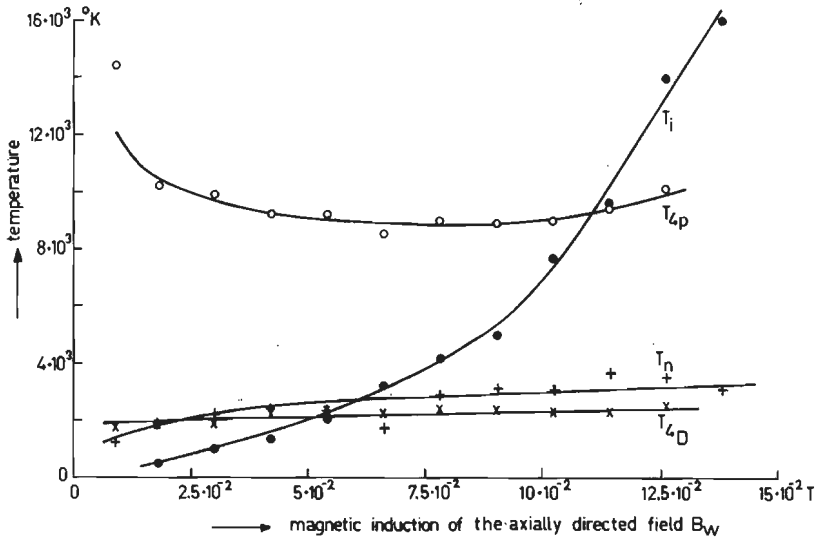
Fig.9 *Configuration and heavy particle temperatures as functions of the magnetic induction B_w for an end-anode discharge. Discharge conditions: discharge current $I_D = 24$ A; Pressure = 1.5×10^{-3} mm of Hg; ● ion temperature T_i; + neutral temperature T_n; O 4p group configuration temperature T_{4p}; x ^{4}D multiplet configuration temperature T_{4D}.*
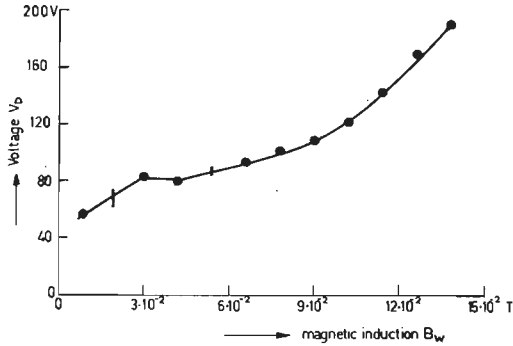
Fig.10 Voltage V_D between the cathode and the end-anode as a function of the magnetic induction B_w. See for discharge conditions Fig.9. Points or bars give the values of the voltage.

Figure 9 gives the values of the various temperatures as functions of the magnetic induction B_w. The discharge conditions are stated in the legend of the figure. T_{4p} shows a small decrement as a function of B_w in the region of small B_w values. This decreasing character of T_{4p} is affirmed by previous measurements with ten measured points in the 0 to 5×10^{-2}T region. A small increment seems to occur for large values of the magnetic induction. T_{4D} on the contrary is nearly constant as a function of B_w.

The curve of T_i shows a rather rapidly growing character as a function of B_w, ranging from 500 to 16×10^3 ^{0}K. All preliminary measurements confirm the form of the presented curve, which for larger discharge currents even has larger maximum values, up to 50×10^3 ^{0}K. The neutral particle temperature T_n only shows a small increase for small values of B_w. For greater values of B_w, T_n is nearly constant, the total variation being between 1.5×10^3 and 3.5×10^3 ^{0}K.

Systematic errors in T_i, due to deconvoluting techniques and to a possible error in the apparatus broadening may range from 50% for temperatures of 1×10^3 ^{0}K to 8% for temperatures of 30×10^3 ^{0}K. Random errors due to the measurements themselves range from about 20% for 1×10^3 ^{0}K to 5% for 30×10^3 ^{0}K. The systematic errors in T_n for a value

of 1.5×10^3 °K are estimated as about 40%, and are partly due to an uncertainty in the calibration of the apparatus broadening for the 4201 Å wavelength, which may give an error in addition. The random error in T_n is larger than that in T_i for the same value of the temperature and is estimated to be 20% for $T_n = 3000$°K. This fact is due to the weak
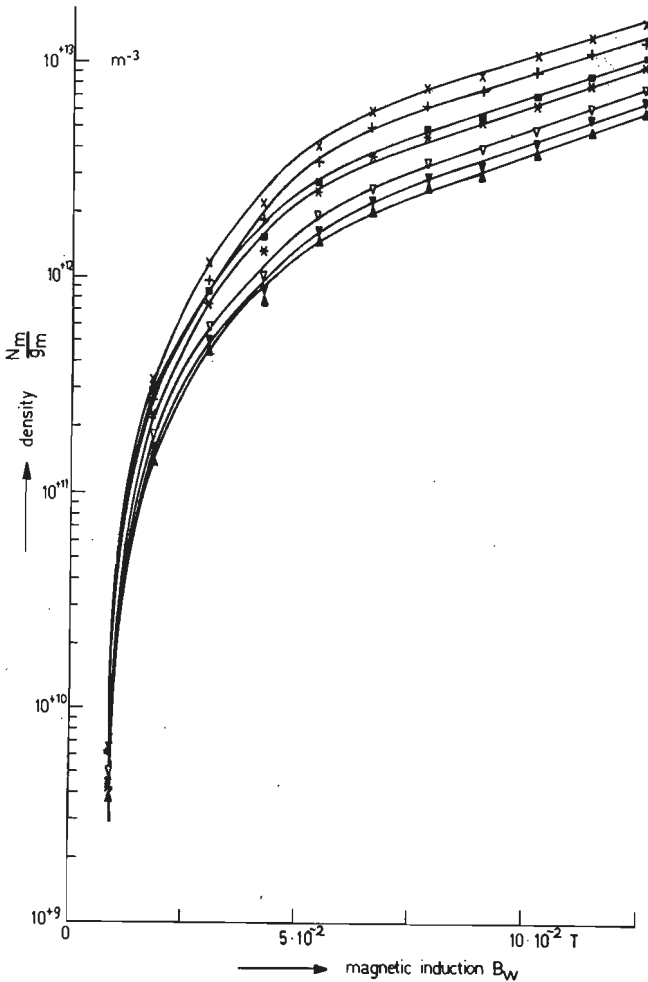
Fig. 11a. Magnetic sublevel populations n_m/g_m for the 4p group as functions of the magnetic induction B_w. See for discharge conditions Fig. 9. $\times\,{}^4P_{5/2}$ level; $+\,{}^4P_{3/2}$; $*\,{}^4P_{1/2}$; $\blacksquare\,{}^2D_{5/2}$; $\blacktriangle\,{}^2D_{3/2}$; $\triangledown\,{}^2P_{1/2}$; $\blacktriangledown\,{}^2P_{3/2}$.

signals of the lines of the neutral spectrum.

The values of the voltage V_D between the end-anode and the cathode for the discharge conditions of Fig.9 are presented in Fig.10.

For the conditions of the measurements presented in Fig.9, the average population densities in the column of the magnetic sublevels of the 4p
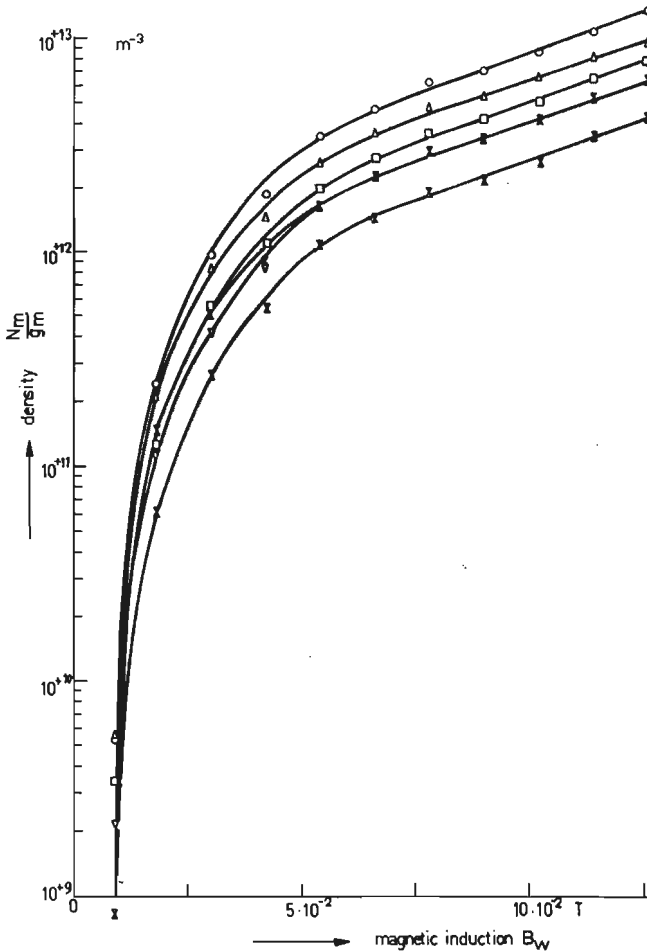
Fig.11b. *Magnetic sublevel populations* n_m/g_m *for the 4p group as functions of the magnetic induction* B_w. *See for discharge conditions Fig. 9.* $\circ\,^4D_{7/2}$; $\triangle\,^4D_{5/2}$; $\square\,^4D_{3/2}$; $\nabla\,^4D_{1/2}$; $\times\,^4S_{3/2}$; $\mathbf{I}\,^2S_{1/2}$. *The* ∇ *and* $\mathbf{I}$ *symbols coincide for many* B_w *values.*

group have been calculated with expression (1). The results are given in Figs. 11a and 11b. We can conclude that in the lower part of the magnetic induction range, the greater part of the confinement of the plasma occurs. From B_w is 9×10^{-3} to 3×10^{-2} T the population densities grow by a factor 100 or more, from 3×10^{-2} to 12×10^{-2} T, however, by about a factor 10. Results of previous measurements with the ring-shaped anode show even more clearly a saturation effect for large magnetic fields.
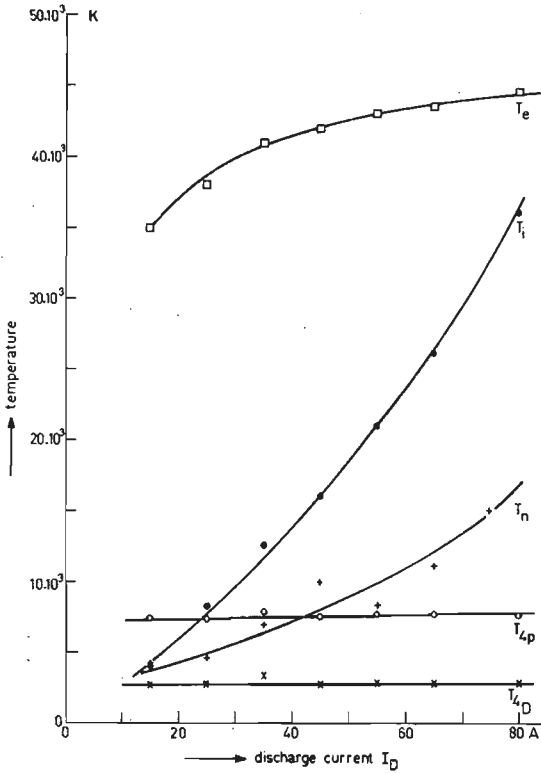
Fig.12 Configuration and particle temperatures as functions of the discharge current I_D. Discharge conditions: ring-shaped anode; magnetic induction $B_w = 9 \times 10^{-2}T$; pressure = 1.65 to 1.70 $\times$ 10^{-3} mm of Hg. □electron temperature T_e; ●ion temperature T_i; +neutral particle temperature T_n; ○ configuration temperature T_{4p}; ✕ configuration temperature T_{4D}.
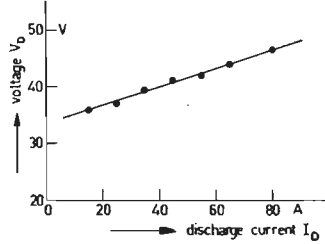
Fig.13 Voltage V_D between the cathode and the ring-shaped anode as a function of the discharge current I_D. See for discharge conditions Fig.12.

In Figure 12 results are presented for the various temperatures of the plasma from measurements, which have been performed as functions of the discharge current I_D, using the ring-shaped anode. The discharge conditions are stated in the legend of the figure. T_i reaches a value of more than 35×10^3 °K for currents of 80 A. Also T_n increases markedly as a function of the discharge current from 3.5×10^3 to 15×10^3 °K. On the contrary, T_{4p} and T_{4D} are constant within very narrow limits, 7.4×10^3 to 7.8×10^3 °K and 2.6×10^3 to 3.3×10^3 °K respectively, while the variation in these values has a random character.

The values of T_e for this set of measurements have been calculated from the ratio of the intensities of the argon III 3286 Å line and the argon II 4348 Å line. The values of T_e increase with the discharge current I_D from 35×10^3 to 45×10^3 °K. The used Corona formulae may lead to systematic errors, which are difficult to estimate. Moreover, the population density of argon^{++} with respect to argon$^+$ will be lower than described by the Corona Equilibrium, due to diffusion losses of the charged particles. These losses will depend on the value of the magnetic induction. Therefore, the T_e will be systematically lowered by the diffusion losses and moreover the error in T_e will be a function of the magnetic induction.

Fig.13 gives the voltage characteristic for the discharge conditions of the measurements of Fig.12. We see a linear variation of V_D with the discharge current.
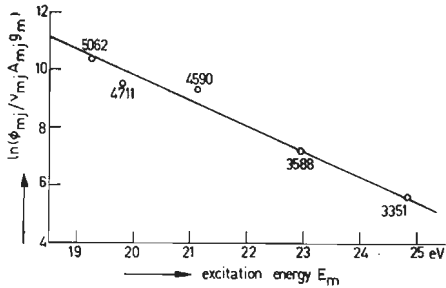
Fig.14 Example of the calculation of an intra group configuration temperature T_{ic} in a semilogarithmic plot as Fig.5. Discharge conditions: ring-shaped anode; discharge current I_D = 25 A; magnetic induction B_w = 13.5 x 10^{-2}T; pressure = 2.5 x 10^{-3} mm of Hg; Result: T_{ic} = 13.2 x 10^3 °K.

In section II it is stated that we can define an inter configuration temperature T_{ic} for a larger range of excitation energies than that of the 4p group, including more than one spectral group. In Fig.14 we show some results from intensity measurements of spectral lines, originating from levels of a large spectral range (19 to 25 eV), including 4p, 4p', 4d and 4d' levels. The discharge parameters are indicated in the legend of the figure. For this example T_{ic} has a value of 13.2 x 10^3 °K. The values of T_{ic} of all other mesurements with various discharge conditions range from 12 x 10^3 to 16 x 10^3 °K. The A-values have been derived from Table 1 of the Appendix for the 5062 and 4965 Å lines and from a recent publication of NERHEIM and OLSEN[9] for the other lines. T_e is estimated to be in the range of 30 x 10^3 to 60 x 10^3 °K for these measurements. These measurements enable us to compare our results in the next section with those of the other references.

VI   DISCUSSION AND CONCLUSIONS

The results, presented in the Figs. 5,9 and 12 are mainly intended to clear the question of thermalization by heavy particles within a spectral group with small energy differences among the subsequent levels.

In section III we saw that contradictory ideas have been published on this topic in the literature on low pressure discharges and argon[+] lasers.

The conclusions which can be drawn from this work, in the first place regard to the argon II 4p group with 13 levels with excitation energies between 19.22 and 19.97 eV and to the parameters of the described plasma, being: $3 \times 10^4 \; ^{\circ}K < T_e < 6 \times 10^4 \; ^{\circ}K$; $2 \times 10^3 \; ^{\circ}K < T_i < 5 \times 10^4 \; ^{\circ}K$; $1.5 \times 10^3 \; ^{\circ}K < T_n < 1.5 \times 10^4 \; ^{\circ}K$; $1 \times 10^{19} \; m^{-3} < n_e = n_i < 6 \times 10^{19} \; m^{-3}$; $2 \times 10^{18} \; m^{-3} < n_n < 4 \times 10^{19} \; m^{-3}$. n_i and n_n are the density of the ions and neutral particles respectively.

In our investigation we calculated the temperature of the various particles to compare them with the configuration temperature T_{4p} for the discharge current and magnetic induction regions available. The main idea for the comparison is, that in the case of rearrangement induced by heavy particles, having temperatures $T_{i,n} < T_e$, the influence of the collisions must be found in the values of T_{4p}. This influence will appear in such a way that the relation

$$T_{i,n} \leq T_{4p} < T_e \tag{5}$$

holds. The value of T_{4p} within the region between $T_{i,n}$ and T_e must depend on the completeness of the thermalization process.

When looking at T_e and T_{4p} in Fig.12, we conclude that the difference between T_e (35×10^3 to $45 \times 10^3 \; ^{\circ}K$) and T_{4p} (7×10^3 to $9 \times 10^3 \; ^{\circ}K$) is very large, indicating that the value of T_{4p} does not give any information on the value of T_e. This conclusion can be drawn with more certainty since the T_e values most probably have to be regarded as minimum values.

A comparison of T_{4p} with T_i, based on the figures 9 and 12 leads to the conclusion that T_{4p} cannot be influenced by collisions with the ions themselves. T_{4p} is more or less constant as a function of the discharge current I_D and for B_w values larger than 2.5×10^{-2} T. T_i is smaller than T_{4p} for small values of B_w, whereas T_i is larger than T_{4p} for larger values of this parameter. The results for the larger B_w values are contrary to the relation (5) which makes it impossible that

thermalization occurs by collisions with ions. Our conclusion is that no detectable quantity of transitions occurs within the 4p group as a whole, initiated by collisions with other ions.

When we compare the values of T_{4p} and T_n as functions of B_w with each others, we see from Fig.9 that the behaviour of these parameters is similar . Besides, it holds that $T_n < T_{4p} < T_e$, which is in agreement with relation (5). In Fig.12, however, the behaviour of T_{4p} and T_n as functions of the discharge current I_D is quite different, resulting in $T_n > T_{4p}$ for $I_D > 40A$, which is in contradiction with relation (5). We conclude that no detectable interaction exists between neutral particles and the excited ions, leading to a thermalization of the whole 4p group.

It appeared from Fig.5, that lines can be drawn through the measured points of the various multiplets. For the ^4P triplet and the ^4D quartet the deviations are small, suggesting the possibility of a thermalization process within the multiplets. The ^4D multiplet configuration temperature T_{4D} has values between 1.8×10^3 and 3×10^3 ^0K. In Fig.9 the curves of T_{4D} and T_n has a similar form. However, T_{4D} is smaller than T_n for the greater part of the curves which is contrary to relation (5), and in Fig.12 the constant value of T_{4D} contrasts with the values of T_n which are growing as a function of I_D. Our conclusion is that from these experiments no reasons can be found to suppose a thermalization process within the multiplets, caused by collisions with neutral atoms. Collisions with ions also do not cause a thermalization.

Reviewing the results of this discussion, we conclude that comparison of the temperatures T_i and T_n of the heavy particles with the configuration temperatures T_{4p} and T_{4D} shows that thermalization processes due to heavy particles must be excluded.

These conclusions can be sustained with an estimation of the minimum value of the cross-section for collisions between excited ions and other heavy particles needed to cause a rearrangement within a spectral group or multiplet. The estimation can be made by comparing the rate of rearrangement with the spontaneous radiation decay rate of a level. One can state that rearrangement will be obvious when:

$$<\sigma_{n,i} \cdot v_{n,i}> \; n_{n,i} \geq \Sigma j \; A_{mj}, \tag{6}$$

where $<\sigma \cdot v>$ denotes an integration of the cross-section over the velocity distribution; n is the suffix for neutrals, i for the ions; $\Sigma j \; A_{mj}$ is the sum of the transition probabilities for the level m. A calculation of σ for the equality of expression (6) for the densities and temperatures, already mentioned gives $\sigma_n \approx 1 \times 10^{-14} \; m^2$ and $\sigma_i \approx 10^{-15}$ to $10^{-14} \; m^{-2}$. These values are about a factor of 10^3 and 10^4 larger than any other cross-section value. These results support our conclusions about the absence of a rearrangement by heavy particles.

Our suggestion is that the locations of the points in Fig.5 are mainly determined by the excitation functions for the levels concerned, resulting in a more or less regular pattern within the ^4P and ^4D multiplets. Thus the physical significance of the parameters T_{4p} and T_{4D} is limited. We conclude from the deviations from other particle temperatures, including T_e, that thermal equilibrium does not exist either within the 4p group or within a multiplet.

In Fig.14, we gave some results of line-intensity measurements and a T_{ic}-value for a region of 6 eV excitation energy. We now want to investigate, what information on T_e is obtainable from the slope of the line in Fig.14. It appears that T_{ic} is 12 x 10^3 to 15 x 10^3 °K. These values must be compared with T_e-values larger than 30 x 10^3 °K. Our conclusion is that even for relative line-intensity measurements from levels with excitation energy differences up to 6 eV, the values of the excitation cross-sections are more important than the factor $\exp(-E_m/kT_e)$. Therefore, a reliable determination of T_e from these measurements is not possible.

We shall now make a comparison of the numerical results of T_{4p} and T_{ic} of this work with the values of other references in order to investigate whether reasonable agreement exists.

The values for T_{4p} are 9 x 10^3 °K for the measurements presented in Fig.9 and 7.5 x 10^3 °K for those presented in Fig.12. It appears that the first value is somewhat larger than the values of the range mentioned in section III. Differences in T_e and n_e between the discharge conditions may cause the greater value of T_{4p} in our experiment.

Our values of T_{ic}, namely 12×10^3 to 15×10^3 °K, are in good agreement with most other values in the literature. We suppose that the large values of LEJEUNE and TIDWELL for T_{ic} are caused by small electron densities. For these circumstances we also found an increasing value of T_{ic}.

We conclude that, apart from errors in A-values, differences in the number of spectral groups and lines and extreme circumstances as very low electron densities, the range of T_{4p} and T_{ic} values is rather small. The values of T_{4p} and T_{ic} are only weak functions of n_e and T_e. We therefore assume that the conclusions from our own investigation may be extended to the other low pressure argon discharges and the argon+ lasers. We expect that thermalization effects are absent for these cases.

As pointed out above, we suppose that the locations of the points in Fig.5 are determined by numerical differences in the excitation of the various levels. This idea is supported by comparing it with the measurement at the very low B_w value of Fig.6. To our opinion, a change in the excitation mechanism takes place when B_w is increased from 9×10^{-3} T to larger values. This opinion is supported by the fact that preliminary measurements showed that the whole region of B-values cannot be described with one excitation process. We suppose that there is a shift from stepwise excitation for normal circumstances to direct excitation from the ion ground levels for very low electron densities. Further detailed experiments in the 0 to 3×10^{-2} T range may give a solution for this problem. It appears to be important in the question on the excitation mechanisms of the argon+ laser and the argon low pressure, high current arc.

ACKNOWLEDGEMENTS

REFERENCES

1 . R.C.Miller, E.F.Labuda and C.E.Webb, Bell System. Techn.J. 46 ,
                                        281 (1967).
2 . R.I.Rudko and C.L.Tang, J.Appl.Phys. 38, 4731 (1967).
3 . J.I.Shipp and E.D.Tidwell, J.Opt.Soc. Am.57, 1061 (1967).
4 . J.I.Shipp, Thesis University of Tenessee, USA, 1967.
5 . S.L.Leonard, Proc. 9th Intern.Conf.Ionized Gases Bucharest p.170
            (1969).
6 . B. van der Sijde, Proc. 9th Intern.Conf.Ionized Gases, Bucharest
                    p. 639 (1969).
7 . C. Lejeune, Proc. 9th Intern.Conf.Ionized Gases, Bucharest, p.216
            (1969).
8 . C.B.Kretschmer, F.Boeschoten and L.J.Demeter, Phys.Fluids 11, 1050
                                        (1968).
9 . N.M.Nerheim and H.N.Olsen, J.Quant.Spectrosc.Radiat.Transf. 10,
                    735 (1970).
10. R.E.Johnson, J.Phys. B 3, 539 (1970).
11. C.A.M.Mouwen, J.Phys.E 3, 27 (1970).
12. R.W.P.McWhirter, Plasma Diagnostic Techniques, Ch. 5 (Editors:
    R.H.Huddlestone and S.L.Leonard) Ac.Press, New York (1965).

APPENDIX

A CONSIDERATION OF THE TRANSITION PROBABILITIES OF THE 4p GROUP OF THE ARGON II SPECTRUM.

Since GARSTANG[1] published the first calculations on transition probability values (abbreviation: A-value) of the argon II spectrum in 1954, a good deal of work has been done in this field, both theoretical [2-4] and experimental[5-11]. Only three of the references are practically complete for the 4p group of the argon II spectrum, having excited levels with energies between 19.22 and 19.97 eV, involving all transitions with A-values larger than $10^5 s^{-1}$ [3,6,8]. The other references range from those giving all important transitions with large A-values to those giving only a few A-values.

Furthermore, lifetime values of the 4p group levels have been published by several authors[12-17]. The values of BENNETT et al[12] agree well with those of RUDKO and TANG[3] and SHUMAKER and POPENOE[8]. Large differences exist between the lifetime values of the ^4P and ^4D multiplets and the ^4S singlet, given by[13-17] and those given by[3,8], whose values are sustained by the A-values of the other authors of [1-11]. The average difference between these two groups of references is more than 50%. The differences in the ^2D and ^2P doublet and the ^2S singlet values are less exceptional. In our calculations we have chosen for the values, according to the references[1-12].

Out of need for the knowledge of the A-values in our own calculations, a systematic comparison has been set up to find one mean value for every A. This comparison involves the work of six selected authors, 1) who have a more or less complete list of the values of the strong transitions and 2) whose values are not totally or partly in great disagreement with the values of the other references. This selection has been made to avoid an arbitrary influence, exerted by one reference on only a small part of the A-values, and to safeguard the procedure against arbitrariness in the choice of rejected and accepted values of some reference. Once having obtained a final result, the work of those authors, so far held out of competition, can be compared with the calculated mean values.

Table 1 *Systematic comparison of the transition probabilities A in $10^{+7}s^{-1}$ of the 4p group of argon II.*

1	2	3	4	5	6	7	8	9	10	11
upper state* and lower state	wave-length λ in Å	Statz 1965 (2)	Rudko 1967 (3)	Kooze-kanani 1969 (4)	mean theoretical value and standard deviation	Schna-pauff 1968 (6)	Chapelle 1968 (7)	Shumaker 1969 (8)	mean experimental value and standard deviation	mean value and deviation§
$(^3P)4p\,^4P_{5/2}$*						x1.43†	x1.13‡			
$(^3P)4s\,^4P_{3/2}$	5009	1.37	1.50	1.48	1.45 3%	1.68	1.51	1.63	1.61 3%	1.53 5%
$(^3P)4s\,^4P_{5/2}$	4806	8.74	8.28	9.62	8.88 5%	8.16	8.88	8.72	8.59 3%	8.73 2%
$(^3P)3d\,^4D_{5/2}$	4431		1.65			1.05	1.08	1.22	1.12 5%	
$(^3P)3d\,^4D_{7/2}$	4401		5.18			2.87	3.3	3.57	3.25 7%	
$(^3P)3d\,^4D_{3/2}$	4461		0.23			0.14		0.173	0.157 10%	
$(^3P)4p\,^4P_{3/2}$*						x1.34†				
$(^3P)4s\,^4P_{1/2}$	5062	2.08	2.16	2.05	2.10 1.5%	2.70		2.45	2.58 5%	2.34 10%
$(^3P)4s\,^4P_{3/2}$	4933	1.61	1.48	1.67	1.59 4%	1.52		1.58	1.55 2%	1.57 1.5%
$(^3P)4s\,^4P_{5/2}$	4736	6.38	6.11	6.76	6.42 3%	6.00		6.5	6.25 4%	6.33 1.5%
$(^3P)3d\,^4D_{1/2}$	4421		0.46			0.21		0.36	0.29 30%	
$(^3P)3d\,^4D_{3/2}$	4400		2.57			1.44		1.82	1.63 12%	
$(^3P)3d\,^4D_{5/2}$	4371		3.90			2.04	2.44	2.58	2.35 7%	
$(^3P)4p\,^4P_{1/2}$*						x1.42†				
$(^3P)4s\,^4P_{1/2}$	4972	0.95	0.97	0.97	0.96 1%	1.15		1.07	1.11 4%	1.04 8%
$(^3P)4s\,^4P_{3/2}$	4848	8.97	8.65	9.44	9.02 3%	9.15		9.4	9.28 1.5%	9.15 1.5%
$(^3P)3d\,^4D_{1/2}$	4352		3.81			2.00	1.74	2.53	2.09 12%	
$(^3P)3d\,^4D_{3/2}$	4332		3.22			1.65		2.3	1.98 16%	

40

Table 1 (continued)

upper state* and lower state	wavelength λ in Å	Statz 1965 (2)	Rudko 1967 (3)	Kooze-kanani 1969 (4)	mean theoretical value and standard deviation	Schna-pauff 1968 (6)	Chapelle 1968 (7)	Shumaker 1969 (8)	mean experimental value and standard deviation	mean value and deviation
$(^3P)4p^4D_{7/2}$*						x0.90†	x1.13‡			
$(^3P)4s^4P_{5/2}$	4348	13.9	13.5	14.6	14.0 2.5%	12.4	·11.6	13.7	12.6 5%	13.3 5%
$(^3P)3d^4F_{7/2}$	6887							0.109		
$(^3P)3d^4F_{9/2}$	6644							1.86		
$(^3P)3d^4D_{5/2}$	4039		0.28			0.13		0.141	0.13^5 5%	
$(^3P)3d^4D_{7/2}$	4014		1.70			1.12	1.10	1.19	1.14 2.5%	
$(^3P)4p^4D_{5/2}$*						x1.31†				
$(^3P)4s^2P_{3/2}$	5145	0.71	0.92	1.97	1.20 35%	1.05		1.08	1.07 2%	1.13 6%
$(^3P)4s^4P_{3/2}$	4426	10.4	9.46	9.07	9.64 4%	8.10	7.84	9.2	8.4 5%	9.0 7%
$(^3P)4s^4P_{5/2}$	4267	1.92	2.10	1.89	1.97 4%	1.62		1.73	1.68 4%	1.82 8%
$(^3P)3d^4F_{5/2}$	6864							0.24		
$(^3P)3d^4F_{7/2}$	6684							1.25		
$(^3P)3d^4D_{3/2}$	3992		0.31					0.169		
$(^3P)3d^4D_{5/2}$	3968		0.66			0.48	0.44	0.52	0.48 5%	
$(^3P)3d^4D_{7/2}$	3944		0.63			0.41		0.447	0.43 5%	
$(^3P)4p^4D_{3/2}$*						x1.41†				
$(^3P)4s^2P_{1/2}$	5287	0.14	0.20	0.38	0.24 30%			0.17		
$(^3P)4s^4P_{1/2}$	4430	6.78	6.22	6.59	6.53 2.5%	5.70	3.8	5.9	5.1 14%	5.8 12%
$(^3P)4s^4P_{3/2}$	4331	6.42	6.27	5.81	6.17 3%	5.23		6.3	5.8 9%	6.0 4%
$(^3P)4s^4P_{5/2}$	4178	0.12	0.15	0.05	0.11 30%			0.14		
$(^3P)3d^4F_{3/2}$	6757							0.1		
$(^3P)3d^4F_{5/2}$	6638							1.43		

41

Table 1 (continued)

upper state[*] and lower state	wavelength λ in Å	Statz 1965 (2)	Rudko 1967 (3)	Kooze-kanani 1969 (4)	mean theoretical value and standard deviation	Schna-pauff 1968 (6)	Chanelle 1968 (7)	Shumaker 1969 (8)	mean experimental value and standard deviation	mean value and deviation
$(^3P)3d^4D_{1/2}$	3931		0.33			0.23		0.22	0.23 3%	
$(^3P)3d^4D_{3/2}$	3915		0.40			0.30		0.36	0.33 9%	
$(^3P)3d^4D_{5/2}$	3892		1.05			0.66		0.81	0.74 10%	
$(^3P)4s^2P_{3/2}$	5018	0.03		0.77	0.4 90%			0.095		
$(^3P)4p^4D_{1/2}$[*]						$\times 1.21$†				
$(^3P)4s^4P_{1/2}$	4380	12.2	11.7	12.8	12.2 2.5%	9.83	12.7	11.5	11.3 8%	11.8 4%
$(^3P)4s^4P_{3/2}$	4283	1.49	1.51	1.44	1.48 1.5%	1.43		1.33	1.38 4%	1.43 4%
$(^3P)3d^4F_{3/2}$	6640							2.01		
$(^3P)3d^4D_{1/2}$	3891		0.62			0.55		0.43	0.49 12%	
$(^3P)3d^4D_{3/2}$	3875		1.21			0.99		0.8	0.90 12%	
$(^3P)4p^2D_{5/2}$[*]						$\times 1.53$†				
$(^3P)4s^2P_{3/2}$	4880	8.96	8.45	8.00	8.47 4%	8.45		8.7	8.58 1.5%	8.52 1%
$(^3P)4s^4P_{3/2}$	4228	0.99	1.31	3.17	1.82 40%	1.00	1.28	1.44	1.24 10%	1.53 20%
$(^3P)4s^4P_{5/2}$	4082	0.36	0.38	0.47	0.40 9%	0.31		0.30	0.31 2.5%	0.35 14%
$(^3P)3d^4F_{7/2}$	6243							0.32		
$(^3P)3d^4D_{5/2}$	3809		0.12			0.11		0.08	0.10 16%	
$(^3P)3d^4D_{3/2}$	3830		0.06					0.04		
$(^3P)3d^4D_{7/2}$	3786		0.02			0.15		0.13	0.14 7%	
$(^3P)4p^2D_{3/2}$[*]						$\times 1.35$†				
$(^3P)4s^2P_{1/2}$	4965	2.63	4.61	3.00	3.41 18%	3.54		3.85	3.70 4%	3.55 4%
$(^3P)4s^2P_{3/2}$	4727	7.27	4.56	6.20	6.01 14%	5.53	5.6	5.6	5.6 0.5%	5.8 4%
$(^3P)4s^4P_{1/2}$	4202	0.11	0.35	0.88	0.45 50%			0.18		

Table 1 (continued)

upper state* and lower state	wave-length λ in Å	Statz 1965 (2)	Rudko 1967 (3)	Kooze-kanani 1969 (4)	mean theoretical value and standard deviation	Schna-pauff 1968 (6)	Chapelle 1968 (7)	Shumaker 1969 (8)	mean experimental value and standard deviation	mean value and deviation
$(^3P)4s\,^4P_{3/2}$	4113	0.11	0.27	1.26	0.55 70%	0.09		0.091	0.09 0%	0.32 70%
$(^3P)4s\,^4P_{5/2}$	3975	0.06	0.04	0.16	0.09 40%			0.09		
$(^3P)3d\,^2P_{1/2}$	6809							0.07		
$(^3P)3d\,^4F_{3/2}$	6240							0.02		
$(^3P)3d\,^4F_{5/2}$	6139							0.11		
$(^3P)3d\,^4D_{1/2}$	3751		0.03					0.01		
$(^3P)3d\,^4D_{3/2}$	3736					0.43		0.025	0.23 90%	
$(^3P)3d\,^4D_{1/2}$	3715		0.07					0.02		
$(^3P)4p\,^2P_{1/2}$ *						x1.21†				
$(^3P)4s\,^2P_{1/2}$	4889	1.98	1.25		1.62 25%	1.74		1.76	1.75 0.5%	1.68 4%
$(^3P)4s\,^2P_{3/2}$	4658	7.55	8.55		8.05 6%	8.5		8.9	8.7 2.5%	8.4 4%
$(^3P)4s\,^4P_{1/2}$	4147							0.02		
$(^3P)3d\,^2P_{1/2}$	6666							0.8		
$(^3P)3d\,^4D_{1/2}$	3707		0.07					0.02		
$(^3P)4p\,^2P_{3/2}$ *						x1.24†				
$(^3P)4s\,^2P_{1/2}$	4765	7.15	4.47	6.94	6.19 14%	5.43		6.37	5.9 8%	6.04 2.5%
$(^3P)4s\,^2P_{3/2}$	4545	2.77	5.19	3.66	3.87 18%	3.88	4.6	4.58	4.35 6%	4.11 6%
$(^3P)4s\,^4P_{3/2}$	3974.5	0.08	0.07		0.08 7%			0.2		
$(^3P)4s\,^4P_{5/2}$	3845	0.02	0.09		0.06 70%	0.11		0.2	0.16 30%	0.11 50%
$(^3P)3d\,^2P_{3/2}$	6861			0.28				0.27		
$(^3P)4p\,^4S_{3/2}$						x0.89†				
$(^3P)4s\,^2P_{1/2}$	4588							0.05		

43

Table 1 (continued)

upper state[*] and lower state	wave-length λ in Å	Statz 1965 (2)	Rudko 1967 (3)	Kooze-kanani 1969 (4)	mean theoretical value and standard deviation	Schna-pauff 1968 (6)	Chanelle 1968 (7)	Shumaker 1969 (8)	mean experimental value and standard deviation	mean value and deviation
$(^3P)4s\,^2P_{3/2}$	4384	0.02	0.09		0.06 70%			0.12		
$(^3P)4s\,^4P_{1/2}$	3929	4.51	4.30	4.94	4.58 4%	2.61	3.6	3.3	3.2 10%	3.9 18%
$(^3P)4s\,^4P_{3/2}$	3851	7.30	6.94	7.76	7.33 3%	4.48	6.0	5.3	5.3 10%	6.3 16%
$(^3P)4s\,^4P_{5/2}$	3729	8.70	8.50	8.77	8.66 1%	6.71	7.0	6.6	6.8 2%	7.7 12%
$(^3P)3d\,^2P_{3/2}$	6500							0.04		
$(^3P)3d\,^4D_{3/2}$	3518		0.02		0.01			0.01		
$(^3P)3d\,^4D_{5/2}$	3500		0.05					0.04		
$(^3P)4p\,^2S_{1/2}$ [*]						x1.03[†]				
$(^3P)4s\,^2P_{1/2}$	4579	8.42	8.99	9.83	9.08 5%	7.9	11.4	9.04	9.4 12%	9.3 2%
$(^3P)4s\,^2P_{3/2}$	4376	3.71	2.30	2.76	2.92 14%	1.89	1.6	2.22	1.90 10%	2.4 20%
$(^3P)3d\,^2P_{3/2}$	6483					1.20		1.1	1.15 4%	
$(^3P)3d\,^2P_{1/2}$	6104							0.13		

Notes:

[*] The upper states have been indicated with an asterisk.

[†] The multiplication factor for each state denotes the ratio between the values, given in column 7 and the original values of Schnapauff himself.

[‡] The multiplication factor for the original values of Chapelle et al is 1.13 for all values.

[§] The deviation is the difference between the overall mean value and the theoretical or experimental mean value.

In accordance with the principle explained before, the theoretical results of STATZ et al[2], RUDKO and TANG[3], and KOOZEKANANI and TRUSTY[4] and the experimental results of SCHNAPAUFF[6], CHAPELLE et al[7], and SHUMAKER and POPENOE[8] have been chosen as the basis of our systematic comparison.

In Table 1 this comparison is presented, leading to a mean value for many transitions. In the following we shall explain the framework of Table 1. The values of some authors have been modified in a systematic way, the reason for the modification being explained below.

At first we shall pay attention to the three selected theoretical papers. GARSTANG[1] carried out calculations on absolute A-values, based on the Coulomb approximation and Intermediate Coupling (I.C.). The latter appeared to be much more adequate than the single L-S coupling. STATZ et al[2] extended the calculations of GARSTANG by introducing more parameters. This led to significantly better results for the values of the $4p \rightarrow 4s$ transitions. Therefore, only the I.C.-values of STATZ et al have been included in our calculation.

Work done by Marantz and presented by RUDKO and TANG[3], moreover yielded the A-values of the $4p \rightarrow 3d$ transitions. KOOZEKANANI and TRUSTY[4] using I.C. and Hartree-Fock wave functions presented values, for the most part in good agreement with[2] and [3].

The values of these three references are indicated in the columns 3 to 5 of Table 1. In column 6 the average of these values is given, presenting a mean theoretical value for the $4p \rightarrow 4s$ transitions. The standard deviation is also stated. The values for the $4p \rightarrow 3d$ transitions will be discussed later on. The degree of agreement for each multiplet or singlet is summarized in Table 2. The applied evaluation is also given.

Reviewing these results, the conclusion arises that the work of the three authors chosen, gives a very good agreement in the great majority of the values of the $4p \rightarrow 4s$ transitions originating from the $^4P, ^4D, ^4S$ and ^2S levels, whereas the agreement for the values of the ^2D and ^2P levels can be qualified as being moderate to very poor with only four favourable exceptions. The great differences between the values for the ^2D and ^2P levels in the treatments give support to the

Table 2 Review of the degree of agreement between the theoretical A-values, based on the value of the standard deviation of the mean theoretical value.

standard deviation	degree of agreement	multiplet or singlet						
		4_P	4_D	2_D	2_P	4_S	2_S	totals
0-5%	very good	7	7	1	-	3	1	19
6-10%	good	-	-	1	2	-	-	3
11-20%	moderate	-	-	2	2	-	1	5
21-40%	poor	-	3	2	1	-	-	6
41-100%	very poor	-	1	2	1	1	-	5
	totals	7	11	8	6	4	2	38

assumption that the three sources are sufficiently independent in their calculations. This conclusion consolidates the opinion that the agreement of the A-values for the other levels is a consequence of the reliability of the obtained results.

SCHNAPAUFF[6] obtained A-values for argon II lines from intensity measurements of a cascade arc with pressures ranging from 1 to 5 atm. The A-values given by Schnapauff, were partly based on lifetime values, derived from BENNETT et al[12], and BAKOS et al[13], and partly on values calculated with the aid of the Coulomb approximation, using tables of BATES and DAMGAARD[18], and of GRIEM[19]. It appears that SCHNAPAUFF'S original A-values are significantly lower than the already calculated theoretical mean values and also lower than the values of SHUMAKER and POPENOE[8], based on experimental data. To our opinion this discrepancy is due to his choice of the lifetime values. Therefore, we have consistently used the lifetime values of BENNETT et al for those levels, for which a value is available. For the values, lacking in the work of BENNETT et al, those of SHUMAKER and POPENOE increased with 10%, have been used; the mean difference between the values, available in the two references, is given by this percentage. This choice assures

us of a set of values, independent of theoretical data. A-values, based on the lifetime values, obtained in the described way and on the relative rates of the transition probabilities for every single upper level, as given by SCHNAPAUFF, are presented in column 7. A small correction has been taken into account for transitions not considered. The multiplication factor for the original values of SCHNAPAUFF is noted in Table 1 for every upper level.

CHAPELLE et al[7] presented A-values of the argon II spectrum (of which 21 are of the 4p group), based on atmospheric pressure arc experiments. The absolute values are based on GARSTANG's value for the 4806 Å line ($A = 7.88 \times 10^{+7}$ s^{-1}). Although the difference between this value and the mean theoretical value of Table 1 ($A = 8.88 \times 10^{+7}$ s^{-1}) is only 13%, the latter value may be expected to be more reliable than GARSTANG's value and is more consistent with our system. The mean theoretical value is in good agreement with the value of SHUMAKER and POPENOE ($8.72 \times 10^{+7}$ s^{-1}). Therefore, the original values of[7] have been multiplied by a factor 1.13. The results are shown in column 8.

SHUMAKER and POPENOE[8] used a wall stabilized atmospheric pressure arc for their A-measurements. The values were obtained in an independent way, assuming that L.T.E.circumstances were valid, and can be found in column 9.

Table 3 *Review of the degree of agreement between the experimental A-values, based on the value of the standard deviation of the mean experimental value.*

standard deviation	degree of agreement	multiplet or singlet						
		^4P	^4D	^2D	^2P	^4S	^2S	totals
0-5%	very good	8	10	5	2	1	1	27
6-10%	good	3	4	2	2	2	1	14
11-20%	moderate	3	3	1	-	-	1	8
21-40%	poor	1	-	-	1	-	-	2
41-100%	very poor	-	-	1	-	-	-	1
	totals	15	17	9	5	3	3	52

The values in the columns 7, 8 and 9 have been averaged in column 10, presenting a mean experimental value. The standard deviation is also indicated. The degree of agreement for each multiplet or singlet is summarized in Table 3.

Reviewing the results of the comparison of the experimental data, we can conclude that the agreement is better than 10% for 41 of the 52 values, while many of the other 11 values have a moderate agreement. None of the levels show deviations, which are systematically greater than others.

Finally, a comparison can be made between the mean theoretical and experimental values. The results are shown in column 11, giving an overall mean value and the difference between this value and each particular value. The degree of agreement for each multiplet or singlet is summarized in Table 4.

Table 4 Review of the degree of agreement between the mean theoretical and the mean experimental A-values, based on the value of the deviation in column 11 of Table 1.

standard deviation	degree of agreement	multiplet or singlet						
		^4P	^4D	^2D	^2P	^4S	^2S	totals
0-5%	very good	5	4	3	3	-	1	16
6-10%	good	2	3	-	1	-	-	6
11-20%	moderate	-	1	2	-	3	1	7
21-40%	poor	-	-	-	-	-	-	0
41-100%	very poor	-	-	1	1	-	-	2
	totals	7	8	6	5	3	2	31

Reviewing the final results of the 4p → 4s transitions, we can conclude that of the 31 values which could be compared, 22 are in good or very good agreement. The 9 values with larger deviations are found in the ^4D quartet (one value), in the ^2D and ^2P doublets due to the unreliable theoretical values, and in the $^4S_{3/2}$ and $^2S_{1/2}$ singlets,

in which the deviations are more or less unexpected and unexplained.

A similar comparison for 4p → 3d transitions was not possible as completely as has been performed for the 4p → 4s transitions being less information available than for the 4p → 4s transitions. The only theoretical data for the first mentioned transitions have been given by RUDKO and TANG[3]. Experimental values have been given by two and sometimes three references, so that a representative mean experimental value for many transitions could be given. 13 values are in good or very good agreement, 8 values are in moderate to very poor agreement with each other. It seems that the values of the 4p → 3d transitions given by RUDKO and TANG are too large in many cases by a factor 1.5 to 1.7.

When the calculations of the Appendix were performed, the survey of WIESE et al[20] was not available to us. We now conclude that the results of their calculations agree well with ours. We can see, however, a systematic difference between many of their values and those of us, due to the different way of calculation. WIESE et al do not describe exactly the method of their calculations. It seems that the lifetime values of BENNETT et al[12] have a dominant position in their calculations. Further detailed information can be found on pages 202 and 203 of[20].

Table 5 A comparison between the results of some authors with the A-values of Table 1.

authors	totals	deviations <2σ	deviations >2σ	average of the absolute differences in %
Garstang[1]	31	13	18	33
Olsen[5]	11	3	8	11
Berg and Ervens[9]	8	2	6	22
Van Houwelingen[10] and Kruithof	4	1	3	12
Nerheim and Olsen[11]	4	1	3	22

A comparison of the results of Table 1 has been made with the A-values of the previously mentioned authors. For each author the total number

Table 6 Selection of transitions with large and reliable A-values.

transition	wavelength λ in Å	A value in $10^{+7}s^{-1}$	deviation in %
$4p\ ^4P_{5/2} \to 4s\ ^4P_{5/2}$	4806	8.73	2
$4p\ ^4P_{3/2} \to 4s\ ^4P_{5/2}$*	4736	6.33	1.5
$4p\ ^4P_{1/2} \to 4s\ ^4P_{3/2}$	4848	9.15	1.5
$4p\ ^4D_{7/2} \to 4s\ ^4P_{5/2}$	4348	13.3	6
$4p\ ^4D_{5/2} \to 4s\ ^4P_{3/2}$	4426	9.0	7
$4p\ ^4D_{3/2} \to 4s\ ^4P_{3/2}$	4331	6.0	4
$4p\ ^4D_{1/2} \to 4s\ ^4P_{1/2}$	4380	11.8	4
$4p\ ^2D_{5/2} \to 4s\ ^2P_{3/2}$	4880	8.52	1
$4p\ ^2D_{3/2} \to 4s\ ^2P_{3/2}$	4727	5.6 †	0.5
$4p\ ^2P_{1/2} \to 4s\ ^2P_{3/2}$	4658	8.4	4
$4p\ ^2P_{3/2} \to 4s\ ^2P_{1/2}$	4765	6.04	2.5
$4p\ ^4S_{3/2} \to 4s\ ^4P_{5/2}$*	3729	7.7	12
$4p\ ^2S_{1/2} \to 4s\ ^2P_{1/2}$	4579	9.3	2

*Two alternative transitions had already been chosen and used for the calculations of this paper. This selection was based on the literature up till 1968. These transitions are:

$4p\ ^4P_{3/2} \to 4s\ ^4P_{3/2}$, 4933 Å, A = 1.57 x $10^{+7}s^{-1}$, dev. 1.5% and
$4p\ ^4S_{3/2} \to 4s\ ^4P_{3/2}$, 3851 Å, A = 6.3 x $10^{+7}s^{-1}$, dev. 16%.

† The mean experimental value has been chosen, the mean theoretical value having a deviation of 14%.

of transitions, the number of values within an interval of two times the
deviation percentage of the overall mean value (2σ) and outside this
interval is indicated. Moreover, the average of the absolute differences
between the value of the regarding author and the overall mean value
is noted. The results are presented in Table 5.

For our own calculations we wanted to know for every excited level
of the 4p group the A-value of at least one transition, originating
from that level. The choice is determined by the strength of the
transition and the reliability of the A-values. Following this principle
we made a selection, presented in Table 6.

REFERENCES TO THE APPENDIX

1 . R.H.Garstang, Mon.Not.Roy.Astr.Soc. 114, 118 (1954).

2 . H.Statz, F.A.Horrigan, S.H. Koozekanani, C.L.Tang and G.F.Koster
J.Appl.Phys. 36, 2278 (1965).

3 . R.I.Rudko and C.L.Tang, J.Appl.Phys. 38, 4731 (1967).

4 . S.H.Koozekanani and G.L.Trusty, J.Opt.Soc.Am. 59,1281 (1969).

5 . H.N.Olsen, J.Quant.Spectrosc.Radiat.Transfer 3, 59 (1963) and 3,
305 (1963).

6 . R.Schnapauff, Zeitschr.f.Astrophys. 68, 431 (1968).

7 . J.Chapelle, A.Sy, F.Cabannes and J.Blandin, J.Quant.Spectrosc.Radiat.
Transfer 8, 1201 (1968).

8 . J.B.Shumaker Jr. and C.H.Popenoe, J.Opt.Soc.Am. 59, 980 (1969).

9 . H.F.Berg and W.Ervens, Zeitschr.f.Phys. 206, 184 (1967).

10. D. van Houwelingen and A.A.Kruithof, J.Quant.Spectrosc.Radiat.
Transfer 11, 1235 (1971).

11. N.M.Nerheim and H.N.Olsen, J.Quant.Spectrosc.Radiat.Transfer 10,
735 (1970).

12. W.R.Bennett Jr., P.J.Kindlmann, G.N.Mercer and J.Sunderland,
Appl.Phys.Letters 5, 158 (1964).

13. J.Bakos, J.Szigeti and L.Varga, Phys. Letters 20, 503 (1966).

14. T.A.Matilsky and J.E.Hesser, J.Opt.Soc.Am.59,579 (1969).

15. A.Denis and M.Gailland, Phys.Letters 31A, 9 (1970).

16. J.A.Kernahan, C.C.Linand and E.H.Pennington, J.Opt.Soc.Am. 60,
898 (1970).

17. G.E.Assousa, L.Brown and W.K.Ford Jr., J.Opt.Soc.Am. 60, 1311
(1970).

18. D.R.Bates and A.Damgaard, Phil.Trans.Roy.Soc.London(A) 242,
101 (1949).

19. H.R.Griem, Plasma Spectroscopy, Mc.Graw-Hill Book Cy, New York,
(1964).

20. W.L.Wiese, M.W.Smith and B.M.Miles, Atomic Transition Probabilities,
Part II, N.B.S., 1969.

TEMPERATURE AND DENSITY PROFILES OF ELECTRONS IN A HOLLOW CATHODE ARGON
ARC DISCHARGE

B. van der Sijde
Department of Technical Physics, University of Technology, Eindhoven,
Netherlands.

Summary- Measurements have been performed of radial radiation profiles
of argon I and II lines in a hollow cathode low-pressure magnetically-
confined argon arc discharge with currents of 15 to 60 A. The working
pressure of the discharge was $\sim 10^{-3}$ mm of Hg and the electron density
was $\sim 10^{19} m^{-3}$. From the radiation profiles radial temperature and
density profiles of the electrons have been calculated. For this
calculation we made use of Corona Equilibrium formulae and we discussed
how far these formulae give a good description of the excitation
phenomena in the plasma. It appears that the decrease of the electron
temperature in most cases is about 10% per 10 mm or smaller and that
the width at half-maximum value of the electron density profile for a
confined plasma is about 18 mm for an end-anode configuration situated
at 1.2 m from the cathode and 27 mm for a ring-shaped anode situated
near the cathode. These widths at half-maximum value are roughly
independent of the magnetic induction value between 3.75 x 10^{-2} and
12.5 x 10^{-2}T.

I   INTRODUCTION

   This investigation deals with measurements of radiation profiles
as functions of the distance r from the axis of argon lines and
calculations of the electron temperatures and electron densities
relative to the values on the axis in a hollow cathode low-pressure
magnetically-confined argon arc discharge. This type of discharge,
having a working pressure of about 10^{-3} mm of Hg, had been introduced
by LIDSKY et al [1] and was investigated by several authors[2-6].
   The discharge device and the equipment for spectral line radiation
measurements were described in a previous paper [7] (see Fig.1). The
radiation profiles have been determined as functions of the distance
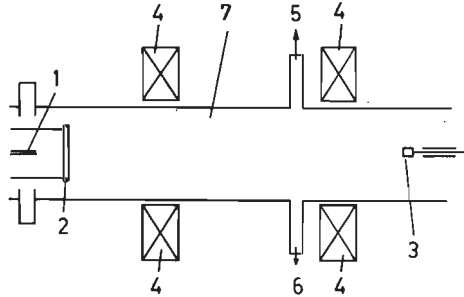
Fig.1 Simplified design of the cathode and anode device. 1 is a hollow-cathode; 2 is a ring-shaped anode; 3 is an end-anode; 4 are magnetic coils; 5 and 6 are tubes for spectral measurements; 7 is a pyrex tube.

x in the vertical direction which is perpendicular to the axis of the plasma column. The profiles are obtainable as functions of the radius r by application of an Abel transformation.

The electron density n_e of the plasma of the discharge when confined by the longitudinal magnetic field B_z was of the order of $10^{19} m^{-3}$. This means that the plasma was in Corona Equilibrium (C.E.), resulting in the phenomenon that the collisional excitation of the levels is balanced by radiative decay only.

The method for calculation of the electron temperature T_e from spectral line-intensities for a plasma in C.E. [8] was given by McWHIRTER [9] and WILNER [10]. In the next section will be discussed the fact that the Corona formulae used give a good qualitative description of the excitation phenomena in the argon II spectrum. The absolute values of T_e, calculated with this method may be greatly in error, due to numerical deviations in the cross-section data used. Therefore we only applied the method for comparing the results of the calculations of $T_{e,o}$ for $r = 0$ and $T_{e,r}$ for $r \neq 0$ with each other. It appears that reduced T_e profiles $T_{e,r}/T_{e,o}$ can be found by comparing the profiles of two or more argon II lines with largely different excitation energies of the upper levels. By making use of this information it is also possible to calculate the reduced n_e profiles $n_{e,r}/n_{e,o}$ from one of these argon II profiles.

The argon I profiles show a more or less complicated picture.
Although the upper levels concerned are mainly populated by direct
excitation from the atomic ground level, the complications in the
picture may be due to an additional stepwise excitation and a small
diffusion of the excited particles of the 5p group. As a consequence
of the weak radiation of other groups than the 4p and 5p group, we
can state that cascade radiation is not important.

II   TEMPERATURE AND DENSITY PROFILES OF THE ELECTRONS

1   Balance equation for argon II levels

We shall discuss the excitation and ionization phenomena that may
occur in the plasma and are of interest for the explication of the
radial radiation profiles. First we shall deal with the profiles of
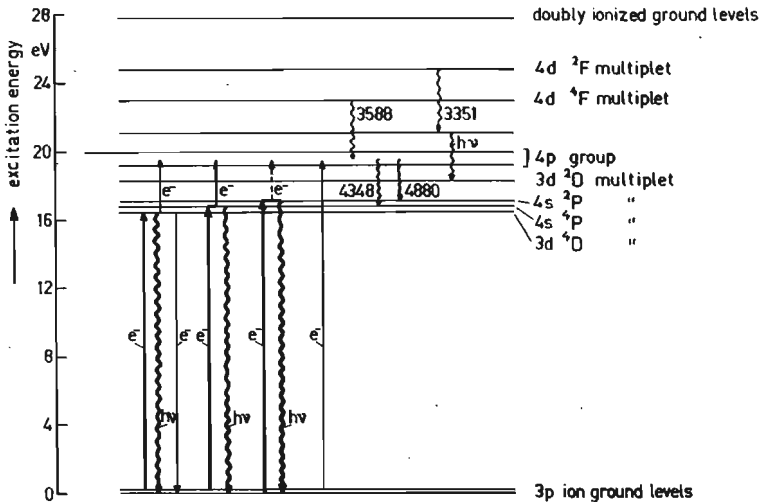
Fig.2 Simplified diagram of the argon II excited levels or groups.
Transitions are indicated with e⁻ (excitation by electrons), hν
(emission of radiation) or a special line, designated with its wave-
length. The thickness of the lines gives a rough qualitative impression
of the importance of the processes.

the argon II lines. The radiation detected is that of spectral lines with upper levels, having excitation energies of 19.49 eV (4p group, $^4D_{7/2}$ level, $\lambda = 4348$ Å), 22.96 eV (4d group, $^4F_{9/2}$ level, $\lambda = 3588$ Å) and 24.85 eV (4d group, $^2\bar{F}_{5/2}$ level, $\lambda = 3351$ Å) (see Fig.2).

The levels concerned may be populated by one or more of the following processes:

1) simultaneous ionization and excitation directly from the atomic ground level;
2) simultaneous ionization and excitation from the atomic metastable levels ;
3) direct excitation from the two ion ground levels;
4) stepwise excitation from the ion ground levels through short-lived levels (e.g. 4s $^4P_{1/2}$ and $^4P_{3/2}$ levels for which the lifetime $\tau = 9 \times 10^{-8}$ and 2.7×10^{-8}s respectively [11]);
5) stepwise excitation from the ion ground levels through metastable levels (e.g. some 3d levels);
6) cascade radiation from 4d and 5s levels to the 4p group and from 5p, 5d and 6s levels to the 4d levels concerned here;
7) recombination of argon doubly ionized particles to excited argon II levels.

The levels concerned may be depopulated by one or more of the processes:

1) spontaneous emission;
2) collisional deexcitation to a lower level;
3) excitation to a higher excited level;
4) ionization to doubly ionized particles.

Other conceivable processes for population as well as depopulation are neglected.

The balance equation for levels marked with suffix 3 can be written as

$$n_e n_a \langle \sigma v_e \rangle_{sim} + n_e n_a^* \langle \sigma v_e \rangle_{sim}^* + n_e n_{ion} \langle \sigma v_e \rangle_{dir} +$$

$$+ n_e^2 n_{ion} \Sigma i \{\langle \sigma v_e \rangle_{II}^i \cdot (\Sigma \langle \sigma v_e \rangle_I^i / \Sigma A_{2i\ 1}) + n_e \Sigma j\ n_{2j}^* \langle \sigma v_e \rangle_{met}^j +$$

$$+ \Sigma k\ n_{4k} A_{4k\ 3} + n_e n_{ion}^{++} R_3 =$$

$$n_3 \Sigma m A_{3\ 2m} + n_3 n_e \langle \sigma v_e \rangle_{deexc} + n_3 n_e \langle \sigma v_e \rangle_{exc} + n_3 n_e \langle \sigma v_e \rangle_{ion} , \quad (1)$$

where n_a is the neutral atom density; n_a^* is the atomic metastable
density; n_{ion} is the ion density; n_2^* is the ion metastable density;
n_4 is the density of a cascading level; n_{ion}^{++} is the doubly ionized
particles density and n_3 the density of the level concerned.
$<\sigma v_e>$ denotes an integration of a cross-section over the electron
velocity distribution. The suffix *sim* denotes the simultaneous
ionization and excitation from the atomic ground level and *sim** from
the atomic metastable level; the suffix *dir* denotes direct excitation
from the ion ground levels; the suffices *I* and *II* the first and second
step of the stepwise process; the suffix *met* excitation from an ion
metastable level to a level 3; the suffices *deexc* and *exc* collisional
deexcitation and excitation from a level 3 to a lower and a higher level
respectively; the suffix *ion* ionization to argon^{++} ions.
The ground levels are marked with 1, the intermediate levels with 2,
the level concerned with 3 and cascading levels with 4.
A_{21} denotes the transition probability for transitions from a level 2
to 1 et cetera; R_3 is the radiative recombination coefficient to a
level 3 .
Σi, j, k and m, denote sums over diverse types of levels.
In setting up the fourth term, it is supposed that absorption phenomena
for the levels designated with 2 may be neglected.

We shall now try to reduce equation (1) by an examination, to find
out which of the terms may be neglected.

The first term $n_e n_a <\sigma v_e>_{sim}$. In section V it will be pointed out
that only for a non-confined discharge with a magnetic induction
$B_w = 6.3 \times 10^{-3}$T, the contribution of simultaneous ionization and
excitation is estimated as approximately 10% for the 4p $^4D_{7/2}$ level.
For a confined plasma with n_e values at least 10 times higher than is
found for $B_w = 6.3 \times 10^{-3}$T and with lower T_e values [12] the contribution
will be < 1‰. We shall neglect this contribution. Moreover, for the
4d levels this process can be neglected altogether.

The second term $n_e n_a^* <\sigma v_e>_{sim}^*$. Cross-section data for simultaneous
ionization and excitation from metastable levels of argon I to excited
argon II levels are not known. Based on the probably small amount of

metastables and the probably small cross-section values due to the large energy gap of 23.5 eV for excitation to 4p levels, we suppose that this process can be neglected.

The third term $n_e n_{ion} <\sigma v>_{e\ dir}^i$ and the fourth term $n_e^2 n_{ion} \Sigma i \{<\sigma v>_{e\ II}^i \cdot (\Sigma <\sigma v>_{e\ I}^i/A_{2i\ 1})\}$. These terms of equation (1) both appear to contribute to the population of the levels denoted with 3, for example the 4p group, as will be shown in a following article [12]. For $n_e > 6 \times 10^{18} m^{-3}$ stepwise excitation through intermediate levels and for $n_e < 6 \times 10^{18} m^{-3}$ direct excitation from the ion ground levels is the dominant process for the 4p group.

The fifth term $n_e \Sigma j\ n_{2j}^* <\sigma v>_{e\ met}^j$. In [12] it also appears that no reasons could be found to suppose that metastable ions contribute to the population densities of levels designated with 3. At one point the assumption of a contribution through metastable levels is in disagreement with the results. We therefore think that the fifth term of equation (1) may be omitted.

The sixth term $\Sigma k\ n_{4k}\ A_{4k\ 3}$. The contribution of cascade radiation to the population density of the 4p levels will also be discussed in [12]. It appears that for the $^4D_{7/2}$ level the contribution is about 6%. It is assumed that for the 4d levels concerned this contribution is smaller. This assumption is based on the fact that the intensities of other lines than originating from the 4p, 4d and 5s groups are very weak. The influence of the cascade radiation on the form of the radiation profiles will be small. This can be seen as follows (see Fig.2). The lifetimes of the 4p and 4d levels are $\leq 10^{-8}$s, so that the diffusion length of hot excited ions ($T_i = 50 \times 10^3$ °K) is about 5×10^{-2}mm. This length is 5% of the width at half-maximum value of the radial profiles, i.e. less than the inaccuracy of this width. This small diffusion length means that the radiation profiles are very nearly the same as curves, presenting the amount of created excited particles. We conclude that the profile of re-radiated cascade radiation has the same form as the profile of the upper level of the cascade radiation. This profile differs from that of the lower level as has been given by the measurements reported in this article, section IV. The 3588 Å line e.g. gives cascade radiation to the 4p $^4D_{7/2}$ level. We remark that neglect of the contribution of the cascade radiation as regards the

the relative method used, only gives errors in the final results for T_e profiles, which are of the same order as the percentage of the cascade radiation, i.e. 4 to 8%.

The seventh term $n_e n_{ion}^{++} R_3$. For the conditions for which the measurements were performed, the argon III spectrum was very weak. The strongest line, with $\lambda = 3286$ Å, had an intensity of only a few pro milles of that of the 4348 Å line. The quantity of argon^{++} ions and accordingly the recombination contribution for every separate level will be toally negligible, say < 1‰.

Now, returning to deexcitation phenomena, we state that the term $n_e \Sigma m A_{3\ 2m}$, representing the spontaneous emission, fully dominates the second term $n_3 n_e <\sigma v_e>_{deexc}$, representing collisional deexcitation, in agreement with C.E.. It can be calculated from our measurements that the density n_e for 4p levels is about 2‰ to 4‰ of that for L.T.E. for the same value of T_e ($\sim 30 \times 10^3$ °K) for large B_w values. The estimated ratio between radiative emission and collisional deexcitation is then 250 to 500 and we conclude that the latter process may be neglected.

The third term $n_3 n_e <\sigma v_e>_{exc}$. The depopulation due to excitation to higher levels will be much smaller than the population due to cascade radiation. This assertion is based on comparison with collisional deexcitation, which mainly is of the same order of magnitude as excitation to higher levels. Furthermore, when excitation from 4p → 4d should occur, a clear difference between the 4d-3588 Å and 4p-4348 Å profiles should be found due to the cumulative n_e dependency for the line profiles of the 4d levels. This point will be discussed further in section V. Based on these facts, we shall neglect the term, dealing with excitation to higher levels.

The fourth term $n_3 n_e <\sigma v_e>_{ion}$. The ionization to argon^{++} ions can be neglected for the same reasons as has been done for recombination from argon^{++}.

We can now reduce equation (1) drastically, with $n_{ion} = n_e$ to

$$n_e^2 <\sigma v_e>_{dir} + n_e^3 \Sigma i\ \{\Sigma <\sigma v_e>_{II}^i (\Sigma <\sigma v_e>_I^i / \Sigma A_{2i\ 1})\} + \Sigma k\ n_{4k} A_{4k\ 3} = n_3 \Sigma m\ A_{3\ 2m}.$$

$$(2)$$

We already argued that the term $\Sigma k \, n_{4k} A_{4k \, 3}$ does not influence the T_e profiles more than 4 to 8%. It will be omitted in the relative comparison.

2. *Corona formulae for stepwise excitation*

The computation, to be developed will be applied here for the higher n_e-values, found in our experiments. Therefore we shall first describe a model based on stepwise excitation in the argon II spectrum and later on we shall improve the results for the case that the contribution of direct excitation is not negligible.

We look for a mathematical description of the stepwise excitation phenomena, which will lead to the form

$$n_3 \, \Sigma m \, A_{3 \, 2m} = K_{3s} \cdot f_1(n_e) \cdot f_2(T_e), \tag{3}$$

where K_{3s} is independent of T_e, n_e and consequently of the radius r, and is characteristic for the level 3, concerned; f_1 and f_2 are functions depending only on n_e and T_e respectively. We shall be able to draw conclusions on n_e and T_e as functions of r by comparing the radiant flux $P_{3,o}$ for $r = 0$ with $P_{3,r}$ for $r \neq 0$.

Considerations of McWHIRTER [9] and WILNER [10] for a C.E.plasma enable us to derive an expression conformable to equation (3). The calculations can only be considered as a general model with possibly great numerical errors in the values of the cross-sections used. We think that the special application of the calculations in this article avoids these errors (see equations (9) and (10)).

Only the most important starting points of the derivation of McWhirter and Wilner will be reviewed here. Their derivation is based on the integrated form of the excitation function of ALLEN [13], given by SEATON [14].

$$<\sigma v_e>_{mn} = 5.44 \times 10^{-29} \, f_{mn}/(T_e^{\frac{1}{2}} E_{nm}) \, \exp(-E_{nm}/kT_e), \tag{4}$$

where $<\sigma v_e>_{mn}$ is the excitation function in $m^3 s^{-1}$, f_{mn} is the absorption oscillator strength and E_{nm} is the excitation energy difference between the levels m and n in Joule; k is Boltzmann's

constant. The Gaunt factor, which appears in the original formulae was given here the value 0.2 [13]. There is a difference of a factor 2 between the expression used by McWhirter and the one used by Wilner We chose the form given by Wilner.

The collisional excitation by electrons is related to radiative absorption by the quantity f_{mn} and related to the spontaneous emission according to the relation

$$g_m f_{mn} = g_n f_{nm} \,,$$ (5)

where f_{nm} is the oscillator strength for emission and g is the statistical weight of a level. The introduction of one of the parameters f_{mn} or f_{nm} into expression (4) means that the description of collisional excitation phenomena is limited to those transitions which also have a spontaneous radiative decay in the reverse direction. Direct excitation starting from the ion ground levels therefore cannot be included in the derivation without some extension as a consequence of the absence of radiative transitions between most of the levels denoted with 3 (e.g. all 4p levels) and the ion ground levels [15]. We can apply the derivation of McWhirter and Wilner for the description of the stepwise excitation phenomena, as all transitions involved are optically permitted (see Fig.2).

The derivation is based on the twice repeated application of the balance equation

$$n_n \, \Sigma i \, A_{n \, mi} = n_e \, \Sigma i \, n_{mi} \, <\sigma v_e>_{mi \, n} \,,$$ (6)

where n mi denotes a process from n → mi and mi n from mi → n. Application of the equations (4), (5), (6) and the relation between A_{nm} and f_{nm} leads to the expression

$$n_3 \, \Sigma m \, A_{3 \, 2m} = 1.035 \times 10^{-147} \cdot \frac{n_e^3 g_3}{T_e \, \Sigma g_1} \cdot \Sigma m \, (\frac{A_{3 \, 2m}}{E_{2m \, 1}^3 \, E_{3 \, 2m}^3}) \cdot \exp(-E_{31}/kT_e),$$ (7)

where Σg_1 is the sum of the two statistical weights of the ion ground levels; E is in Joules. Note that Σi in expression (2) has been replaced by Σm, due to equation (5). The expression is conformable to

relation (3).

With the help of the expression, giving the spontaneous radiant flux P_{3p} of a level 3p

$$P_{3p} = h\nu_{3p\ 2m}\ A_{3p\ 2m}\ n_{3p}, \tag{8}$$

where $h\nu_{3p\ 2m}$ is the energy of the quantum for a transition from $3p \rightarrow 2m$, we can state that

$$P_{3p,r}/P_{3p,o} = (n_{e,r}/n_{e,o})^3 \cdot (T_{e,o}/T_{e,r}) \cdot \exp\{-E_{3p\ 1}/k\ (1/T_{e,r} - 1/T_{e,o})\}. \tag{9}$$

We can also compare the radiation of the levels 3p and 3q with different excitation energies with each other. This comparison gives, in combination with (9)

$$\frac{(P_{3p,r}/P_{3p,o})}{(P_{3q,r}/P_{3q,o})} = \exp\left\{-\frac{(E_{3p\ 1} - E_{3q\ 1})}{k} \cdot \left(\frac{1}{T_{e,r}} - \frac{1}{T_{e,o}}\right)\right\}. \tag{10}$$

When the P values are measured, relation (10) provides us with the term $(1/T_{e,r} - 1/T_{e,o})$. When the value of $T_{e,o}$ is known we are able to present a $T_{e,r}$ profile as a function of r. Relation (9) then enables us to calculate the $n_{e,r}/n_{e,o}$ profile.

3. Extended Corona formulae

We shall also mention the changes in expression (10) when direct excitation furnishes an additional contribution to the population of the levels denoted with index 3. ALLEN [13] gives an expression for the cross-section σ_f for forbidden transitions for electron energies $E_e > E_{exc}$, the excitation energy. The expression is

$$\sigma_f = 2.18 \times 10^{-20} \cdot \pi a_0^2 \cdot \Omega/(\Sigma g_1\ E_e) \quad m^2, \tag{11}$$

where $\pi a_0^2 = 8.80 \times 10^{-21} m^2$ is the cross-section of the hydrogen atom, Ω is the collision strength in m^{-1} [13] and E_e is the electron energy in J. When integrated over a Maxwellian distribution function one finds for the direct excitation

$$<\sigma v_e>_{dir} = 3.2 \times 10^{-25} \cdot \Omega/\Sigma g_1 \cdot (kT_e)^{-\frac{1}{2}} \cdot \exp(-E_{exc}/kT_e) \quad m^3 s^{-1}, \tag{12}$$

where E_{exc} is the excitation energy in J.

When introducing constant factors K_{3s} and K_{3d} for stepwise and direct excitation respectively, we can replace equation (7) by

$$n_3 \Sigma m \, A_{3\ 2m} = K_{3s} \cdot (n_e^3/T_e) \cdot \exp(-E_{31}/kT_e) + K_{3d} \cdot (n_e^2/T_e^{\frac{1}{2}}) \cdot \exp(-E_{31}/kT_e). \tag{13}$$

For the levels 3p and 3q is found an extended formulation of equation (10) , given by

$$\frac{(P_{3p,r}/P_{3p,o})}{(P_{3q,r}/P_{3q,o})} = \exp\left\{ -\frac{(E_{3p\ 1} - E_{3q\ 1})}{k} \left(\frac{1}{T_{e,r}} - \frac{1}{T_{e,o}}\right) \right\} \cdot$$

$$\cdot \left\{ 1 + \left(\frac{K_{3p,d}}{K_{3p,s}} - \frac{K_{3q,d}}{K_{3q,s}}\right) \cdot \left(\frac{T_{e,r}^{\frac{1}{2}}}{n_{e,r}} - \frac{T_{e,o}^{\frac{1}{2}}}{n_{e,o}}\right) \right\}. \tag{14}$$

This equation is valid when the factors $(K_{3d}/K_{3s}) \cdot (T_e^{\frac{1}{2}}/n_e) \ll 1$. It appears that for n_e values $> 1 \times 10^{19} m^{-3}$ this condition is fulfilled [12]. We remark that the sum of the last part of the equation, apart from the original values of the terms, strongly depends on the value of $(K_{3p,d}/K_{3p,s} - K_{3q,d}/K_{3q,s})$. It means that only when the partition between direct and stepwise excitation for the two levels concerned is more or less equal the contribution of the second factor within braces may be omitted. If not, then the terms of the factor $(T_{e,r}^{\frac{1}{2}}/n_{e,r} - T_{e,o}^{\frac{1}{2}}/n_{e,o})$ will still partly compensate each other. It is clear that from this equation it cannot be decided whether the exponential term dominates enough to find a proper T_e profile. Further discussion on this subject will be referred to section V.

4. *Balance equation for argon I levels*

The lines measured of the argon I spectrum are the 6965 Å line of the $2p_2$ level and the 4259 Å line of the $3p_1$ level. The former originates from the 4p group, with excitation energies of 13.0 to 13.3
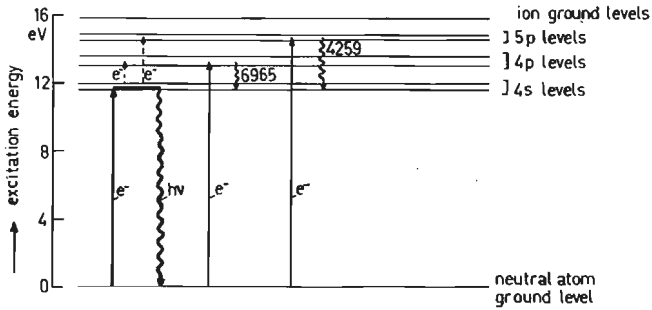
Fig.3 Simplified diagram of the argon I excited levels or groups. See for further explanation Fig.2.

eV and the latter from the 5p group with energies of 14.4 to 14.7 eV (See Fig.3). Radiation from other groups is very weak.

To be able to discuss the argon I profiles we shall first survey the possible excitation phenomena in the argon I spectrum. The levels may be populated by one or more of the processes:

1) direct excitation from the neutral ground level;
2) stepwise excitation through the 4s resonance or metastable levels;
3) recombination of ions by a radiative process.

The levels may be depopulated by one or more of the processes:

1) spontaneous emission;
2) ionization by collisions with electrons to argon ions.

Other conceivable processes are neglected for the same reasons as given for the argon II spectrum.

The contributions of recombination and ionization are unknown, but are expected to be small. It appears that depopulation of the levels occurs by spontaneous emission, while direct or stepwise excitation must be responsible for the excitation. In [12] it appeared that in any case the dominant process will be direct excitation from the atomic ground level. The additional contribution of stepwise excitation may give some tens of percents of the population.

The balance equation for the levels concerned can be written as

$$n_e n_a \langle \sigma v_e \rangle_{dir} + n_e^2 n_a \Sigma i \langle \sigma v_e \rangle_{II}^i \langle \sigma v_e \rangle_I^i / A_{2i \ 1} = n_3 \Sigma m A_{3 \ 2m}. \qquad (15)$$

The interpretation of argon I profiles is still complicated by the influence of the variation of T_e itself as function of r and by a diffusion of 5p excited particles before radiating, due to a $\tau = 3 \times 10^{-7}$s for the $3p_1$ level. The diffusion distance for the $3p_1$ level is estimated to be $\lambda_d = 0.15$ mm for the neutral particle temperature $T_n = 500\ ^0$K and $\lambda_d = 0.5$ mm for $T_n = 5 \times 10^3\ ^0$K.

III METHOD OF MEASUREMENT; ABEL TRANSFORMATION

The radiation profiles were registered with the help of an equipment, capable of measuring the line-intensities over a vertical distance x of 32.5 mm, perpendicular to the axis of the plasma column. An RCA IP28 or an EMI 9698 QB photomultiplier was used. The argon II measurements on which the radial T_e- and n_e-profiles are based, were performed with the RCA type, which is insensitive to the magnetic field of the coils. To be able to measure both argon I and II lines the EMI type was used. This type appeared to be more sensitive to the magnetic field, even when μ metal plates were applied to screen off the cell. As a consequence, the measurements of the argon I and II lines have not been performed in one sequence. It appears, by comparison with the help of one line (4348 Å) measured with both cells, that there is a good agreement between the two sequences for the end-anode measurements and that the agreement is moderate for the ring-shaped anode measurements (see Fig.1).

The radiance profiles $L_e(x)$ have been subjected to an Abel transformation if they could be measured down to about 10% of the maximum intensity or less. The first derivative $L_e'(x)$ for these curves at the end of the measured part of the curve is 1% to 6% of the maximum value $L_e'(x)_{max}$. At the end of the extrapolated part of the curve $L_e'(x)/L_e'(x)_{max}$ was always $\leq$ 1% while it appeared that omitting a part of the curve with $L_e'(x)/L_e'(x)_{max} <$ 2% gave less than 1% error in the transformed curve. It is therefore supposed that the errors due to extrapolating the measured curve can be neglected.

The Abel transformation was performed with N = 65, 85 or 105 equidistant points on one half of the curve. Every fifth point has been weighed by a formula given in [16]. These points with a number of N/5 were used as bases of a third order "spline" function (a set of

third degree polynomials). The first derivative of the spline function
was determined in the N/5 points and a linear interpolation between
the points gave a continuous curve for $L_e'(x)$ [17]. The transformation
itself was performed with the aid of the well-known Abel integral.

IV   RESULTS

In the following we shall present successively the results of four
series of measurements with special purposes, one run with four
different values of the magnetic induction B_w for the end-anode with
50 A discharge current and one similar run for the ring-shaped anode
with 60A discharge current. Important parameters as discharge current
I_D, magnetic induction B_w, back ground pressure p_b and for the runs
with various magnetic fields also the discharge voltage V_D, the
electron temperature $T_{e,0}$ and density $n_{e,0}$, the ion temperature T_i,
the neutral particle temperature T_n and gasflow Q are indicated in the
captions of the figures as far as these data are available.

In Fig.4 the reduced profiles $L_e(x)/L_e(0)$ of the argon II 4348 Å
line, and of the argon I 4259 Å and 6965 Å lines are given. B_w is
6.3×10^{-3}T and the discharge was only slightly confined. It can
easily be seen that the symmetry of the curves is poor and that the
three tops have been shifted with respect to each other. The zero
point of the scale in the direction x is arbitrary. We assume that
$T_{e,r}$ and $n_{e,r}$ are not symmetrical and that the tops of both profiles
are situated at different positions. The curves have not been subjected
to an Abel transformation. Also for this low B_w-value there is a great
difference in the widths of the argon I and II line profiles. These
measurements have been carried out in connection with the problem of
the simultaneous ionization and excitation.

Fig.5a gives the results of three argon II lines after Abel trans-
formation with λ = 4348 Å, 3588 Å and 3351 Å. The points indicated in
this figure and in following similar figures are the N/5 points given
by a computer program, performing the Abel transformation. The maximum
current values of the RCA IP28 photomultiplier were 9.6×10^{-7}A,
2.0×10^{-8}A and 4.0×10^{-10}A respectively for the lines concerned. As
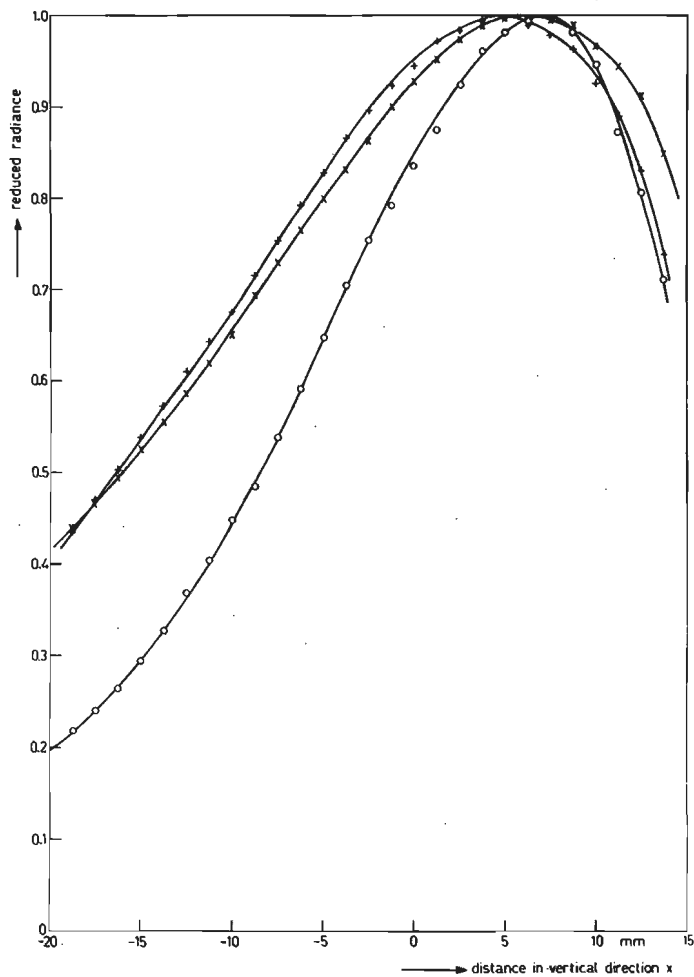a consequence of the signal to noise ratios the errors in the 3588 Å

Fig. 4 The reduced radiance profiles $L_e(x)/L_e(0)$ for some lines as functions of the distance in the vertical direction x. ○ denotes the 4348 Å-argon II line; + the 4259 Å-argon I line and × the 6965 Å-argon I line. Conditions: end-anode; discharge current $I_D = 50$ A; magnetic induction $B_w = 6.25 \times 10^{-3}$ T, background pressure $p_b = 1.25 \times 10^{-3}$ mm of Hg.
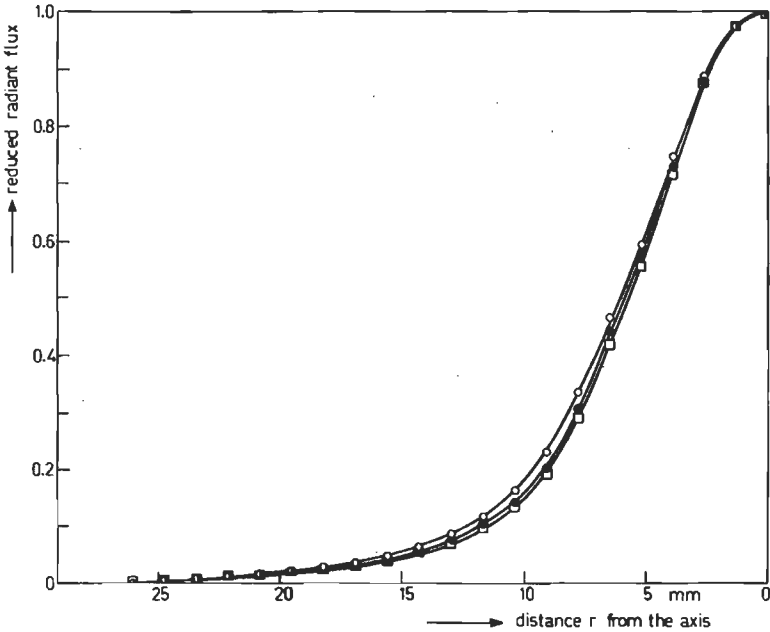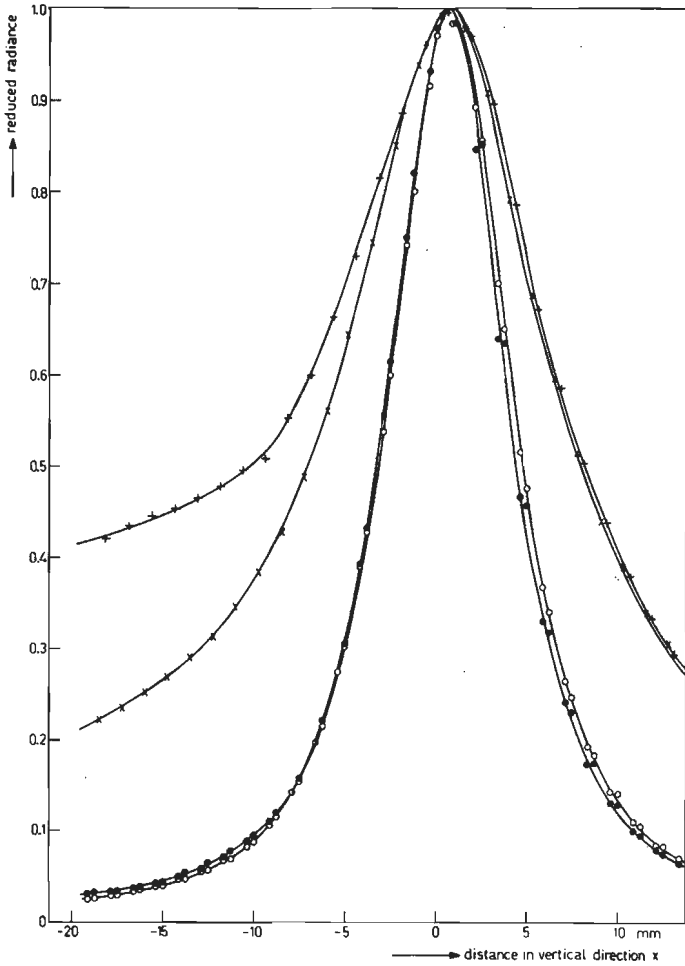
*Fig.5a The reduced **radiant flux** P(r)/P(0) of three argon II lines as functions of the distance r from the axis. ○ denotes the 4348 Å-line ● the 3588 Å-line and □ the 3351 Å-line, all of the argon II spectrum. Conditions: ring-shaped anode; discharge current I_D = 60 A; magnetic induction B_w = 7.5 x 10^{-2}T, background pressure p_b = 1.25 x 10^{-3} mm of Hg.*

profile are a little larger and in the 3351 Å profile markedly larger than in the 4348 Å profile. This could easily be seen from the measured profiles. The radial T_e profile, calculated according to expression (10), has been found from the ratio of the intensities of the 3588 Å and 4348 Å lines and that of the 3351 Å and 4348 Å lines as given in the figure. The results are presented in Fig.5b. It appears that there is a reasonable agreement between the two sets of points. One can roughly estimate that the random error from the measurements in the expression exp {-(E/k)(1/$T_{e,r}$-1/$T_{e,o}$)} is 0.020 to 0.030, which agrees fairly well with the deviations of the points from the drawn lines in Fig.5b.
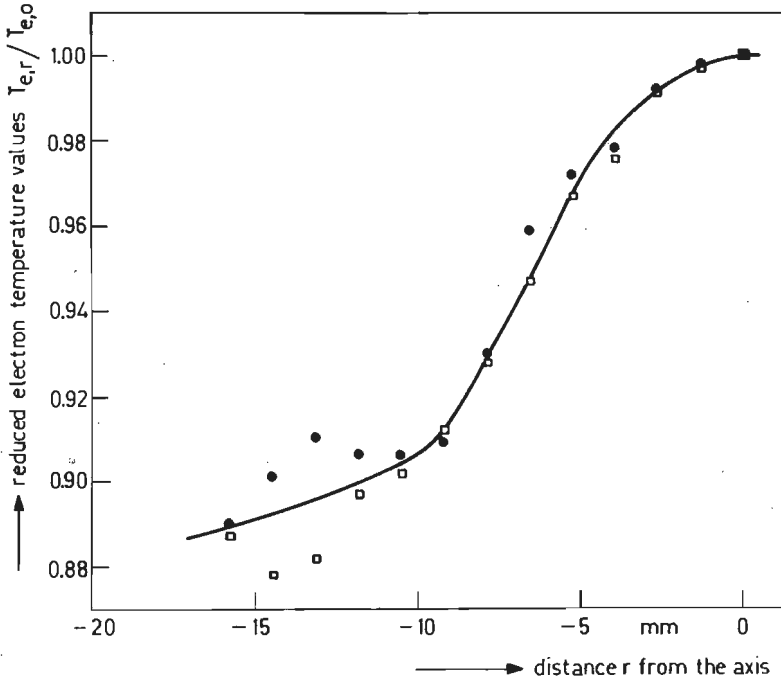
Fig.5b The reduced electron temperature profile $T_{e,r}/T_{e,o}$ *as function
of the distance r from the axis for the conditions given in Fig.5a.*
● *calculated from the ratio of the 3588 Å- and the 4348 Å-lines;*
□ *calculated from the ratio of the 3351 Å and the 4348 Å-lines.* $T_{e,o} =$
$= 32 \times 10^3 \, °K.$

In Fig.6 the direct results of argon I and II profiles are presented
for a situation in which asymmetrical radiation profiles were found. The
asymmetry of the arc could be seen visually, as well as the asymmetrical
heating of the end-anode. It can be seen from the figure that there is
an inverse position for the 3588 Å and 4348 Å lines in comparison with
each other at one side. The radial T_e profile must be strongly
asymmetrical. It appears also that at one side there is a great
difference between the curves of the 4259 Å and 6965 Å.

Fig.7 gives a comparison between the 4348 Å line, a "common" line
of the 4p group, and the 4880 Å line, a laser line of that group. The

Fig.6 The reduced radiance $L_e(x)/L_e(0)$ of some argon II and argon I
lines as functions of the distance in vertical direction x.
o denotes the 4348 Å and ● the 3588 Å argon II lines; + denotes the
4259 Å and x the 6965 Å argon I lines. Conditions: end-anode, asymmetri-
cal profiles; discharge current I_D = 40 A; magnetic induction B_w =
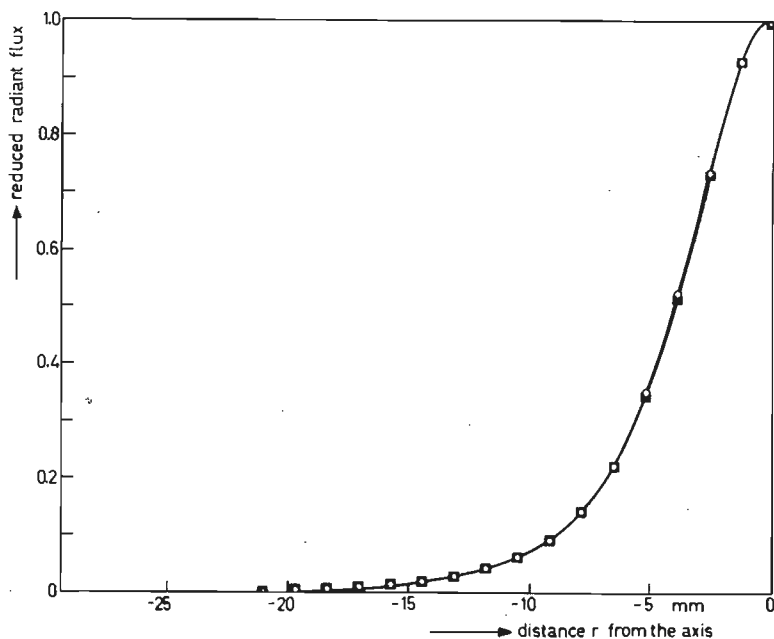= 12.5 x 10^{-2}T; background pressure p_b = 1.5 x 10^{-3} mm of Hg.

Fig.7 The reduced radiant flux P(r)/P(0) of two argon II lines as functions of the distance r from the axis. ○ denotes the 4348 Å and ■ the 4880 Å line. Conditions: discharge current I_D = 50 A; magnetic induction B_w = 12.5 × 10^{-2} T.

results have been given after application of an Abel transformation. We conclude that there is hardly any difference between the radiant fluxes P(r)/P(0) of the two lines.

From a run of four B_w-values with the end-anode, a total set of curves for one B_w-value is presented in Fig.8a. Fig.8b gives the argon II lines after Abel transformation. The calculated $T_{e,r}$ and $n_{e,r}$ profiles of all four B_w-values are shown in the Figs. 9 and 10 respectively. One can conclude from Fig.8a that the 4259 Å profile is broader than that of 6965 Å. This is valid for the whole run. The differences between the 3588 Å and 4348 Å profiles become smaller for larger B_w values, which can also be seen from Fig.9. The T_e-profile for B_w = 12.5 × 10^{-2} T is estimated based on the fact that the differ-
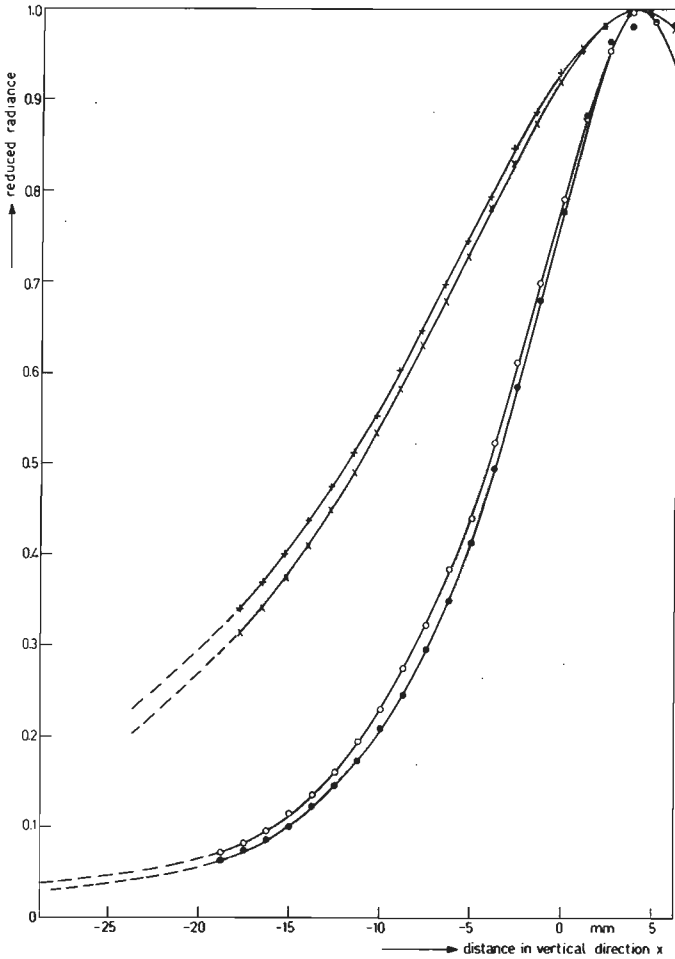
Fig.8a The reduced radiance $L_e(x)/L_e(o)$ of some argon II and argon I
lines; ○ denotes the 4348 Å and ● the 3588 Å argon II lines; + denotes
the 4259 Å and × the 6965 Å argon I lines. Conditions: end-anode;
discharge current I_D = 50 A; magnetic induction B_w = 1.88 × 10^{-2}T;
background pressure p_b = 1.20–1.25 × 10^{-3}mm of Hg; electron temperature
$T_{e,o}$ = 32.5 × 10^3 °K; ion temperature T_i = 600 °K; neutral particle
temperature T_n = 800 °K, electron density $n_{e,o}$ = 0.91 × $10^{19}m^{-3}$;
gas flow Q = 1.90 × 10^{-3} mm of Hg $m^{+3}s^{-1}$.
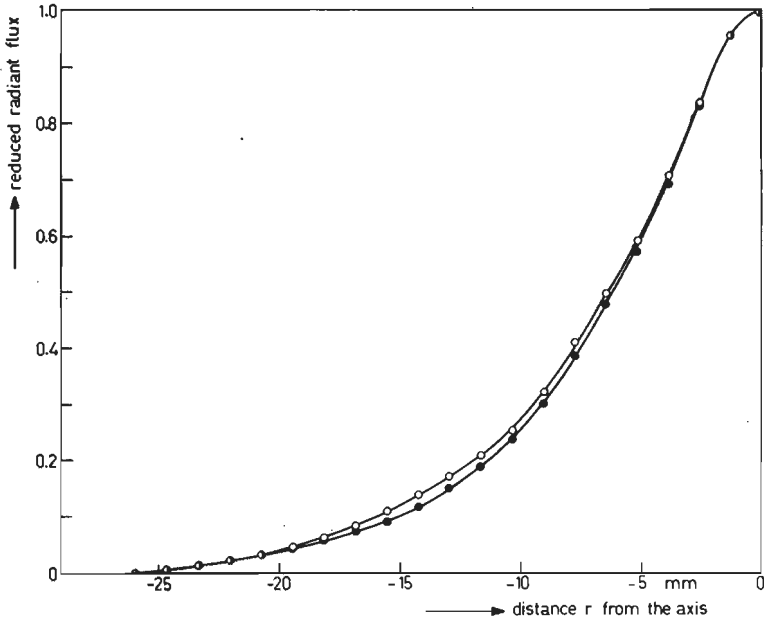
Fig.8b The reduced radiant flux P(r)/P(0) of two argon II lines.
○ denotes the 4348 Å and ● the 3588 Å line. Conditions: see Fig.8a.

ences between both profiles are smaller than 1% of the top value.

The n_e profiles of Fig.10 have been calculated with the smoothed $T_{e,r}$ curves. The results presented in Fig.8 of [12] have the consequency that reduced n_e-profiles, based on a n_e^3 dependency for the argon II profiles (equation (9)) are more or less in error. They were improved with the help of a reduced profile, based on a n_e^2 dependency for the profiles. The proper reduced n_e-profile is found by linear interpolation with the help of the results of [12]. It is believed that this interpolation is sufficient as a consequence of the limited differences between the two profiles and the limited accuracy of the profiles themselves. The maximum n_e-values $n_{e,o}$ have also been calculated by linear interpolation between the two values, obtained from the two extreme approximations.

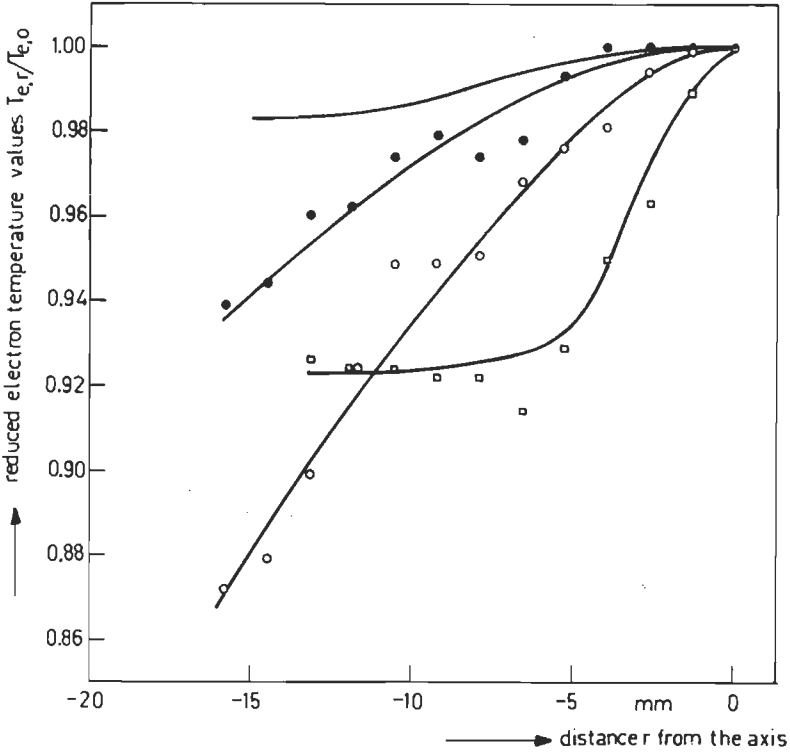The Figs. 11a, 11b, 12 and 13 give the information on a similar

Fig.9 *The reduced electron temperature profiles $T_{e,r}/T_{e,o}$ as functions of the distance r from the axis for four values of the magnetic induction B_w.* ○ : *1.88 x 10^{-2}T;* ● *3.75 x 10^{-2}T;* □ *7.5 x 10^{-2}T;* ■ *12.5 x 10^{-2}T. Conditions: end-anode; discharge current I_D = 50 A; background pressure p_b = 1.25 x 10^{-3} mm of Hg. The electron temperatures $T_{e,o}$ are 32.5 x 10^3 ^{o}K, 30.0 x 10^3 ^{o}K, 34.0 x 10^3 ^{o}K and 40.5 x 10^3 ^{o}K respectively; the ion temperatures T_i are 600 ^{o}K, 2.2 x 10^3 ^{o}K, 5.4 x 10^3 ^{o}K and 14 x 10^3 ^{o}K respectively; the neutral particle temperatures T_n are 800 ^{o}K, 800 ^{o}K, 1 x 10^3 ^{o}K and 4 x 10^3 ^{o}K respectively; the gas flows Q are 1.90 x 10^{-3} to 2.10 x 10^{-3} mm of Hg $m^{+3}s^{-1}$.*

run for the ring-shaped anode. The differences between the profiles of the 4259 Å and 6965 Å lines are much smaller here and for some parts
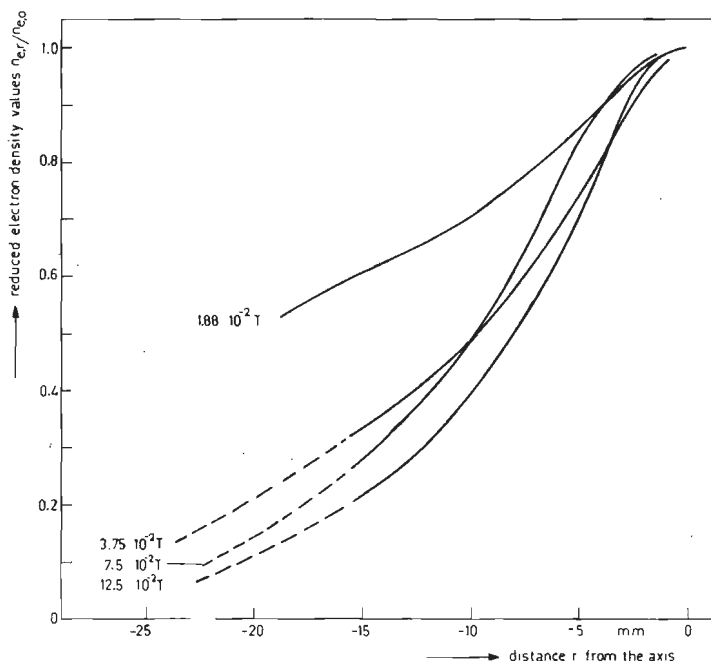
Fig.10 The reduced electron density profiles $n_{e,r}/n_{e,o}$ as functions of
the distance r from the axis for four values of the magnetic induction
B_w, indicated in the figure. Conditions: see Fig.9. The electron
densities $n_{e,o}$ are 0.91 x $10^{19}m^{-3}$, 1.92 x $10^{19}m^{-3}$, 1.70 x $10^{19}m^{-3}$ and
1.57 x $10^{19}m^{-3}$ respectively.

of the curve of reversed sign. The temperature curves are quite similar
for all B_w-values. The inaccuracy of the n_e-profiles due to errors in
the $T_{e,r}$ profiles, intensity errors and errors due to interpolation can
be estimated as about 5% of the top value.

V   DISCUSSION AND CONCLUSIONS

The results of Fig.4 are intended to solve the question of simultane-
ous ionization and excitation of argon II-4p levels. Though the profiles
of the three lines are not symmetrical, the 4348 Å line profile is the
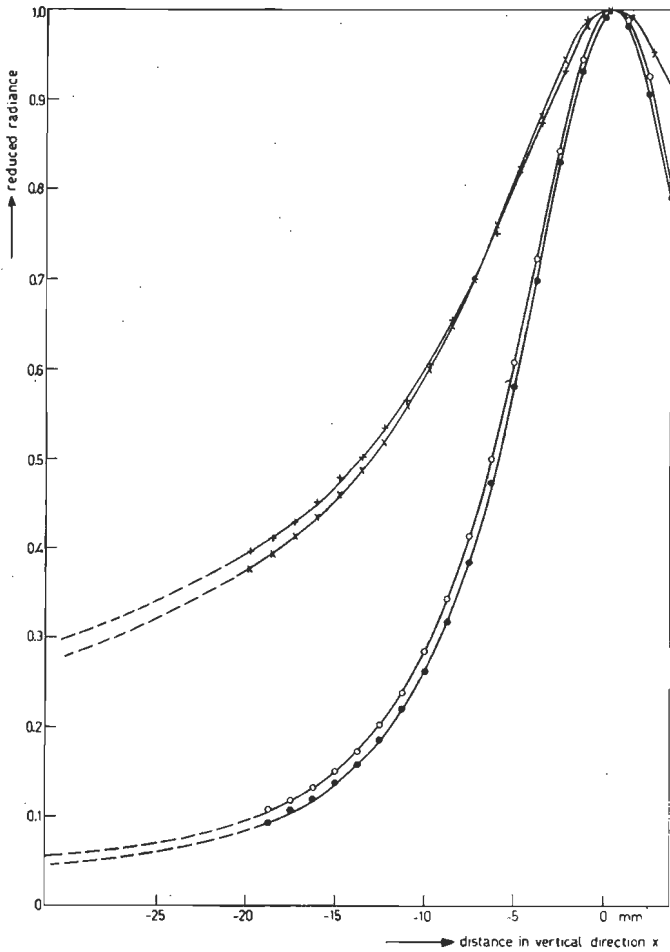steepest at both sides, indicating that a stronger dependency on n_e may

Fig.11a The reduced radiance $L_e(x)/L_e(0)$ of some argon II and argon I
lines. ○ denotes the 4348 Å and ● the 3588 Å argon II lines; + the
4259 Å and x the 6965 Å argon I lines. Conditions: ring-shaped anode;
discharge current $I_D = 60$ A; magnetic induction $B_w = 12.5 \times 10^{-2}$T;
background pressure $p_b = 1.2 \times 10^{-3}$mm of Hg; electron temperature $T_{e,o}$
$= 38 \times 10^3$ °K; ion temperature $T_i = 1.4 \times 10^3$ °K; electron density
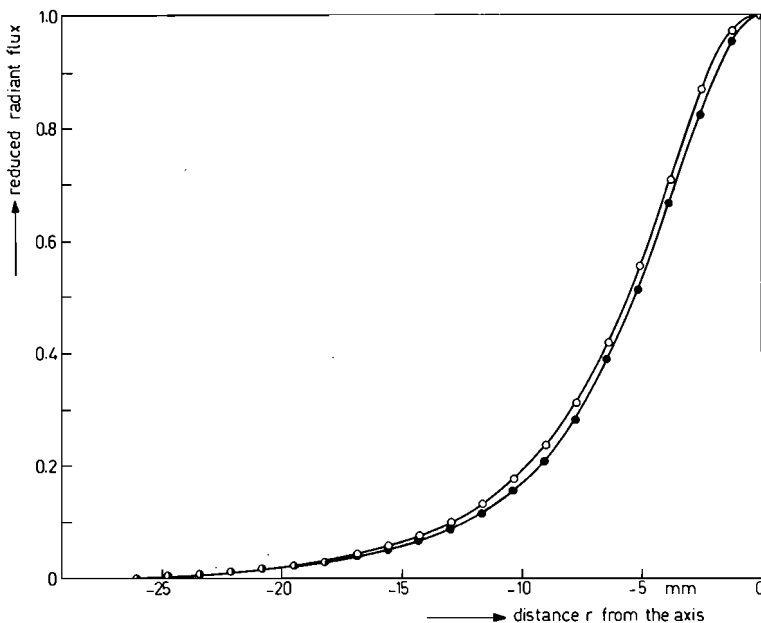$n_{e,o} = 1.89 \times 10^{19} m^{-3}$.

Fig.11b The reduced radiant flux P(r)/P(0) of two argon II lines; ○
denotes the 4348 Å and ● the 3588 Å lines. Conditions: see Fig.11a.

be supposed than for the argon I lines. The shift of the maxima of the
curves can only be caused by a combination of the already mentioned
shift of the top of the n_e and T_e profiles and a different dependency
on n_e of argon I and argon II profiles. The argon II maximum and the
n_e maximum coincide better than those of the other curves.

From the ratios of the maxima of the line-intensities we can also
show that simultaneous ionization and excitation cannot be a dominant
process even for $B_w = 6.3 \times 10^{-3}$T. The measured ratio of the 6965 Å
and 4348 Å signals is 23 and is estimated to be $\sim$ 15 after Abel trans-
formation. The ratio of the intensities of these lines, calculated on
the basis of direct excitation for the 6965 Å line and simultaneous
ionization and excitation for the 4348 Å line and with the help of
literature data on cross-sections for both processes [18-22], appears
to be 100 to 350 for $T_e = 80 \times 10^3$ °K . Therefore the contribution of
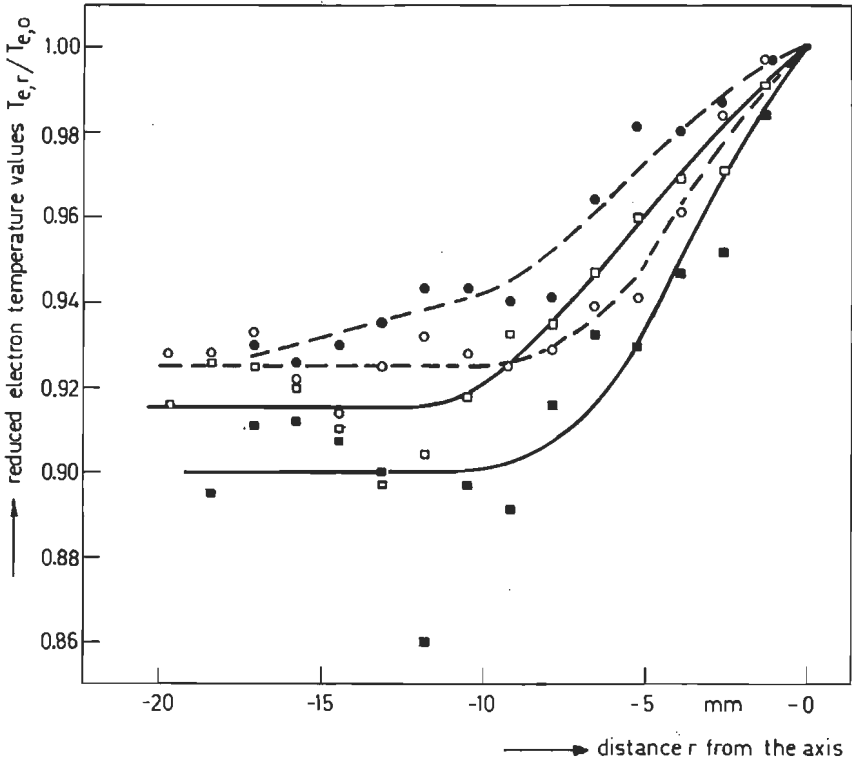
Fig.12 *The reduced electron temperature profiles* $T_{e,r}/T_{e,o}$ *as functions of the distance r from the axis for four values of the magnetic induction* B_w. O $1.88 \times 10^{-2}T$; ● $3.75 \times 10^{-2}T$; □ $7.5 \times 10^{-2}T$; ■ $12.5 \times 10^{-2}T$. *Conditions: ring-shaped anode; discharge current* $I_D = 60$ A; *background pressure* $p_b = 1.20 \times 10^{-3}$ mm *of Hg. The electron temperatures* $T_{e,o}$ *are* 30.0×10^3 $^{\circ}K$, 27.5×10^3 $^{\circ}K$, 32.0×10^3 $^{\circ}K$ *and* 38.0×10^3 $^{\circ}K$ *respectively; the ion temperatures* T_i *are* 1.4×10^3 $^{\circ}K$, 3.7×10^3 $^{\circ}K$, 11×10^3 $^{\circ}K$ *and* 13.3×10^3 $^{\circ}K$ *respectively; the atom temperatures* T_n *are* 1.3×10^3 $^{\circ}K$, 3.5×10^3 $^{\circ}K$ *and* 5×10^3 $^{\circ}K$ *respectively. For* $B_w = 12.5 \times 10^{-2}T$, T_n *has not been measured.*

the simultaneous process to the population of the $^4D_{7/2}$ level can only be 5 to 15%. About the same contribution can be found for the 4806 Å
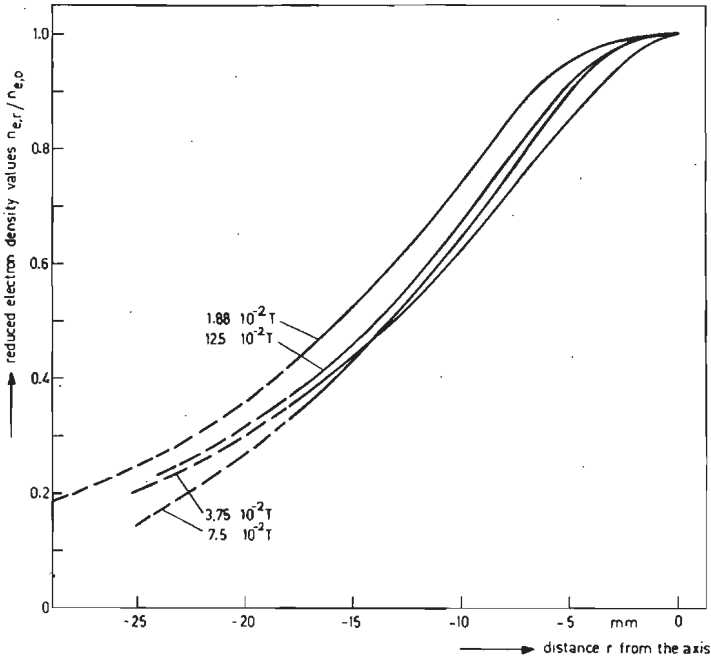
Fig.13 The reduced electron density profiles $n_{e,r}/n_{e,o}$ as functions of the distance r from the axis for four values of the magnetic induction B_w, indicated in the figure. Conditions: see Fig.12. The electron densities $n_{e,o}$ are 1.17 x $10^{19}m^{-3}$, 2.26 x $10^{19}m^{-3}$, 2.35 x $10^{19}m^{-3}$ and 1.89 x $10^{19}m^{-3}$ respectively.

line of the 4p $^4P_{5/2}$ level and the 4880 Å line of the 4p $^2D_{5/2}$ level. The conclusion that for a fully confined plasma the contribution of simultaneous ionization and excitation is smaller than 1‰ has been based on this estimation.

By applying equation (10) for the calculation of the T_e profiles it is assumed implicitly that the contribution of the terms $\neq$ 1 of the second factor within braces in equation (14) cancels each other, although this cannot be verified by measurements. We conclude, however, that the results, shown in Fig.5b and derived from the two ratios, indicated in the caption of the figure, are in good agreement with each

other and support the use of equation (10).

From Fig.6 it can be seen that the position of the 4348 Å and 3588 Å lines can be reversed. From the fact that reversal of the position of the two lines occurs we conclude that ratios of the 3588 Å and 4348 Å lines slightly smaller than 1 can not be explained by a small additional excitation from the 4p group to the 4d group. Therefore, excitation from 4p → 4d could be neglected in equation (2).

One of the most striking features in Fig.6 is the great difference between the 4259 and 6965 Å profiles at one side indicating that partition between direct and stepwise excitation for both groups is not equal. It is evident that the difference of the ratio of direct and stepwise excitation for the 4p and 5p group of argon I, combined with the effect due to the T_e-profile makes the interpretation of the differences between the profiles of the 6965 Å and 4259 Å lines difficult. We conclude from these measurements, combined with the results of [12] that there will be some stepwise excitation to the 4p group and to a smaller amount also to the 5p group.

The results, presented in Fig.7 are to demonstrate explicitly that there is no evident difference between the profiles of laser lines and other lines of the 4p group, indicating that the excitation mechanisms for the whole 4p group are the same.

Fig.9 shows clearly that the T_e-profiles for the end-anode become flatter for increasing B_w-values. From Fig.12, it appears that the T_e differences are quite similar for all B_w-values. It seems that the decrease of T_e stops for r > 10 mm. Although this effect was stated for the greater part of the measurements, it may be that inaccuracy of the measurements for these r-values was the cause thereof.

Inspection of the n_e-profiles, given in the Figs. 10 and 13 shows that the confining effect can be clearly seen by comparison of the 1.88×10^{-2}T measurement for the end-anode with the other measurements for this anode. The n_e-profiles for the ring-shaped anode are broader than those for the end-anode. It is possible that the rotation of the plasma column causes a decrease of confinement as can be established for the 12.5×10^{-2}T measurement for the ring-shaped anode. [23]

We finally conclude that by determination of the argon II and I profiles it is possible to give a contribution to the explanation of

the excitation mechanisms in the argon II and argon I spectra and to determine reduced $T_{e,r}$ and $n_{e,r}$ profiles with a reasonable accuracy.

ACKNOWLEDGEMENTS

REFERENCES

1 . L.M.Lidsky, G.D.Rothleder, D.J.Rose, S.Yoshikawa, C.Michelson and R.J.Mackin Jr., J.Appl.Phys. 33, 2490 (1962).

2 . S.L.Leonard, Proc. 9th Intern.Conf.Ionized Gases, Bucharest, p.170 (1969).

3 . C.B.Kretschmer, F.Boeschoten and L.J.Demeter, Phys. Fluids 11, 1050 (1968).

4 . E.D.Tidwell and J.I.Shipp, Proc. 8th Int.Conf.Ionized Gases, Vienna, p. 453 (1967).

5 . J.L.Delcroix, H.Minoo and A.R.Trindade, Proc. 9thInt.Conf.Ionized Gases, Bucharest, p. 169 (1969).

6 . M.Hudis, K.Chung and D.J.Rose, J.Appl.Phys. 39, 3297 (1968).

7 . B. van der Sijde, J.Quant.Spectr.Radiat.Transf., in press.

8 . G.Elwert, Z.Naturforsch. 7a, 432 (1952).

9 . R.W.P.McWhirter, Plasma Diagnostic Techniques, Ch. 5 (Ed.: R.H. Huddlestone and S.L.Leonard) Ac.Press, New York (1965).

10. B.Wilner, Acta Polyt.Scand., Physics and Nucleonics 41, 1 (1966).

11. H.Statz, F.A.Horrigan, S.H.Koozekanani, C.L.Tang and G.F.Koster, J.Appl.Phys. 36, 2278 (1965).
G.F.Koster, H.Statz, F.A.Horrigan and C.L.Tang, J.Appl.Phys. 39, 4045 (1968).

12. B. van der Sijde, to be published .

13. C.W.Allen, Astrophysical Quantities, Athlone Press, London (1964).

14. M.J.Seaton, Atomic and Molecular Processes, Ch. 11 (Ed.: D.R.Bates) Ac.Press, New York (1962).

15. J.C.Boyce, Phys. Rev. 48, 396 (1935).

16. K.Bocharten, J.Opt.Soc, 51, 943 (1961).

17. J.Leclair, to be published .

18. I.P.Zapesochnyi and P.V.Feltsan, Opt.Spectr.20, 291 (1966).

19. L.M.Volkova and A.M.Devyatov, Opt.Spectr. 7, 480 (1959).

20. W.R.Bennett Jr., G.N.Mercer, P.J.Kindlmann, B.Wexler and H.Hyman, Phys.Rev.Letters, 17, 987 (1966).

21. I.D.Latimer and R.M.St.John, Abstracts of 6th Intern.Conf.Phys. Electr.Atomic Collisions, Boston, p. 287 (1969).

22. J.M.Hammer and C.P.Wen, J.Chem.Phys. 46, 1225 (1967).

23. B. van der Sijde and P.A.W.Tielemans, Proc. 10thIntern.Conf.Ionized Gases, Oxford, p. 192 (1971).

EXCITATION MECHANISMS AND TEMPERATURES AND DENSITIES OF ELECTRONS IN A HOLLOW CATHODE ARGON ARC DISCHARGE

B. van der Sijde
Department of Technical Physics, University of Technology, Eindhoven, Netherlands.

Summary- For a hollow cathode low-pressure magnetically-confined argon arc discharge an investigation was made of spectral line-intensities of the argon II spectrum to ascertain the excitation mechanisms in this spectrum, especially for the 4p group (excitation energy 19.2 to 20.0 eV). It appears that for n_e-values of 1 x 10^{19} to 2 x $10^{19} m^{-3}$ stepwise excitation from the ion ground levels through short-lived intermediate levels (16.3 to 16.8 eV) contributes at least 70% to the 4p- argon II group population. Direct excitation from the ion ground levels is dominant for considerably smaller n_e-values. Cascade radiation plays a minor role in populating the 4p group. The stepwise excitation may lead to laser action in this type of discharge in the same way as occurs in the common argon ion laser. The proposed mechanism is not cited in the literature as a possible mechanism for laser action.

Furthermore, the electron temperature T_e was determined from absolute line-intensity measurements of the argon I and II spectra. For argon I the method is based on cross-section data for the 4p group, for argon II on Corona Equilibrium formulae. For a well-confined plasma $T_{e,o}$ on the axis was 30 x 10^3 to 40 x 10^3 °K at an axial distance of 0.6 m from the cathode.

The value of the electron density n_e was calculated from phase shift measurements with microwaves, accounting for the non-linear relation between n_e and the refractive index μ. The calculation was performed with the help of a method described in a previous paper. The influence of the slice breadth, interacting with the microwaves and of diffraction are discussed. It appeared that $n_{e,o}$ on the axis is 1 x 10^{19} to 2 x $10^{19} m^{-3}$ for a confined plasma.

I   INTRODUCTION

For the hollow cathode low-pressure magnetically-confined argon arc discharge described in [1], the excitation mechanisms in the argon II spectrum will be discussed. The phenomena are related to those of the argon ion laser, as about the same region of electron temperatures and densities are apparent. In the discussion on the excitation mechanisms a method is developed to determine the electron temperature T_e from absolute spectral-line measurements and from the value of the electron density n_e.

The n_e-values were calculated from phase-shift measurements, performed with a 70 GHz microwave interferometer. A method is discussed to determine the $n_{e,o}$-values on the axis of a plasma column with a refractive index μ, continuously changing as function of the radius r. Therefore, we applied a method as pointed out in [2], where reduced n_e-profiles were determined. A spatial mean value of n_e was determined from the phase-shifts, caused by the breadth of the plasma slice interacting with the microwaves perpendicular to the direction of wave propagation. To find a proper $n_{e,o}$-value, the mean value was improved by a method, described in section II. Diffraction effects did not appear apparent.

The T_e-values were determined from absolute line-intensity measurements, both of the argon I and II spectrum and with the help of the n_e-values, determined. For argon I cross-section data of direct excitation by electron collisions are available with moderate accuracy [3,4]. For argon II the Corona Equilibrium (C.E.) formulae described by McWHIRTER [5] and WILNER [6] were used after a numerical improvement. The results of both methods appeared to be in disagreement with each other for small n_e-values.

Changes in the relative population densities of the 4p levels of argon II as functions of the magnetic induction B_w, the minor significance of cascade radiation and calculations of relative cross-section values for the transitions 4s group → 4p group and 3d group → 4p group give arguments to suppose a change of the excitation mechanisms as function of B_w.

It appeared possible to develop a consistent system for the

excitation in the argon II spectrum, initiated by the differences
between the two methods of determining T_e and based on the different
dependency on n_e for the different forms of excitation. Stepwise
excitation through short-lived intermediate levels with lifetimes of
$\sim 5 \times 10^{-8}$ s and excitation energies of ~ 16.5 eV mainly determines the
densities of the 4p levels for n_e greater than $6 \times 10^{18} m^{-3}$. Direct
excitation from the ion ground levels is supposed to be dominant for
n_e-values smaller than this value.

Finally, the complete results of four series of measurements with
$0 < B_w \leq 15 \times 10^{-2} T$ are presented. The results involve the n_e- and
T_e-values, and the ion temperature T_i and neutral particle temperature
T_n, obtained from Doppler broadening measurements. The equipment for
these measurements and the method for the calculations have been
described in [1]. The values of the radiant flux P(0) on the axis of
the column for the 7384 Å argon I and the 4806 Å argon II lines, the
ionization degree α and the voltage characteristics complete the data,
obtained.

II   DETERMINATION OF THE ELECTRON DENSITY

1   Interferometer

A 70 GHz microwave interferometer with wavelength $\lambda = 4.3$ mm was
used to measure the phase shift $\Delta\phi$ caused by the plasma column. The
experimental device is presented in Fig.1. The antenna system was
situated inside the vacuum tube and the wave guides were sealed-off
with mica sheets. The interferometer was adjusted to zero without the
plasma to measure the phase ϕ_0 and also with the plasma to measure ϕ_p.
These two values were corrected, if necessary, for temperature
influences due to heating effects of the plasma on the waveguides
within the vacuum system.

This type of interferometers is suitable to determine $\Delta\phi$ with an
accuracy of 2° to 5°, but with an uncertainty of $k \times 2\pi$, where k is an
integer. The problem to find k was solved by careful determination of
$\Delta\phi$-values for $B_w \rightarrow 0$, corresponding with $\Delta\phi \rightarrow 0$ and by some check
measurements with a "zebra stripe" type of interferometer, which has
an oversized delay-line [7]. This type yields absolute $\Delta\phi$-values with
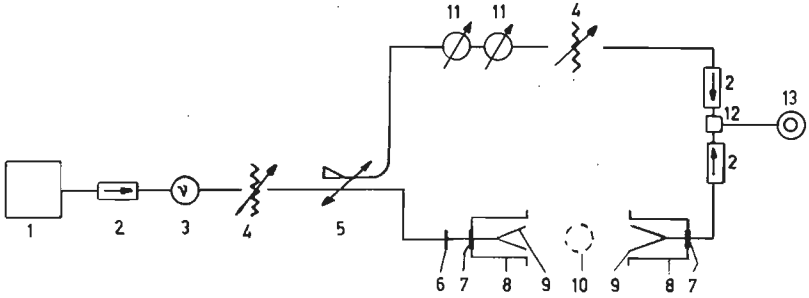limited accuracy.

Fig.1 Scheme of the microwave equipment. 1 is a microwave source; 2 is an isolator; 3 is a frequency meter; 4 is a calibrated attenuator; 5 is a directional coupler; 6 is an adaptor; 7 is a vacuum-window (mica); 8 are side-tubes; 9 is an antenna; 10 is the plasma column; 11 is a phase-shifter; 12 is a hybrid tee; 13 is a crystal detector.

2   *One dimensional slab approximation*

The interferometer was used in the ordinary-wave mode, so that the electrical field vector $\vec{E}$ was parallel to $\vec{B}_z$, the direction of the static magnetic field. The relation between the refractive index μ and the plasma frequency ω_p is then given by a simplified form of the Appleton equation [7]

$$\mu^2 = 1 - \frac{\omega_p^2/\omega_0^2}{1-j\nu/\omega_0} \ , \tag{1}$$

where ω_0 is the angular frequency of the microwaves and ν is the collision frequency of the electrons with ions for momentum transfer.

An expression for the collision frequency for electron-ion interaction is given in [8]. The expression can be written in S.I. units as

$$\nu_{ei} = \frac{n_e \ \ln(1.24 \times 10^7 \cdot T_e^{3/2}/n_e^{1/2})}{3.8 \times 10^5 \cdot T_e^{3/2}} \ . \tag{2}$$

For $n_e = 10^{19} m^{-3}$ and $T_e = 3 \times 10^4 \ °K$, ν_{ei} appears to be about 5×10^7 s^{-1}. Whereas $\omega_0 = 2\pi \times 7 \times 10^{10} s^{-1}$, the term $j\nu/\omega_0$ can be neglected.

Equation (1) can be reduced to

$$\mu^2 = 1 - \omega_p^2/\omega_0^2 = 1 - n_e/n_{ec} \;,\tag{3}$$

where n_{ec} is the critical electron density for the frequency applied.

The basic equations for the relationship between the phase shift $\Delta\phi$ caused by a plasma slab, which is non-homogeneous in the direction of wave propagation x and homogeneous in planes perpendicular to that direction at one hand and $n_e(x)$ at the other hand, are given by relation (3) and

$$\Delta\phi = \phi_0 - \phi_p = k_0 \, D'(1-\bar{\mu}),\tag{4}$$

where k_0 is the wave vector in vacuo; D' is the thickness of the slab defined by relation (5) and $\bar{\mu}$ is the average refractive index, given by relation (6) (see Fig.2). It is supposed that the plane wave approximation is satisfactory. The boundary of the slab has been more or less arbitrarily chosen by the statement that the thickness D' is determined by

$$n_e(x) = 0.05 \, n_{e,o} \quad ,\tag{5}$$

where $n_{e,o}$ is the maximum n_e-value. $\bar{\mu}$ is determined by

$$\bar{\mu} = (1/D') \int_{-\frac{1}{2}D'}^{\frac{1}{2}D'} \mu(x)dx.\tag{6}$$

With the relations (3) and (4) we can state

$$\Delta\phi = k_0 D'\{1 - \frac{1}{D'} \int_{-\frac{1}{2}D'}^{\frac{1}{2}D'} \sqrt{1 - \frac{n_e(x)}{n_{ec}}} \, dx\} \cdot\tag{7}$$

When the reduced values $n_e(x)/n_{e,o}$ are known the value of $n_{e,o}/n_{ec}$ and thus of $n_{e,o}$ can be calculated with relation (7).

The plasma column considered can be assumed to be homogeneous in the axial direction and to have radial symmetry with a certain $n_{e,o}$ value on the axis and some $n_e(r)$ profile in the x-y plane,

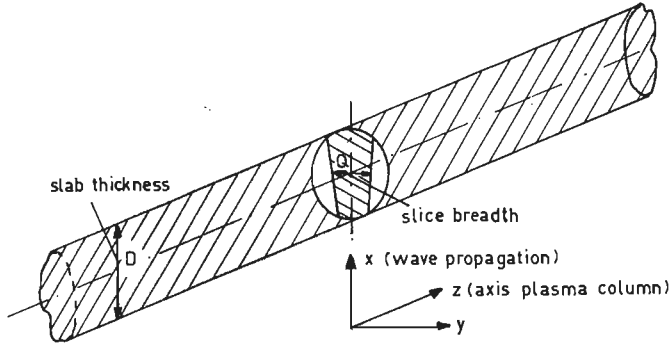slab thickness

slice breadth

Q

D

x (wave propagation)

z (axis plasma column)

y

*Fig.2 Simplified design of the plasma column, interacting with micro-
waves.*

corresponding with a variable $\mu < 1$. In [2] a method was pointed out
to calculate $n_e(r)/n_{e,o}$ from spectroscopic measurements. One can use
the plasma slab approximation, replacing $n_e(r)/n_{e,o}$ by $n_e(x)/n_{e,o}$ to
calculate a first approximate value $n_{e,o1}$, neglecting at the moment
the dependency of n_e in the y direction.

3. Slice breadth approximation

For a real plasma column, the relation between $\Delta\phi$ and the n_e-
profile is more complicated as given in relation (7). To be able to
improve the slab approximation, we consider the refraction phenomena
in a cylinder more in detail. Extending the derivation of HEALD and
WHARTON [7], we can calculate the breadth Q of a slice interacting
with the microwaves for a cylindrical rod with a dielectricum, having
a constant $\mu < 1$ (see Fig.3). This model is supposed to be an
equivalent of the real plasma column in interaction with the micro -
waves. The relations between the various angles in Fig.3 are based on
the geometrical optical approximation and on the small angle
approximation. They are

$$\begin{array}{ll}
\theta_1 = \mu\,\theta_2 & ; \quad \theta_1 - \theta_i = P/D \quad ; \\
\theta_e = \theta_i + 2(\theta_2 - \theta_1); & \theta_i + 2\theta_2 - \theta_1 = P'/D.
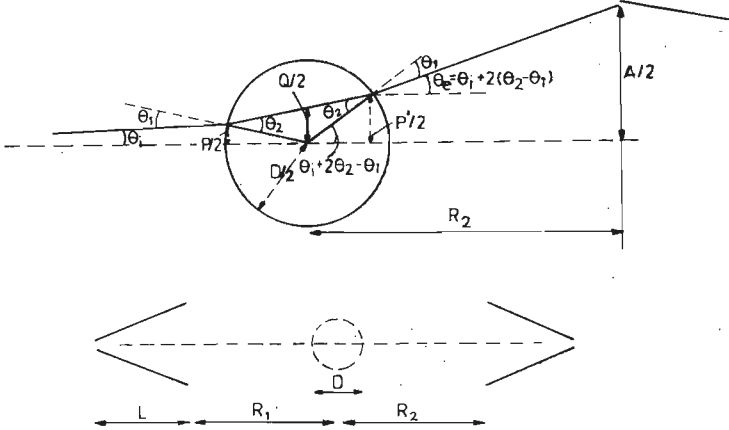\end{array} \tag{8}$$

Fig.3 *Refraction of microwaves by a cylindrical rod. The parameters are indicated in the figure and explained in the text.*

These relations are valid for the ray just received by the antenna. The first three expressions of (8) result in

$$\theta_e = 2(1/\mu - 1) P/D + \{2(1/\mu - 1) + 1\} \theta_i. \qquad (9)$$

With (8),(9) and the relations

$$\theta_i = \frac{P}{2(L+R_1)-D} \quad \text{and} \quad \theta_e = \frac{A-P'}{2R_2-D} \quad , \qquad (10)$$

one can derive an expression for P/D, only based on geometrical quantities and μ:

$$P/D = \frac{A(L+R_1 - D/2)}{4(1/\mu-1)R_2(L+R_1) + D(L+R_1+R_2)} . \qquad (11)$$

A similar expression for P'/D, being the largest breadth, interacting with the microwaves, can be derived. One finds

$$P'/D = \left\{ \frac{2(L+R_1)}{\mu(L+R_1-D/2)} -1 \right\} P/D. \tag{12}$$

We shall approximate the breadth Q of the slice in interaction in the y direction with $Q = (P+P')/2$, giving

$$Q/D = \frac{(L+R_1)A}{4(1-\mu)R_2(L+R_1) + \mu D(L+R_1+R_2)} \tag{13}$$

Now we shall try to correct the $n_{e,o1}$-value already found for the influence of the slice breadth Q. We chose two extreme approximations for the plasma column, to be able to estimate the parameter Q/D.

The first approximation is a rod having a diameter D' as defined by relation (5) and a $\bar{\mu}$ value as defined by the relations (4),(5) and (6). Due to the large value of D' and consequently the small value of $1-\bar{\mu}$ in this approximation, it appears that the value Q' in relation (13) is a major estimate for the slice breadth. As $0.8 < \mu < 1$ in most cases, the value of μ itself is less influenced by the approximation.

The second approximation is a rod with a diameter D" as defined by the width at half-maximum value of the reduced n_e-profile and a μ"-value corresponding with $n_{e,o1}$. The D"-value may be considered as a more or less small estimate of D. It is obvious that the value $1-\mu$" is too large. Consequently, the value Q" will be a minor estimation for the slice breadth. As it is impossible from these elementary estimates to decide which of the two approximations is the better, we shall adopt for the parameter Q the value given by $(Q'+Q'')/2$. We are now able to replace the slab approximation $n_{e,o1}$ by a second approximation $n_{e,o2}$, based on the estimation of the slice breadth. We suppose that the approximation of the top of the n_e-distribution by a triangular shape is good enough for the estimates, so that

$$n_{e,o2} = 2\, n_{e,o1} - n_{eQ} \qquad \text{or}$$

$$n_{e,o2} = \frac{2\, n_{e,o1}}{1 + n_{e\, red\, Q}}, \tag{14}$$

where n_{eQ} and $n_{e\ red\ Q}$ are the n_e-value and reduced n_e-value,
respectively at a distance $r = Q/2$ from the axis.

The differences found for both approximations are the largest for a
well-confined plasma column and negligible for non-confined plasmas.
The maximum error in relation (14) is estimated to be 5% from the
differences between the two approximations. The total amount of the
correction is $\leq$ 15% so that a second iterative step with improved
$n_{e,o}$-values appears to be superfluous.

4. *Miscellaneous questions*

Another question to be considered is, whether "rays" cross each
other due to the r-dependent μ-value, in such a way that information
of an inner layer does not reach the antenna, in contradiction with an
outer layer of the plasma slice. One can approach this problem by
replacing Q by y and A by y' in equation (13) and differentiating the
variables y and y' with respect to each other. One can formulate the
demand that for $\Delta y > 0$ the shift in the antenna plane $\Delta y'$ must be ≥ 0.
With the differentiated form and equation (13) itself the expression

$$\left| \frac{\partial n_e}{\partial y} \right| \leq \frac{2\mu\ n_{ec}}{y} \left\{ \frac{4(1-\mu)R_2(L+R_1) + D(L+R_1+R_2)}{4\ R_2(L+R_1) - D(L+R_1+R_2)} \right\} \qquad (15)$$

is obtainable and when $(L+R_1) \approx R_2 \approx R$ is introduced, one finds

$$\left| \frac{\partial n_e}{\partial y} \right| \leq \frac{2\mu\ n_{ec}}{y} \left\{ \frac{\mu(D-2R) + 2R}{2R-D} \right\}. \qquad (16)$$

It appears that for the nearly triangular n_e-profiles found, equation
(16) is fulfilled, so that no complications on this point need be
expected.

We shall now pay attention to eventual diffraction problems of the
system of microwaves and plasma column. We can state for the plasma
that $3 \lessapprox D''/\lambda \lessapprox 10$, where $\lambda = 2\pi/k_o$. ROSEN [8], and HEALD and WHARTON[7]
treat the refraction for a system of a "plasma rod" with a value of
$n_e/n_{ec} = 0.56$. The diffraction losses can be estimated from the
difference between the experimental values of Fig.4.16 and the
theoretical values of Fig.4.18 of [7] (see Fig.4). It appears
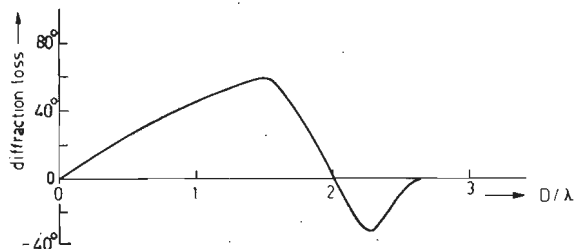
Fig.4 Diffraction loss caused by a cylindrical rod as function of D/λ
i.e. the diameter of the rod divided by the wavelength of the micro-
wave .

that errors due to diffraction are largest for $D/\lambda = 1.5$ and are
totally negligible for $D/\lambda \gtrsim 3$.

When for plasma columns with continuously varying refractive index
μ the expression

$$\lambda \, (\vec{\nabla}\mu/\mu) \ll 1 \tag{17}$$

holds, it is assumed that diffraction phenomena may be neglected. For
the profiles measured, the values of expression (17) appeared to be
< 0.1, so that errors due to diffraction are expected to be small.

Based on these facts, we suppose that the errors due to diffraction
phenomena are in any case less than 10% and are probably negligible
and we abondon to improve the calculated n_e-values.

The estimation of the total error in the n_e-values is somewhat
complicated by the fact that the $\Delta\phi$ measurements were performed in a
plane shifted about 15 cm from that of the spectroscopic measurements
from which the reduced n_e-profiles were calculated. Though there are
differences between the spatial radiation profiles as a function of z
and hence of the n_e-profiles, we suppose that the number of electrons
per unit length in axial direction is more or less constant. Due to
the non-linear relation between μ and n_e expressed in (3), it may be
expected that the $\Delta\phi$-values slightly change when the n_e-profile varies

as a function of z. We assume that the total error, due to the
different location of the measurements is about 10%.

Finally, we estimate the error, caused by errors in the reduced
n_e-profiles to be about 10%, so that we can state with the errors in
the slice breadth and in the $\Delta\phi$ measurement, that $\Delta n_{e,o}/n_{e,o}$ is about
30%. The error in the ratio of two $n_{e,o}$-values of various conditions
is estimated as about 10%.

III DETERMINATION OF THE ELECTRON TEMPERATURE

The calculation of the electron temperature T_e will be performed
starting from absolute line-intensity measurements both of the argon I
and the argon II spectrum.

For the first method, the radiant flux P(0) of the 7384 Å line of
argon I, originating from the $2p_3$ level was obtained after an Abel
transformation. For this level the transition-probability values
(A-values) and the cross-section value σ found in the literature were
the most reliable. For ΣA of the $2p_3$ level $3.6 \times 10^7 s^{-1}$ was adopted and
for A of the 7384 Å line $0.92 \times 10^7 s^{-1}$, which are mean values of [10-14].
For the maximum value of σ of the $2p_3$ level $3.5 \times 10^{-22} m^2$ was adopted,
a mean value of [3,4], accounting for deviations due to cascade
radiation.

When direct excitation is the dominant populating process for the $2p_3$
level and according to C.E. circumstances, spontaneous radiation decay
is the dominant depopulating process, we may write

$$n_{2p_3} \Sigma A = n_e n_a <\sigma v_e> \quad , \tag{18}$$

where n_{2p_3} is the population density of the $2p_3$ level; n_{2p_3} can be
calculated with the A- and P(0)-values for the 7384 Å line. n_a is the
neutral particle density and was calculated with the relation
$p = n_a k T_n$ for $T_n = 500°K$, whose value is valid for discharge currents,
smaller than 50A. The pressure p was measured with an ionization gauge
at some distance from the discharge. ∇p in the discharge volume due to
neutral particles is small, so that the pressure measurement is a good
representation of the pressure near the axis. $<\sigma v_e>$ denotes the

integration of the excitation cross-section function σ over the electron velocity distribution. For the mathematical description of σ we used the approximation given by Fabrikant [15] from threshold to top-value and a straight-line approximation for the remaining part. A curve giving T_e as a function of the $<\sigma v_e>$-values is presented in Fig.5. From the curve T_e can be read when $<\sigma v_e>$ is calculated from relation (18).
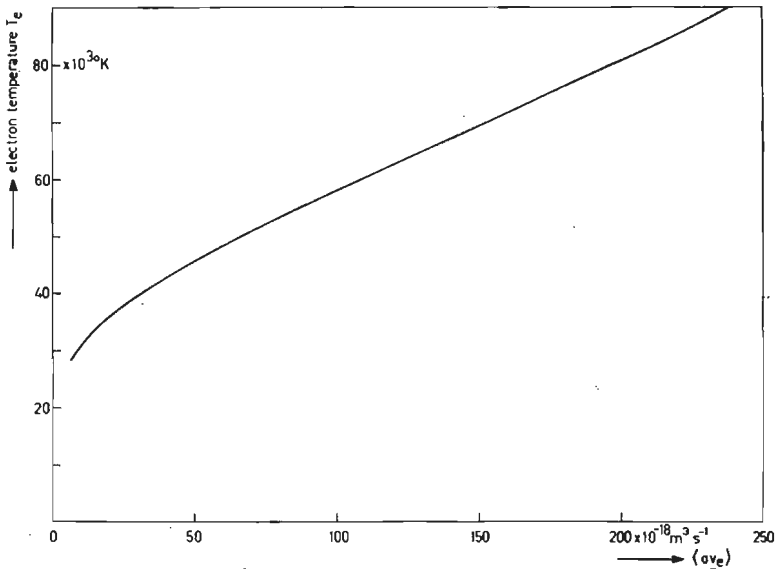
Fig.5 The electron temperature T_e as a function of the value of $<\sigma v_e>$ of the $2p_3$ level (7384 Å line).

The errors in $<\sigma v_e>$ are estimated to be 10% due to n_{2p3}, 10% to ΣA, 30% to n_e, 30% to n_a, 30% to σ and 20% to the approximation for $<\sigma v_e>$, used. These errors are for an important part uncorrelated systematic errors. We estimate the total error due to the parameters in relation (18) to be 25 to 50%. These errors cause 5 to 10% uncertainty in the determination of T_e for $T_e = 35 \times 10^3$ °K. Also systematic errors, due to other population mechanisms up to about 50% do not harm the method severely. The random error in T_e between the various points is 3% or
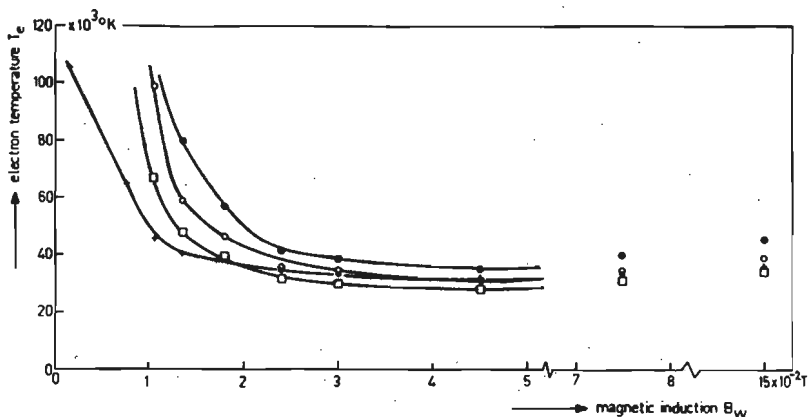
Fig.6 The electron temperature T_e as function of the magnetic induction B_w. + symbols from the radiant flux of the argon I 7384 Å line. ●
o and □ symbols from the radiant fluxes of argon II lines for f = 50, f = 100 and f = 200, respectively. Conditions: end-anode; discharge current I_D = 40A; pressure p_b = 1.5 × 10^{-3} mm of Hg.

less.

The second method is based on measurements of the argon II-4p group line-intensities and on a Corona Equilibrium (C.E.) formula, described in [2], equation (7). The level populations are calculated from the radiant fluxes P(0) of four lines (4765 Å, 4806 Å, 4848 Å and 4880 Å) and A-values of [1]. The n_e-values were calculated as described in section II.

As pointed out in [2], the method to determine T_e, is based on stepwise-excitation through short-lived intermediate levels. Assuming at the moment that stepwise-excitation is the proper mechanism, still great errors may occur. The σ-values used in the C.E. model can only be considered as very rough approximations of the absolute values. To obviate this problem, we introduced a factor f in the expression, given in equation (7) of [2]. The factor f has to be regarded as the multiplication $f = f_1 × f_2$ of the two errors in the values of σ for the first and the second step of the excitation. We calculated T_e-values for several f-values and compared the results with those of the above described method.

In fact, the factor f varies from one to the other 4p level with about a factor 4 between the smallest and largest value. The variation of f for the various transitions accounts for differences in the P(0) values as far as not caused by differences of the excitation energy of the 4p levels. The parameter f introduced in Fig.6, is the factor belonging to the 4p $^4P_{5/2}$ level and the 4806 Å line.

This figure shows a series of results for T_e as functions of the magnetic induction B_w. The f-values range from 50 to 200. Irrespective of the f-values used, we may conclude from the figure that between the two methods of determining T_e there are large deviations for small B_w-values. For f = 100 there is a good agreement for large B_w-values. Further discussion on these deviations are delayed to section V.

IV   MISCELLANEOUS REMARKS ON EXCITATION

1   *Population densities*

In [1] it has been remarked that the ratios of the population densities of the 4p levels of argon II seem to change when the magnetic induction B_w is lowered to small values. For this paper, we measured the line-intensity of one line of every level of the 4p group to calculate the population density of that level for a set of B_w-values. A part of the results is presented in Fig.7. The changes in the population densities as functions of B_W can be seen in the subsequent figures of Fig.7. This example is in agreement with the other measurements. The measurements presented in Fig.7 are not subjected to an Abel transformation.

We note from large to small B_w-values a shift of the points, representing the $^4P_{3/2}$ and $^4P_{1/2}$ levels, with respect to each other, the lift of the $^4D_{5/2}$ point with respect to the neighbouring points, the lift of the $^2D_{5/2}$ point, the ^2P doublet and the $^2S_{1/2}$ point with respect to the other multiplets and the lower position of the $^4S_{3/2}$ point. 0.1 of the vertical scale corresponds with about 10% change in the population density. We conclude that changes of about 40 to 60% in the density ratios occur when changing from large to small B_w-values.

It has already been suggested [1] that a possible reason for the changes in the ratios of the population densities occur by changes in the excitation mechanisms when the B_w-value is varied widely. This
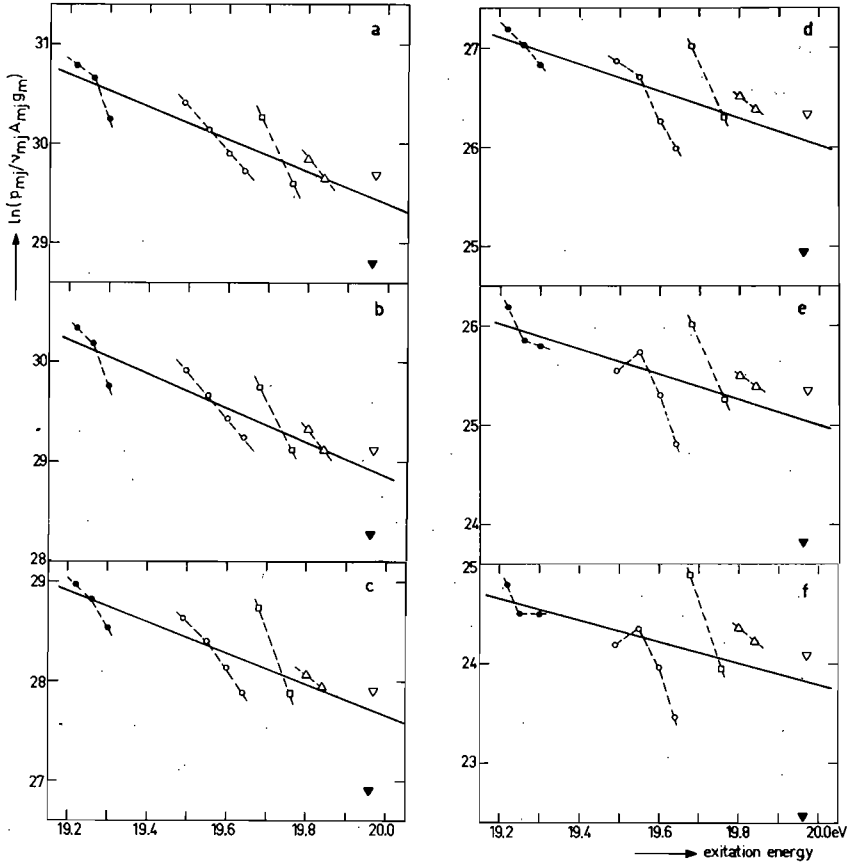
Fig.7 Magnetic sublevel populations on an arbitrary scale as functions
of the excitation energy E_m. a: Magnetic induction $B_w = 15 \times 10^{-2}T$;
b: $B_w = 7.5 \times 10^{-2}T$; c: $B_w = 3 \times 10^{-2}T$; d: $B_w = 1.8 \times 10^{-2}T$;
e: $B_w = 1.5 \times 10^{-2}T$; f: $B_w = 1.2 \times 10^{-2}T$. Significance of the symbols
from left to right: • $^4P_{5/2}$, $^4P_{3/2}$ and $^4P_{1/2}$ level; ○ $^4D_{7/2}$, $^4D_{5/2}$,
$^4D_{3/2}$ and $^4D_{1/2}$ level; □ $^2D_{5/2}$ and $^2D_{3/2}$ level; ▵ $^2P_{1/2}$ and $^2P_{3/2}$
level; ▼ $^4S_{3/2}$ level and ▽ $^2S_{1/2}$ level. Conditions: ring-shaped
anode; discharge current $I_D = 25A$; pressure $p_b = 1.0 \times 10^{-3}$ mm of Hg.

variation corresponds with large differences in n_e-values. A possible explanation of the phenomena is that direct excitation from the ion ground levels to the 4p levels is dominant for small n_e-values and that stepwise excitation through short-lived intermediate levels ($\tau \approx 5 \times 10^{-8}$s) occurs for large n_e-values. However, it may be that metastable levels act as intermediate levels, either for small n_e-values or for large n_e-values. Also the contribution of cascade-radiation has to be taken into account. From Fig.7 alone, we cannot decide which mechanism occurs for large and small n_e-values respectively.

2 Cascade radiation

The contribution of the cascade radiation from 4d and 5s levels to the population density of the 4p levels was determined as part of the investigation of the excitation mechanisms for the 4p levels. The calculation of the percentage of cascade-radiation for a particular level is based on the measurement of all line-intensities involved; this means the intensities of lines having the level concerned either as lower, or as upper level. When cascading levels are designated with 4k, the 4p level with 3 and lower intermediate levels with 2m, the contribution is defined as

$$\frac{\Sigma k \, P_{4k\,3}/h\nu_{4k\,3}}{\Sigma m \, P_{3\,2m}/h\nu_{3\,2m}} \quad , \tag{19}$$

where P is the radiant flux of a line. It is assumed that spontaneous emission is completely dominant as deexcitation mechanism [2].

The results are presented in Table 1. The first column gives the various 4p levels, the second column is the average value of two conditions, namely the discharge current I_D = 75 A with the ring-shaped anode and I_D = 40 A with the end-anode, both for B_w = 2.4 $\times$ 10^{-2}T. The electron temperature T_e is more or less equal for these two circumstances. The third column is a mean value for I_D = 75 A with the ring-shaped anode and I_D = 35 A with the end-anode, both for B_w = 7.5 $\times$ 10^{-2}T.

We conclude that there is an increment of the amount of cascade radiation of about 20% for B_w = 2.4 $\times$ 10^{-2}T in comparison with that

Table 1 Percentages of the population densities of the argon II 4p levels due to cascade radiation from the 4d and 5s groups for two values of B_w.

excitation levels of the 4p group of argon II	percentage of cascade radiation $B_w = 2.4 \times 10^{-2}$ T	percentage of cascade radiation $B_w = 7.5 \times 10^{-2}$ T
$^4P_{5/2}$	4.8	3.6
$^4P_{3/2}$	6.9	3.7
$^4P_{1/2}$	6.0	3.7
$^4D_{7/2}$	6.4	6.3
$^4D_{5/2}$	5.7	8.0
$^4D_{3/2}$	8.1	5.8
$^4D_{1/2}$	8.5	5.6
$^2D_{5/2}$	11.2	9.4
$^2D_{3/2}$	4.8	8.0
$^2P_{1/2}$	5.7	4.0
$^2P_{3/2}$	2.3	1.9
$^4S_{3/2}$	16.9	15.0
$^2S_{1/2}$	0.2	0.3
mean value	6.7	5.6

for $B_w = 7.5 \times 10^{-2}$ T for the mean value. The part of the population due to cascade radiation is small in any case. We expect that the contribution of cascade radiation to the densities of the 4p levels is also limited for $B_w < 2.4 \times 10^{-2}$ T. There is no connection at all between the changes of Fig.7 and those of Table 1. We conclude that it is not apparent that the contribution of cascade radiation is an explanation for the changes in Fig.7.

3   Excitation cross-sections

Information on excitation cross-sections can be found from calculations based on a method introduced by RACAH [16] and extended by EDMONDS [17]. With this method, relative values of the cross-sections for transitions from one to another multiplet were calculated, using the dipole-dipole interaction approximation. The method is restricted to optically permitted transitions, as it is based on the L-S coupling approximation. We give for example the results for $4s\,^4P \rightarrow 4p\,^4P$ transitions and for $3d\,^4D \rightarrow 4p\,^4P$ transitions in Table 2. Multiplication of a number in the table with

Table 2 Relative cross-section values for excitation by electrons for $4s\,^4P \rightarrow 4p\,^4P$ and $3d\,^4D \rightarrow 4p\,^4P$ transitions in the argon II spectrum.

	$4p\;^4P_{5/2}$	$4p\;^4P_{3/2}$	$4p\;^4P_{1/2}$
$4s\;^4P_{5/2}$	1.4	1.8	0
$4s\;^4P_{3/2}$	1.8	.18	.18
$4s\;^4P_{1/2}$	0	.18	.11
$3d\;^4D_{7/2}$	1.6	2.88	0
$3d\;^4D_{5/2}$	.36	.84	0
$3d\;^4D_{3/2}$	.04	.14	.33
$3d\;^4D_{1/2}$	0	.07	1.0

the population density of a 4s or 3d level is proportional to the excitation rate to the level, concerned. As these densities are unknown, the numbers in the columns can not be added up.

The most important conclusion, to be drawn from Table 2, is that the population of the $4p\,^4P$ multiplet cannot be dominated by excitation from the $3d\,^4D$ multiplet. The reason is that every separate $3d\,^4D$ level yields more transitions to $4p\,^4P_{3/2}$ than to $4p\,^4P_{5/2}$, which is in disagreement with the results of Fig.7. This implies that the suggestion that possibly metastable levels as the $3d\,^4D_{7/2}$ level and perhaps the $3d\,^4D_{1/2}$ level are dominant for either small B_w-values or large B_w-

values is not right for the 4p ^{4}P multiplet and very doubtful for other multiplets.

The population of the 4p ^{4}P multiplet may be in agreement with the data of Table 2, when it is assumed that the majority of the excitations occurs through the 4s ^{4}P multiplet, perhaps with some additional excitations through the 3d ^{4}D multiplet.

Similar calculations for 4s ^{4}P → 4p ^{4}D and 3d ^{4}D → 4p ^{4}D transitions show that it is not possible to decide whether the majority of the excitation phenomena occurs through the 3d ^{4}D or through the 4s ^{4}P multiplet.

We finally conclude that stepwise excitation through short-lived levels is in agreement with the data of these calculations and that excitation through metastable levels is at least at one point in disagreement with these data.

V   EXCITATION MECHANISMS

In Fig.6 we found large differences between the values of T_e, based on direct excitation in the argon I spectrum and those, based on stepwise excitation in the argon II spectrum. An interpretation of these differences will be given now.

The curve of T_e calculated from the argon I line-intensity is the flattest curve which can be found for argon I, for direct excitation is proportional to n_e. Assumption of partly or almost totally stepwise excitation should give a much steeper curve, as this phenomenon is proportional to n_e^2. The largest deviations with respect to the curve drawn in Fig.6, should occur for large B_w- and n_e-values.

On the contrary the T_e curve determined from argon II line-intensities is the steepest curve which can be found for argon II, as stepwise excitation is proportional to $n_e^2 \times n_i = n_e^3$. Contribution of direct excitation from the ion ground levels should give a flatter curve with the largest deviations with respect to the curves drawn for small B_w- and n_e-values. It can be seen from Fig.6 that factors 2 and 4 in the factor f used, give variations of T_e from $T_e > 200 \times 10^3$ $^\circ$K to $T_e = 99 \times 10^3$ $^\circ$K and to 67×10^3 $^\circ$K respectively for $B_w = 1 \times 10^{-2}$T. It appears from this example that large contributions of direct excitation in the argon II spectrum for small B_w-values may give large

errors in the calculation of T_e.

The contributions of direct excitation and stepwise excitation in the argon II spectrum can be calculated if we assume that the T_e-curves from the argon I line-intensity are correct. We then are able to set up a balance equation for the population density n_3' for a 4p level, accounting for contributions of direct and stepwise excitation[2]

$$n_3' \, \Sigma m \, A_{3 \, 2m} = K_d(n_e'^2/T_e'^{\frac{1}{2}})\exp(-E_3/kT_e) + K_s(n_e'^3/T_e')\exp(-E_3/kT_e), \qquad (20)$$

where ' denotes a particular discharge condition. K_d and K_s are constants for a particular level 3. m is a summation over all intermediate levels, involved. E_3 is the excitation energy of the level 3. A similar equation holds for n_3'', T_e'' and n_e'' for a second discharge condition, denoted with ".

We call $n_3' \, \Sigma m \, A_{3 \, 2m} = z$, $K_d(n_e'^2/T_e'^{\frac{1}{2}})\exp(-E_3/kT_e) = x$ and $K_s(n_e'^3/T_e')\exp(-E_3/kT_e) = y$. The equation (20) can be written as

$$x + y = z \qquad (20a)$$

and the equation for the condition with " as

$$(n_e''/n_e')^2 \cdot (T_e'/T_e'')^{\frac{1}{2}} \cdot \exp\{-E_3/k(1/T_e'' - 1/T_e')\} \, x \qquad +$$
$$(n_e''/n_e')^3 \cdot (T_e'/T_e'') \cdot \exp\{-E_3/k(1/T_e'' - 1/T_e')\} \, y = (n_3''/n_3') \, z \, . \qquad (20b)$$

As the n_e, T_e and n_3 values are known, x/z and y/z can be solved. Their ratios give the contribution of the two kinds of excitation mechanisms for the condition, denoted with '. The equations can also be solved to find the ratios for the condition, denoted with ". By comparing every possible pair of two conditions (B_w-values) with each other for one series of measurements, one can derive a set of values for x/z and y/z for every condition. This set can be averaged to find t the most proper result for the condition concerned. The deviations due to errors in n_e, T_e and n_3 of the other conditions are thus averaged by this procedure.
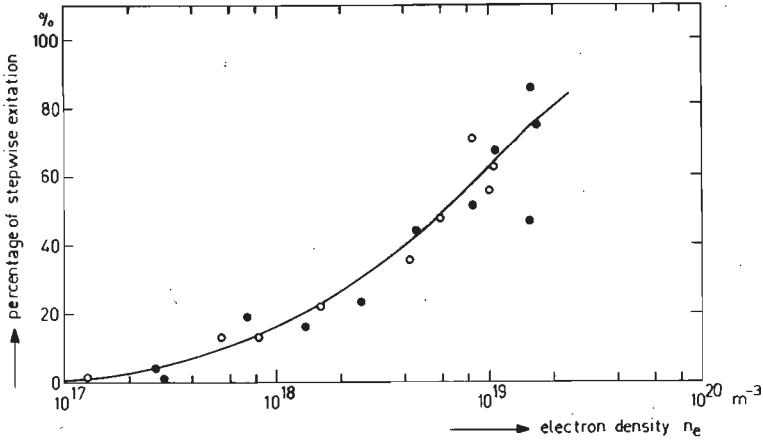
Fig.8 Percentage of the stepwise excitation mechanism for the populating of the argon II 4p levels as function of the electron density n_e. Conditions: o end-anode, discharge current I_D = 20 A; • end-anode, I_D = 40 A.

The results of the calculations for two series of measurements are presented in Fig.8 as functions of n_e. They appear to lead to the same curve. The contribution of the stepwise excitation ranges from about 1% for n_e = $10^{17} m^{-3}$ to about 80% for n_e = 2 x $10^{19} m^{-3}$.

In [2], it has already been discussed that proper n_e-values can be derived by interpolation between values, based on reduced n_e-profiles, related to stepwise excitation and those, related to direct excitation. These corrections have already been performed for the results of Fig.8. Also the T_e-values have been adjusted to the proper n_e-values. The improvements for n_e were 10 to 35% from large to small n_e-values, and correspondingly for T_e,1 x 10^3 to 5 x 10^3 °K. It appeared that only one step of the iteration process to find the partition between stepwise and direct excitation was sufficient, as the values of y/z became only 10% larger by the changes mentioned.

It appears from the results of Fig.8 that stepwise excitation is the dominant process for n_e > 6 x $10^{18} m^{-3}$ and that direct excitation is dominant for n_e < 6 x $10^{18} m^{-3}$. The random error in y/z for most points

is about 5 to 10%. The results can be considered as the explanation of the large deviations for the two methods of T_e-determination, illustrated in Fig.6.

These calculations are based on the T_e-values, derived from the argon I line-intensities, i.e. on direct excitation in the argon I spectrum. When this assumption is not fully correct, and T_e-values for large B_w-values should be somewhat lower, then the contribution of stepwise-excitation should be slightly higher. It can be calculated that stepwise excitation in the argon II spectrum becomes $\gtrsim$ 90% in stead of 75% when direct excitation in the argon I spectrum contributes only 50% of the population of the $2p_3$ level. The values of Fig.8 have to be regarded as minimum values. It is not possible with the method used to distinguish whether the percentages given in Fig.8 are correct, or somewhat too low.

We may conclude now that the calculation of T_e from argon I spectral line-intensities is satisfactory for n_e-values $\lesssim 1 \times 10^{19} m^{-3}$ with an accuracy of approximately 10% and that for larger n_e-values there may be an error in addition up to about 10%. The definite calculations with argon II line-intensities show that the T_e-values for f = 100 and $n_e \gtrsim 7 \times 10^{18} m^{-3}$ are in agreement with those from the argon I line-intensities.

VI   RESULTS

The results of four series of measurements as functions of the magnetic induction B_w are presented in the Figs. 9 to 16. The conditions are stated in the caption of Fig.9. The radiant flux P(0) of the 4806 Å argon II line and the 7384 Å argon I line are shown in the Figs. 9 and 10 respectively. By comparing both figures we state that the P(0) value of the 4806 Å line changes more than a factor 10^3 and that the P(0) value of the 7384 Å changes about a factor 10. This difference in variation is mainly due to the difference in the dependency on n_e. The curves for the ring-shaped anode are somewhat steeper than those for the end-anode.

The results of the calculations of the electron density n_e can be found in Fig.11. The confining effect of the magnetic field can clearly
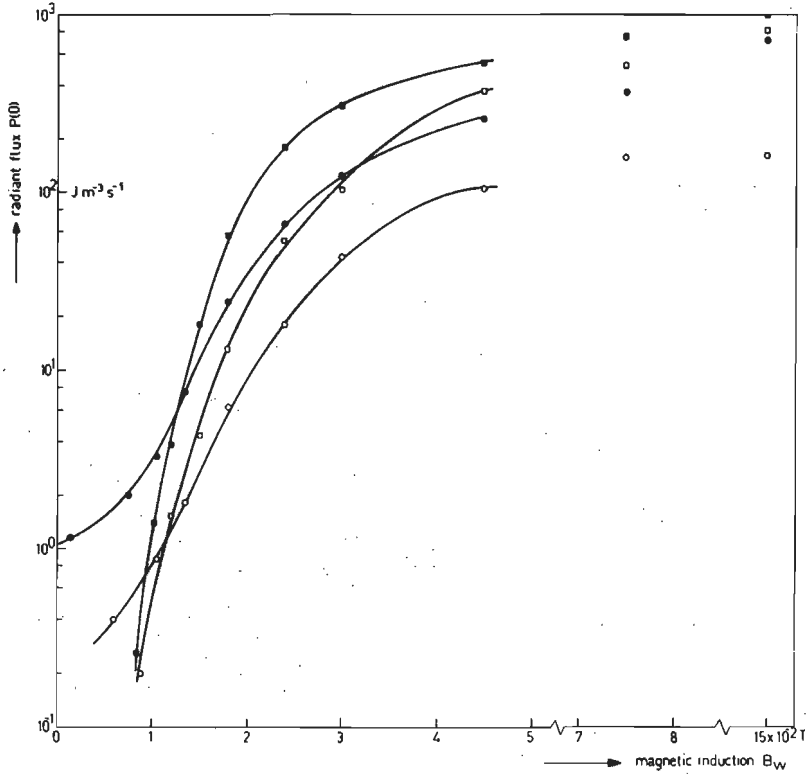
Fig.9 The radiant flux P(0) of the argon II 4806 Å line as function of the magnetic induction B_w. Conditions: o end-anode, discharge current I_D = 20 A, background pressure p_b = 1.0 x 10^{-3} mm of Hg ; • end-anode, I_D = 40 A, p_b = 1.5 x 10^{-3} mm of Hg; □ ring-shaped anode, I_D = 25 A, p_b = 1.0 x 10^{-3} mm of Hg; ■ ring-shaped anode, I_D = 75 A, p_b = = 1.25 x 10^{-3} mm of Hg.

be seen from the changes of $\dot{n}_e$ by a factor 40 or more.

The results for the electron temperature T_e are presented in Fig.12. We can see from the figure that for B_w > 3 x 10^{-2}T, the T_e-values are 28 x 10^3 to 38 x 10^3 °K, with a small increment for large B_w-values. For small B_w-values a marked increase can be stated. We remark that for 0.75 x 10^2T < B_w < 1.05 x 10^2T the discharge was unstable for the end-anode configuration. For B_w-values of about 0.5 x 10^{-2}T, T_e-values
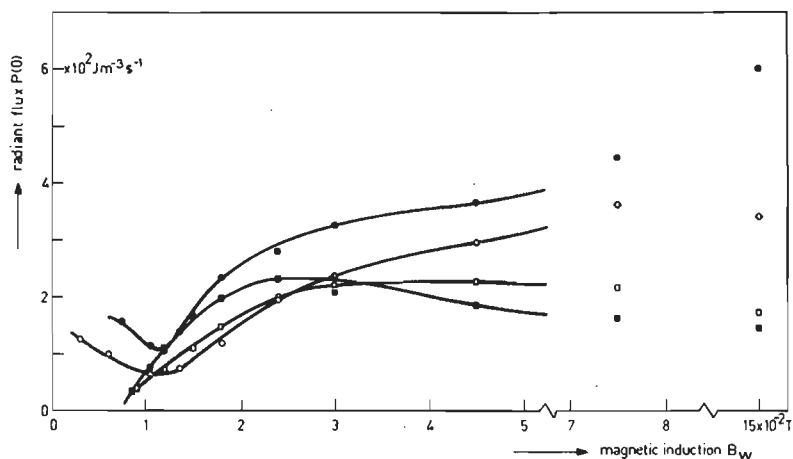
Fig.10 The radiant flux P(0) of the argon I 7384 Å line as function of B_w. See for explanation of the symbols Fig.9.
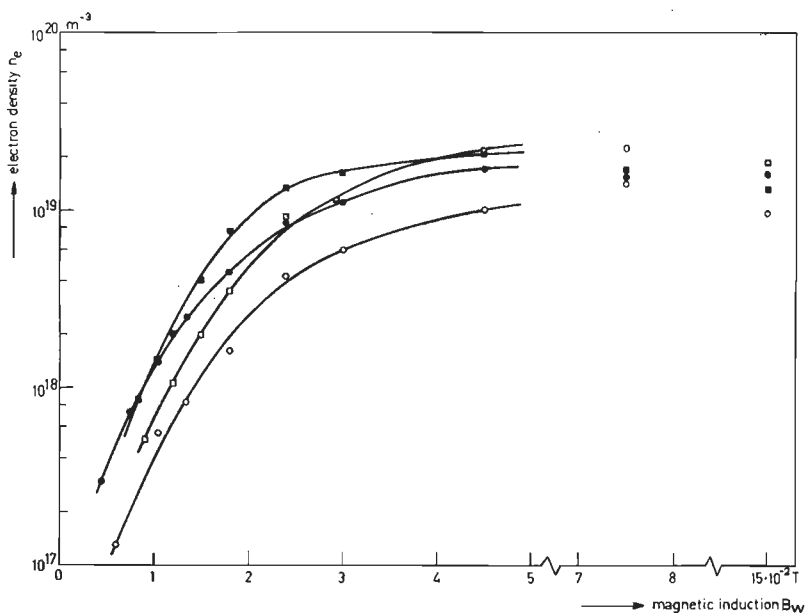

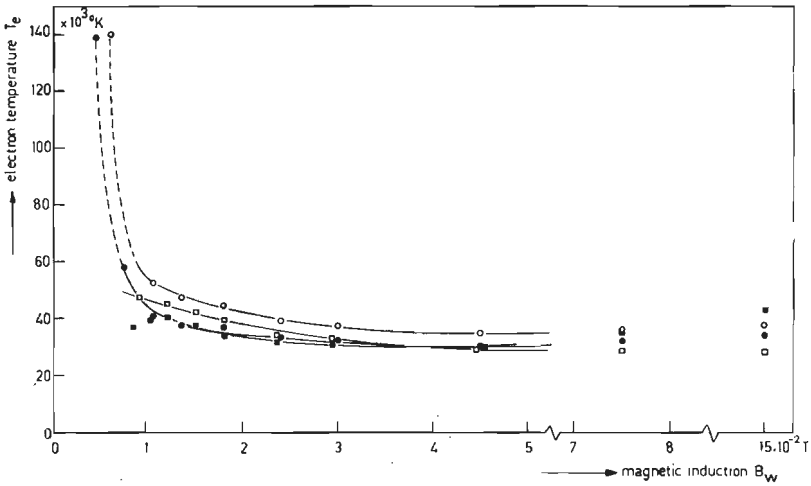Fig.11 The electron density n_e as function of B_w. See for explanation of the symbols Fig.9.

Fig.12 *The electron temperature* T_e *as function of* B_w. *See for explanation of the symbols Fig.9.*

larger than 10^5 ^oK were found. These last values have large errors.
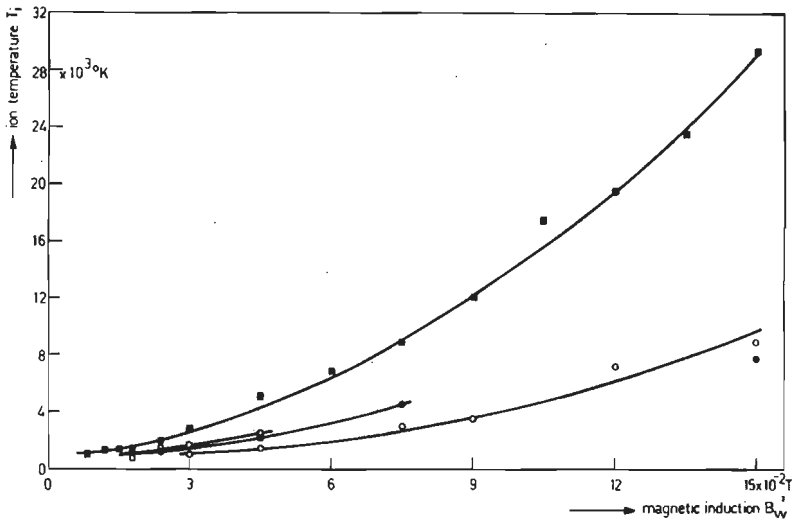For the 75 A ring-shaped anode series the T_e-values were calculated

Fig.13 *The ion temperature* T_i *as function of* B_w. *See for explanation of the symbols Fig.9.*

based on argon II line-intensities with the factor f = 100. It appeared
that due to the large T_n-values of this series (see Fig.14), n_a could
not be calculated accurately. The relations $p = n_a k T_n$ and n_a = constant
does not satisfy and give too large and too small values, respectively
in comparison with the method used.

In the Figs. 13 and 14 the results of the ion temperature T_i and
neutral atom temperature T_n are presented. Both temperatures were found
with the aid of a Fabry-Perot interferometer.
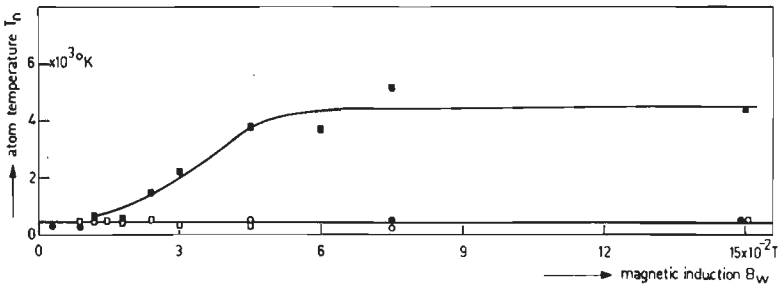
*Fig.14 The atom temperature T_n as function of B_w. See for explanation
of the symbols Fig.9.*

The B_w-values of the measured points do not always coincide with those
of the other figures. We can state a rapid growing of T_i with the
discharge current and with B_w. T_n is approximately 400 to 500 ^oK
for three series. Only for the discharge current I_D = 75 A, a larger
T_n value was found. We do not discuss here the problem whether the
large T_n-values are corresponding with a Maxwellian distribution or
not.

The ionization degree $\alpha = n_e/(n_e + n_a)$ was calculated and the
results are stated in Fig.15. Also here a marked dependency on
I_D and B_w can be seen. The α-values for the ring-shaped series are
larger than for the series with the end-anode.

Finally, the voltage characteristics of the four series can be
found in Fig.16. The most striking phenomenon is a difference between
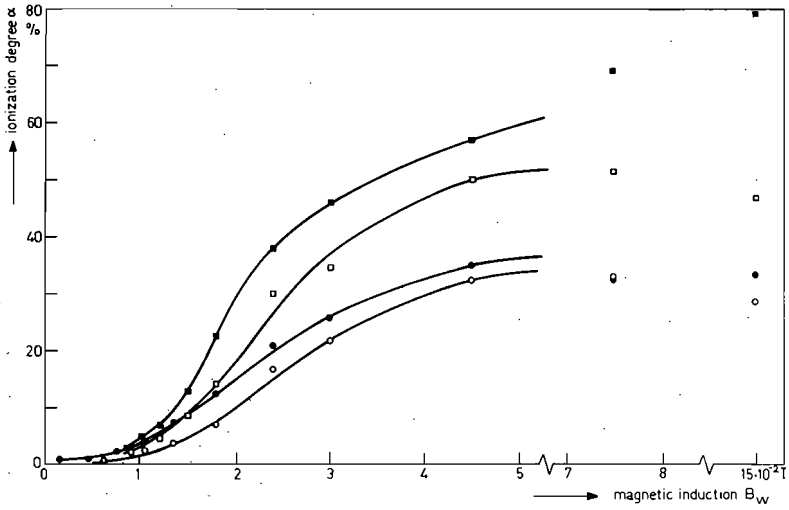the values for the ring-shaped anode and the end-anode. The difference

Fig.15 *The ionization degree α of the plasma as function of* B_w*. See for explanation of the symbols Fig.9.*
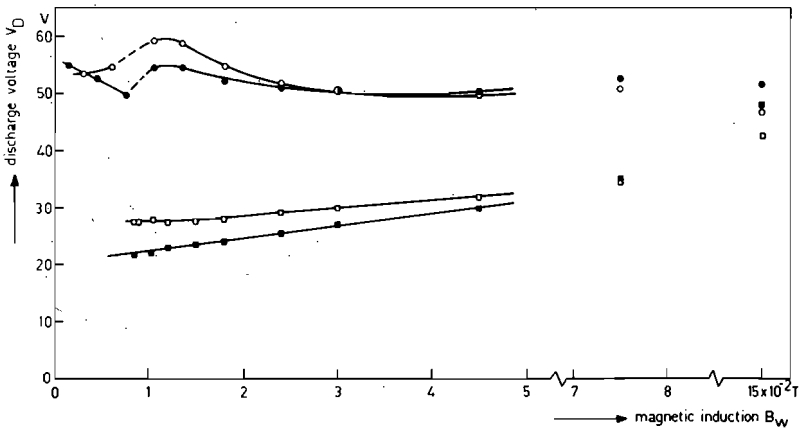

Fig.16 *The voltage characteristics of the discharge as function of* B_w*. See for explanation of the symbols Fig.9.*

of about 25 V may be explained as due to the electrical field E_z along the axis. From this difference E_z is found to be 15 to 20 V m^{-1}, in agreement with [18]. The increase of the voltage V_D for large B_w - values for the ring-shaped anode is probably due to increasing E_r - fields in the surrounding of this anode.

Measurements of the gas flow gave the following results: approximately 1.55 x 10^{-3}, 2.30 x 10^{-3}, 1.65 x 10^{-3} and 2.90 x 10^{-3} mm of Hg.m^{3}s^{-1} for discharge currents I_D of 20, 40, 25 and 75 A respectively .

VII   DISCUSSION AND CONCLUSIONS

One of the most important results of this work is the ascertainment that stepwise excitation through short-lived intermediate levels contributes to the population of argon II-4p levels. The percentage of the population due to this excitation mechanism as function of n_e is given in Fig.8. In fact, a small amount of the percentages is due to cascade radiation from that part of the population of the cascading levels, also created by stepwise excitation. When the partition of direct and stepwise excitation for the cascading levels is similar to that of the 4p levels, the percentages presented should be corrected with approximately 5% for large n_e-values. For small n_e-values the correction is not exactly known, but it is supposed that it has about the same ratio to the stepwise excitation as for large n_e-values.

It may be assumed that the 4p ^{4}P multiplet is mainly populated through the 4s ^{4}P multiplet and that the 4p ^{4}D multiplet is probably populated both through the 4s ^{4}P and 3d ^{4}D multiplets. It is not possible to make a decision for the doublets and singlets. Perhaps there is an additional population by stepwise excitation through the 4s ^{2}P doublet (17.2 eV) but the lasering effects of transitions between some of the 4p levels and this doublet must be caused by population through other multiplets.

We have seen that direct excitation from the ion ground levels is the main excitation mechanism for small n_e-values. In Fig.7 it can be seen that the doublet levels show a larger density for small n_e - values relative to the density of the multiplets, probably caused by

a preferential direct excitation from the 3p ^{2}P ground level doublet
to the 4p group doublets. The so-called configuration temperature T_{4p}[1]
increases from about 6.5 x 10^3 to 10.5 x 10^3 °K from large to small
B_w-values. This effect is mainly caused by the lift of the doublet
points.

An affirmation of the excitation mechanisms proposed can be found
in the following consideration. We calculate for the levels with
excitation energies 19.22 eV and 19.97 eV the ratio of the population
densities, a) when it depends on the expression $(1/E_{13})exp(-E_{13}/kT_e)/\Sigma A$,
corresponding with direct excitation and

b) also on $(1/E_{23})^3 exp-(E_{13}/kT_e)/\Sigma A$, corresponding with
stepwise excitation[2].

E_{13} is the total excitation energy with values 19.22 and 19.97 eV
respectively, and E_{23} is the excitation energy of the second step
from ~ 16.5 eV for both levels. For T_e = 30 x 10^3 °K, the configuration
temperatures T_{4p}, corresponding with the ratios found were > 30 x 10^3 °K
for direct excitation and approximately 10 x 10^3 °K for stepwise
excitation. The results can be compared with a T_{4p} for the Figs. 7a
and 7b, being 7 x 10^3 °K. We see that the slopes, found in Fig.7 may
be explained by stepwise excitation formulae with reasonable
satisfaction. The deviations of the population densities from the
straight lines are to be considered as differences between the
excitation cross-sections of neighbouring levels.

Finally, we show a combined argon I and II excitation energy
diagram in Fig.17, in which the contributions of the various excitation
mechanisms are inserted for T_e = 30 x 10^3 °K and n_e = 2 x 10^{19}m^{-3}.
The results are also based on discussions in [2].

The excitation mechanism proposed for the 4p argon II group is
contrary to the arguments of BENNETT et al [19], who assumed that
direct excitation from the neutral ground level causes the laser
action of the argon ion laser and also of KITAEVA et al [20], who
argue that direct excitation from the ion ground levels is the dominant
process. The contribution of cascade radiation is smaller than found
by RUDKO and TANG [21].

Comparison of our results with the calculations of KITAEVA et al
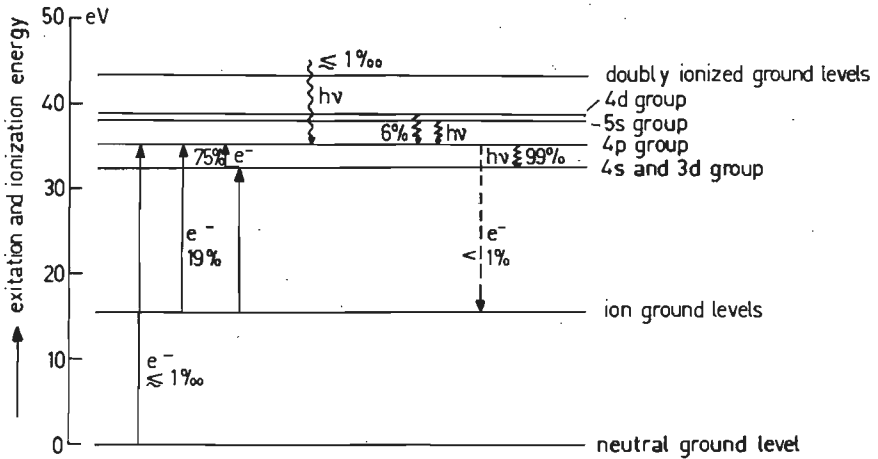[20], also discussed in [22] and [23], shows a complete disagreement.

Fig.17 Simplified diagram of the argon I and II spectrum with the excitation and deexcitation balance for the argon II 4p group for $T_e = 30 \times 10^3 \, ^oK$ and $n_e = 2 \times 10^{19} m^{-3}$.

The first reason can be found by comparing the $<\sigma v_e>$ values. An estimation for the 4p $^4P_{5/2}$ level from our results gives $<\sigma v_e> \approx 3 \times 10^{-18} m^3 s^{-1}$ for $T_e = 30 \times 10^3$ to $35 \times 10^3 \, ^oK$ against $<\sigma v_e> \approx 3 \times 10^{-17} m^3 s^{-1}$ in [20], both for direct excitation. On the contrary, the values for $<\sigma v_e>_I \times <\sigma v_e>_{II}$ for the stepwise process through 4s levels are $5 \times 10^{-30} m^6 s^{-2}$ and $1.5 \times 10^{-29} m^6 s^{-2}$, respectively. The second reason is the very large A-value of $2.5 \times 10^9 s^{-1}$, supposed by KITAEVA for the 4s levels, against the A-value of $2 \times 10^7 s^{-1}$, adopted by us [24]. These two differences, and mainly the second, cause the large differences between the results.

In [2] we found that the reduced radiant flux profile of the 4880 Å laser line and the 4348 Å line are similar within very narrow limits, indicating that no differences exist between the excitation mechanisms of laser lines and normal spectral lines.

It may be remarked that HUCHITAL and RIGDEN [25] and also JENNINGS et al [26] found laser action for a hollow cathode argon arc discharge, similar to our type of discharge. We therefore conclude that stepwise excitation may lead to laser action in this type of discharge in the

same way as occurs in the common argon ion laser.

The determination of the T_e-values is in rough agreement with values of LEONARD [27] and of LIDSKY et al [28], who for certain circumstances also found values of about 30×10^3 °K. The range of values for T_e, found in the literature is 30×10^3 to 100×10^3 °K. The n_e-values are in reasonable agreement with values of GERRY and ROSE [29] and of LEONARD [27]. The range of n_e-values, found in the literature is for confined plasmas $1 \times 10^{19} m^{-3}$ to approximately $10 \times 10^{19} m^{-3}$.

In conclusion, we may state that for the argon plasma an alternative method for the determination of the electron temperature T_e is presented. It is valuable to compare the results of this method with those of other methods as probe measurements and Thomson scattering.

ACKNOWLEDGEMENTS

REFERENCES

1 . B. van der Sijde, J.Quant.Spectrosc.Radiat.Transfer, in press.

2 . B. van der Sijde, to be published.

3 . I.P.Zapesochnyi and P.V.Feltsan, Opt.Spectr. 20, 291 (1966).

4 . L.M.Volkova and A.M.Devyatov, Opt.Spectr. 7, 480 (1959).

5 . R.W.P. McWhirter, Plasma diagnostic Techniques, Ch. 5 (Ed.: R.H.Huddlestone and S.L.Leonard) Ac.Press, New York (1965).

6 . B.Wilner, Acta Polyt.Scand., Physics and Nucleonics 41, 1 (1966).

7 . M.R.Heald and C.B.Wharton, Plasma diagnostics with microwaves, J.Wiley, New York (1965).

8 . E.H.Holt and R.E.Haskell, Plasma Dynamics, McMillen Cy, New York (1965).

9 . B.B.Rosen, Project Matterhorn Tech.Memo 85, Princeton Univ., Princeton (1959).

10. J.B.Shumaker Jr. and C.H.Popenoe, J.Opt.Soc.Am. 57, 8 (1967).

11. H.N.Olsen, J.Quant.Spectrosc.Radiat.Transfer 3, 59 (1963).

12. L.R.Doherty, Ph.D.Thesis, Univ.Michigan, Ann Arbor, Michigan (1961).

13. P.D.Johnson, Proc.Phys.Soc. 92, 896 (1967).

14. R.H.Garstang and J. van Blerkom, J.Opt.Soc.Am. 55, 1054 (1965).

15. A.Rutscher, Beiträge Plasmaphys. 6, 195 (1966).

16. G.Racah, Phys.Rev. 62, 438 (1942).

17. A.R.Edmonds, Angular momentum in quantum mechanics, Princeton Univ. Press, Princeton (1957).

18. J.L.Delcroix, H.Minoo and A.R.Trindade, Rev.Roum.Phys. 13, 401 (1968).

19. W.R.Bennett Jr., J.W.Knutson Jr., G.N.Mercer and J.L.Detch, Appl. Phys. Letters 4, 180 (1964).

20. V.F.Kitaeva, Yu.I. Osipov, P.L.Rubin and N.N.Sobolev, I.E.E.E. J.Quant.Electr. QE-5, 72 (1969).

21. R.I.Rudko and C.L.Tang, J.Appl.Phys. 38, 4731 (1967).

22. I.L.Beigman, L.A.Vainshtein, P.L.Rubin and N.N.Sobolev, J.E.T.P.- Letters 6, 343 (1967).

23. S.C.Lin and C.C.Chen, A.I.A.A. J. 9, 14 (1971).

24. H.Statz, F.A.Horrigan, S.H.Koozekanani, C.L.Tang and G.F.Koster, J.Appl.Phys. 36, 2278 (1965).
    G.F.Koster, H.Statz, F.A.Horrigan and C.L.Tang, J. Appl.Phys. 39, 4045 (1968).

25. D.A.Huchital and J.D.Rigden, Rev.Scient.Instr. 39, 1472 (1968).

26. W.C.Jennings, J.H.Noon and E.H.Holt, Rev.Scient.Instr. 41, 322 (1970).

27. S.L.Leonard, Proc. 9th Intern.Conf.Ionized Gases, Bucharest, p. 170 (1969).

28. L.M.Lidsky, G.D.Rothleder, D.J.Rose, S.Yoshikawa, C.Michelson and R.J.Mackin Jr., J.App.Phys. 33, 2490 (1962).

29. E.T. Gerry and D.J.Rose, J.App.Phys. 37, 2715 (1966).

ALGEMENE SLOTBESCHOUWING

We zullen in dit gedeelte een overzicht geven van de resultaten die
verkregen zijn uit de metingen van de intensiteiten van lijnen uit de
spektra van argon I en II, de stralingsprofielen als funktie van de af-
stand tot de as van de ontlading en de faseverschuivingen van 4 mm mikro-
golven. De informatie omtrent de uit Dopplerverbreding verkregen ionen-
temperaturen T_i en temperaturen van neutrale deeltjes T_n is alleen in
de diskussie betrokken, voor zover nodig voor de interpretatie van het
waargenomen spektrum [2].

Zoals in [1] is opgemerkt, worden ionisatie en aanslag bepaald door
botsingen van atomen en ionen met voldoend energierijke elektronen. We
moeten verwachten dat de numerieke waarden van werkzame doorsneden voor
exciterende botsingen van groot belang zijn voor de grootte van de be-
zetting van de aangeslagen niveaus en dat deze van niveau tot niveau
verschillen in de bezetting kunnen veroorzaken. Een gevolg daarvan is
dat de bezetting van deze niveaus zowel in absolute maat [1] als rela-
tief ten opzichte van elkaar [2] niet aan een Boltzmann-verdeling zal
voldoen. Verandert het mechanisme van de aanslag als funktie van de
elektronendichtheid van bij voorbeeld direkte aanslag vanaf het grond-
niveau naar stapsgewijze aanslag via tussengelegen niveaus dan kan men
verwachten ook veranderingen in de verhoudingen van de bezettingen van
de aangeslagen niveaus te zullen waarnemen. Voorbeelden hiervan zijn de
veranderingen in de bezettingen van de 4p groep van argon II, zoals
weergegeven in de figuren 5 en 6 van [2] en Fig.7 van [4]. In deze
figuren is een relatieve maat voor de bezetting van de aangeslagen
niveaus uitgezet als funktie van de aanslagenergie.

Een nauwkeurig beeld van de bezettingen van aangeslagen niveaus kan
afgeleid worden uit de resultaten van lijnintensiteitsmetingen met
behulp van de betrekking

$$P_{32} = h\nu_{32} A_{32} n_3 ,\qquad\qquad (1)$$

waarin P_{32} de stralingsstroom voor een overgang tussen een niveau 3 (bij
voorbeeld de 4p groep bij $\sim$19.5 eV) en een niveau 2 (bij voorbeeld de 3d
of 4s groep bij $\sim$16.5 eV) is, $h\nu_{32}$ de energie van het betreffende kwant,

A_{32} de bijbehorende overgangswaarschijnlijkheid en n_3 de bezetting van het niveau 3. Voor een goede bepaling van de bezetting is het vereist dat voor minstens één overgang uitgaande van niveau 3 de waarde A_{32} binnen 5 tot 10% nauwkeurig bekend is. Door een zorgvuldige en kritische beschouwing van de beschikbare literatuur zijn we er voor de 4p groep van argon II in geslaagd, deze waarden zo nauwkeurig te verkrijgen. De resultaten zijn vastgelegd in de tabellen 1 en 6 van de Appendix van [2].

In [2] is verder de reeds in [1] genoemde veronderstelling uit de literatuur betreffende de thermalisatie van de bezetting van niveaus binnen een spektrale groep getoetst voor de 4p groep van argon II. Aangezien een rechte met een bepaalde helling in de reeds genoemde figuren van [2] en [4] overeenkomt met een bepaalde waarde van een zo genoemde konfiguratietemperatuur T_{4p} voor de 4p groep, is het duidelijk dat een mogelijke thermalisatie zich moet uiten in een rangschikking van de gemeten punten langs een bepaalde helling met niet te grote afwijkingen daarvan. Op grond hiervan kan men uit de genoemde figuren al opmaken dat de 4p groep als geheel waarschijnlijk geen thermalisatie vertoont. Deze veronderstelling is in overeenstemming met het feit dat niet steeds voldaan wordt aan het in [2] aangelegde kriterium voor thermalisatie

$$T_{i,n} \leq T_{4p} < T_e \quad , \tag{2}$$

waarin T_e de elektronentemperatuur is.
Uit de genoemde figuren blijkt dat voor waarden van de magnetische induktie $B_w \gtrsim 3 \times 10^{-2}$T de punten van het ^{4}P multiplet redelijk en voor het ^{4}D multiplet goed op een rechte liggen. We merken op dat de waarden van de konfiguratietemperatuur voor de diverse multiplets verschillen te zien geven. Ze variëren van 1500 tot 2600 K volgens Fig.5 van [2]. De vergelijking van de waarden van de konfiguratietemperatuur T_{4D} voor het ^{4}D multiplet met T_i en T_n in Fig.12 van [2] leidt tot de konklusie dat niet altijd aan uitdrukking (2), waarin T_{4p} is vervangen door T_{4D}, is voldaan.
In [4] is besproken dat de hellingen voor de 4p groep als geheel voor magneetvelden groter dan 3×10^{-2}T in redelijke overeenstemming zijn met hellingen die berekend kunnen worden uit de Coronaformules voor

stapsgewijze aanslag, zoals weergegven in uitdrukking (7) van [3].
Berekeningen met de theorie van Racah en Edmonds [4] laten zien dat de
relatief grote hellingen van de multiplets te begrijpen zijn, indien
de bezettingen van de tussenniveaus bij 16 à 17 eV geen al te grote
onderlinge verschillen vertonen.

Op grond van bovenstaande beschouwingen kunnen we de veronderstel-
ling van thermalisatie door neutrale deeltjes of ionen binnen een be-
paalde groep of multiplet van het spektrum verwerpen en aannemen dat
de ligging der punten in de betreffende figuren bepaald wordt door het
evenwicht tussen de vorming van aangeslagen deeltjes door een aantal
botsingsprocessen en de verdwijning ervan door spontane emissie. Voor
grote magneetvelden kan dit evenwicht met enige verwaarlozing weerge-
geven worden door de vergelijking

$$n_e \; \Sigma m \; A_{3 \; 2m} = n_e^{\;3} \; \{ \Sigma i \; <\sigma v_e>_{II}^i (\Sigma <\sigma v_e>_I^i / \Sigma A_{2i \; 1}) \} \; , \qquad (3)$$

waarin de indices 1, 2 en 3 respektievelijk één van beide grondniveaus,
een tussenniveau en een 4 p niveau aanduiden. $<\sigma v_e>$ in een integratie
over het produkt van elektronenenergieverdeling en werkzame doorsnede,
I voor de eerste en II voor de tweede stap.

Eén van de doeleinden van dit onderzoek is geweest te komen tot een
bepaling van de elektronentemperatuur T_e uit spektroskopische metingen.
De bepaling van T_e in ontladingen die afwijkingen van L.T.E. vertonen
of daar in het geheel niet aan voldoen, is bij aanwezigheid van een
magneetveld in het algemeen moeilijk.

De resultaten van sondemetingen kunnen worden verstoord door elek-
tronenemissie van de sonde zelf bij nadering van de plasmapotentiaal
als gevolg van verhitting van de sonde door het elektronenbombardement.
Bovendien is de theorie betreffende sondemetingen in magneetvelden
niet genoeg ontwikkeld om geheel zeker te zijn van een goede interpre-
tatie van de meetresultaten.

Bepalingen uit de elektrische geleidbaarheid σ volgens

$$\sigma = \frac{1.5 \times 10^{-2} \cdot T_e^{\;3/2}}{\ln(8.25 \times 10^6 \cdot T_e^{\;3/2} / n_e^{\;1/2})} \qquad (4)$$

vraagt een goede kennis van de stroomdichtheid J, de longitudinale

elektrische velsterkte E_z en van de elektronendichtheid n_e. Bovendien blijkt dat voor onze ontlading de waarden van T_e, berekend met uitdrukking (4) grote absolute verschillen laten zien ten opzichte van de resultaten van Fig.12 van [4]. Bovendien wordt het verloop van T_e als funktie van de magnetische induktie B_w ook niet goed weergegeven. E_z is daarbij geschat uit de spanningskarakteristieken van Fig.16 van [4].

Bepaling van T_e uit de Thomson verstrooiing kan beschouwd worden als de meest universele methode, geldig voor alle gassen onder alle omstandigheden mits de elektronendichtheid groot genoeg is ($\gtrsim 10^{19} m^{-3}$) en de Rayleigh verstrooiing van atomen niet teveel invloed heeft. Het is experimenteel echter een lastige methode, die een lange voorbereidingstijd vereist. Deze methode kon niet worden toegepast.

Er is daarom gezocht naar een alternatieve methode, die gebruik maakt van absolute lijnintensiteiten, vooral van argon I lijnen. De elektronendichtheid n_e, de dichtheid van de neutrale deeltjes n_a, de werkzame doorsnede σ voor aanslag door elektronen en de betreffende overgangswaarschijnlijkheden moeten voor deze methode bekend zijn. Zie uitdrukking (18) van [4]. Voor de bepaling van T_e is de lijn bij $\lambda = 7384$ Å uit de 4p groep gekozen, omdat hiervoor de kombinatie van overgangswaarschijnlijkheden en werkzame doorsnede het best bekend is. Andere lijnen van de 4p groep geven overeenstemmende informatie. De methode kan fysisch relevante informatie geven als een redelijk deel (meer dan 30%) van de bevolking van het aangeslagen niveau door het betreffende mechanisme, direkte aanslag, wordt geleverd. Naarmate de direkte aanslag meer domineert neemt de systematische fout af. Een groot voordeel van deze methode is dat elektronentemperaturen reeds bepaald kunnen worden bij een elektronendichtheid van $\gtrsim 5 \times 10^{17} m^{-3}$, hetgeen bij Thomson verstrooiing waarschijnlijk met grote onnauwkeurigheden zou samengaan.

De elektronendichtheid n_e, bepaald uit de faseverschuiving van mikrogolven, moet bekend zijn voor de berekening van T_e. De dichtheidsbepaling is alleen dan redelijk nauwkeurig wanneer de effektieve breedte van de plasmakolom voldoende nauwkeurig bekend is. In uitdrukking (7) van [4] is weergegeven hoe $n_{e,o}$ op de as berekend kan worden, wanneer een gereduceerd-profiel $n_{e,r}/n_{e,o}$ bekend is. Deze gereduceerde

profielen zijn berekend uit de intensiteitsprofielen van argon II
lijnen [3].

Met het model van stapsgewijze aanslag zijn zowel $T_{e,r}$ als $n_{e,r}$ ten
opzichte van $T_{e,o}$ en $n_{e,o}$ bepaald (uitdrukkingen 9 en 10 van [3]) .
In [4] is gevonden dat de stapsgewijze aanslag minder dan 100% van de
bevolking van de 4p niveaus levert. Enige korrektie is daarom nodig. De
nauwkeurigheid in de bepaling van de profielen kan hierdoor minder goed
worden, inzonderheid die van T_e. Vergelijking van de resultaten van de
drie lijnen met elkaar laat echter zien dat de onnauwkeurigheid
minder groot is, dan vermoed zou kunnen worden.

De onnauwkeurigheden in de T_e- en n_e-profielen werken slechts in
geringe mate door in de absolute waarden van deze grootheden zodat de
uiteindelijke resultaten van [4] niet worden aangetast door deze
systematische fouten in de profielen.

De resultaten voor de T_e-profielen laten een geleidelijke afname
van $\sim$ 10% zien in het gebied waar deze profielen redelijk betrouwbaar
zijn (zie de figuren 9 en 12 van [3]). De n_e-profielen hebben een half-
waardebreedte van ongeveer 18 en 27 mm voor respektievelijk eindanode
en ringanode voor de meeste waarden van de magnetische induktie (zie de
figuren 10 en 13 van [3]).

Met behulp van de kennis van de gereduceerde dichtheidsprofielen van
[3], is de methode om absolute waarden van n_e te bepalen verder ontwik-
keld [4]. Om te kunnen korrigeren voor systematische fouten, die ont-
staan omdat de mikrogolven in interaktie treden met een plakje van het
plasma dat inhomogeen is in één richting loodrecht op de voortplantings-
richting van de mikrogolven, zijn twee uiterste benaderingen van "staaf"
modellen ingevoerd om de dikte van het plakje te kunnen afschatten en
een korrektie voor n_e te kunnen aanbrengen. Verder is aandacht geschon-
ken aan eventuele buigingsverschijnselen en aan de eenduidige informa-
tieoverdracht uit een plakje naar de antenne van de mikrogolfopstel-
ling.

Uit de vergelijking van de resultaten voor de elektronentemperaturen
bepaald uit de intensiteit van de 7384 Å lijn van argon I en die uit de
intensiteiten van een aantal argon II lijnen met behulp van Corona for-
mules (uitdrukking 7 van [3]) als funktie van het magneetveld kon binnen
vrij nauwe grenzen worden vastgelegd dat direkte aanslag voor het argon I

spektrum en stapsgewijze aanslag voor het argon II spektrum dominerend
moeten zijn. Bij de vergelijking blijkt dat het produkt $<\sigma v_e>_{II} <\sigma v_e>_I$
voor het stapsgewijze proces, afhankelijk van het niveau,ongeveer een
faktor 50 tot 120 groter moet zijn dan volgens de Coronaformules wordt
gegeven. De zo gevonden waarde blijkt binnen een faktor 3 overeen te
stemmen met waarden die Kitaeva e.a. (zie ref. 20 van [4]) hebben bere-
kend.

De percentuele bijdrage van stapsgewijze aanslag als funktie van de
elektronendichtheid is te vinden in Fig.8 van [4] en een totale balans
van bevolking en ontvolking van een 4p niveau voor $n_e = 2 \times 10^{19} m^{-3}$ in
Fig.17 van [4]. Berekeningen en schattingen, vermeld in [3], zijn
hierin verwerkt.

De gevonden resultaten houden in dat de opvattingen over de mechanis-
men van de laserwerking van de argon ion laser vrij zeker moeten worden
herzien. De tot nu toe meest gangbare opvatting dat de direkte aanslag
van de grondniveaus van het ion naar de 4p groep het dominerende proces
zou zijn, dient vervangen te worden door dat van stapsgewijze aanslag
via kortlevende tussengelegen niveaus. Dat deze opvatting ook geldig is
voor niveaus met laserwerking, bewijst Fig.7 van [3], waar een vrijwel
volledige overeenkomst betreffende het uitgezonden lichtprofiel tussen
de 4348 Å lijn (normale lijn) en de 4880 Å lijn (laser lijn) te zien is.
De konklusie hieruit is dat de aanslag mechanismen voor beide lijnen
dezelfde zijn.

Het feit dat laserwerking gekonstateerd is voor gelijksoortige ont-
ladingen met gasdrukken $\geq 10^{-2}$ torr (ref. 25 en 26 uit [4]), welke
hoger zijn dan in onze ontlading, kan erop wijzen dat een vorm nodig is,
waarin relatief grote elektronendichtheden voorkomen. De aanwezigheid
van doorboorde ronde schijven met gaten van 3 tot 6 mm diameter wijst
ook in die richting. Dit zou in overeenstemming zijn met onze bevindingen.

Als algemene konklusie mag nog genoemd worden dat het ook in gas-
ontladingen en plasma's mogelijk is om dominerende processen te vinden
in het te onderzoeken systeem door een optimale variatie van parameters
(hier vooral het magneetveld) zonder dat een komplete kennis van basis-
gegevens als overgangswaarschijnlijkheden en werkzame doorsneden voor-
handen is en dat het zelfs mogelijk is redelijke schattingen voor een
deel van deze gegevens te vinden.

REFERENTIES

1. Algemene inleiding, p 5-10.
2. Configuration temperatures in a hollow cathode argon arc and
   transition probabilities of the argon II spectrum; p. 11-52.
3. Temperature and density profiles of electrons in a hollow
   cathode argon arc discharge; p. 53-82.
4. Excitation mechanisms and temperatures and densities of electrons
   in a hollow cathode argon arc discharge; p. 83-114.

SAMENVATTING

Voor een holle kathode boogontlading in argon met een lage achter-
gronddruk en die bijeen gehouden werd door een magneetveld, is een on-
derzoek verricht naar intensiteiten van lijnen van de argon I en II
spektra en naar de stralingsprofielen ervan als funkties van de afstand
tot de as van de ontlading. De ontladingsstromen varieerden van 10 tot
80 A, de axiale magnetische velden van $\sim 5 \times 10^{-3}$ tot 15×10^{-2}T en
de achtergronddruk was ongeveer 10^{-3} torr.

Het aanslagmechanisme van de 4p groep van het argon II spektrum kon
worden vastgesteld; stapsgewijze aanslag van de grondniveaus der ionen
via kortlevende tussenliggende niveaus draagt tenminste voor 70% bij in
de bezetting van de 4p groep, wanneer de elektronendichtheid n_e ongeveer
$10^{19}m^{-3}$ bedraagt. Voor aanzienlijke kleinere waarden van n_e overheerst
direkte aanslag vanuit de grondniveaus der ionen. Het is vrijwel zeker
dat de laserwerking van de argon ion laser het gevolg is van deze staps-
gewijze aanslag.

Het bleek dat "thermalisatie" door ionen of neutrale deeltjes, dit is
een herrangschikking van aangeslagen deeltjes tussen de verschillende
aanslagniveaus tengevolge van botsingen met zware deeltjes, in de 4p
groep niet voorkomt. Voor dit deel van het onderzoek werd een vergelij-
kende studie van de overgangswaarschijnlijkheden van de 4p groep gemaakt.

De elektronentemperatuur T_e is bepaald uit absolute lijnintensiteits-
metingen. De waarde van T_e op een afstand van 0.6 m van de kathode was
ongeveer 35×10^3K voor een plasma met een magnetische induktie
$B_w > 5 \times 10^{-2}$T. Uit de stralingsprofielen werd T_e als funktie van de af-
stand tot de as der ontlading bepaald. T_e daalde ongeveer 10% per 10 mm.

De elektronendichtheden n_e zijn bepaald uit faseverschuivingsmetingen
met mikrogolven. Er werd rekening gehouden met de vorm van het n_e-profiel
en met het niet homogeen zijn van het plakje plasma dat in interaktie is
met de mikrogolven. De n_e-waarden op de as waren 1×10^{19} tot $2 \times 10^{19}m^{-3}$
voor een magnetische induktie $B_w > 5 \times 10^{-2}$T. Elektronendichtheidspro-
fielen werden ook bepaald uit de stralingsprofielen. De halfwaardebreedte
van de profielen was ongeveer 18 mm bij gebruik van een anode op 1.2 m
afstand van de kathode en ongeveer 27 mm voor een ringvormige anode
vlakbij de kathode voor $B_w > 5 \times 10^{-2}$T.

SUMMARY

An investigation was made of intensities of lines of the argon I and II spectra and of the radiation profiles thereof, as functions of the distance to the discharge axis for a hollow cathode low-pressure magnetically-confined argon arc discharge. The discharge currents varied from 10 to 80 A, the axial magnetic fields from $\sim 5 \times 10^{-3}$ to 15×10^{-2}T, and the background pressure was about 10^{-3} mm of Hg.

The excitation mechanism of the 4p group of the argon II spectrum could be ascertained; stepwise excitation from the ion ground levels through short-lived intermediate levels contributes at least 70% to the 4p group population density for electron densities n_e of approximately $10^{19} m^{-3}$. Direct excitation from the ion ground levels is dominant for considerably smaller n_e-values. It is almost certain that the laser action of the argon ion laser results from this stepwise excitation mechanism.

It was found that thermalization by ions or neutral particles, i.e. a rearrangement of excited particles between the various excitation levels caused by collisions with heavy particles does not occur within the 4p group. For this part of the investigation, a comparative study of the transition probabilities of the 4p group was made.

The electron temperature T_e was determined from absolute line-intensity measurements. The value of T_e at a distance of 0.6 m from the cathode was about 35×10^3K for a well-confined plasma with magnetic induction values $B_w > 5 \times 10^{-2}$T. From the radiation profiles T_e as a function of the distance to the axis could be determined. The decrease of T_e was approximately 10% per 10 mm.

The electron densities n_e were determined from phase-shift measurements with microwaves. The form of the n_e-profiles and the non-homogeneity of the slice, interacting with the microwaves were accounted for. The n_e-values on the axis were 1×10^{19} to $2 \times 10^{19} m^{-3}$ for a magnetic induction $B_w > 5 \times 10^{-2}$T. Electron density profiles were also determined from the radiation profiles. The width at half-maximum value of the profiles was about 18 mm when using an anode at 1.2 m from the cathode, and approximately 27 mm for a ring-shaped anode near the cathode, both for $B_w > 5 \times 10^{-2}$T.

CURRICULUM VITAE

geboortedatum en - plaats:
    15 mei 1938 te Soest.

middelbare schoolopleiding:
    Chr.Lyceum te Dordrecht, 1950-1956.
    Gymnasium-β diploma in juni 1956.

universitaire opleiding:
    Technische Hogeschool te Delft,
    afdeling der Technische Natuurkunde, 1956-1962.
    Assistent aan de Hogeschool, 1960-1962.
    Diploma natuurkundig ingenieur in oktober 1962.
    Het afstudeerwerk werd verricht o.l.v. Prof. dr. M.J.Druyvesteyn
    en betrof een onderzoek naar de ordeningsverschijnselen
    in een goud-zilver legering.

militaire dienst:
    Detachering bij de Technisch Physische Dienst TNO-TH
    en werkzaam voor een departementale
    "Adviescommissie geluidhinder door vliegtuigen", 1962-1964.

dienstverband Technische Hogeschool Eindhoven:
    vanaf november 1964 werkzaam als wetenschappelijk medewerker in de
    afdeling der Technische Natuurkunde, groep Atoomfysica.

Stellingen, behorende bij het proefschrift van B. van der Sijde.
Eindhoven, 14 december 1971.

1

In een argon plasma met zeer lage gasdruk worden, in tegenstelling met
de suggestie van MILLER e.a., de bezettingen van dicht bij elkaar gele-
gen aangeslagen niveaus in het spektrum van geioniseerd argon niet
beinvloed door botsingen tussen aangeslagen ionen en neutrale deeltjes
of ionen.

R.C. Miller e.a., Bell System. Techn. J. 46,281 (1967).
Dit proefschrift, p.33-36.

2

De door McWHIRTER en WILNER beschreven methode om voor een plasma in
Corona evenwicht de elektronentemperatuur te bepalen uit een vereenvou-
digde balansvergelijking voor een aangeslagen niveau, levert bij toe-
passing in het argon ion spektrum zeer onnauwkeurige resultaten op.

R.W.P.McWhirter in Plasma Diagnostic Techniques, p. 208-214, Ac.Press, New York (1965)
B.Wilner, Acta Polyt.Scand., Physics and Nucleonics 41, 1 (1966).
Dit proefschrift, p. 93-96 en p.101-104.

3

Het blijkt mogelijk om voor een argon plasma in Corona evenwicht de
elektronentemperatuur te bepalen uit een vereenvoudigde balansverge-
lijking van een aangeslagen niveau van atomair argon, wanneer gebruik
gemaakt wordt van de uit de literatuur bekende gegevens omtrent de
optredende elementaire processen.

Dit proefschrift, p. 93-96 en p. 101-104.

4

Het is voor een argon boogontlading met holle kathode onmogelijk om uit
de relatieve bepaling van twee of meer lijnintensiteiten van het argon
ion spektrum een indruk te verkrijgen van de elektronentemperatuur.

C.B. Kretschmer e.a., Phys.Fluids 11, 1050 (1968).
Dit proefschrift, p. 33 en 36.

5

De door KITAEVA e.a. voorgestelde direkte aanslag vanuit de ion grond-
niveaus naar de bovenniveaus van de laserlijnen in het argon ion spektrum
ter verklaring van de inversie in het spektrum, dient vervangen te worden
door het beeld van stapsgewijze aanslag via kortlevende tussengelegen
niveaus.

V.F.Kitaeva e.a., I.E.E.E.J. Quant. Electr. QE-5, 72 (1969).
Dit proefschrift, p. 96-104 en p. 110-113.

6

"Partial Local Thermal Equilibrium" en het "Collisional-Radiative Model"
zijn twee verschillende benamingen voor één en dezelfde plasmakonditie.

7

Het verdient overweging een onderzoek in te stellen naar de mogelijkheden
om luchtverontreinigende moleculen als CO, NO, SO_2 en dergelijke af te
breken met een holle kathode ontlading.

8

Het is mogelijk om bij experimenten ter bepaling van de absolute waarde
van de totale werkzame doorsnede voor aanslag door elektronen, die uit-
gevoerd worden met een cilindervormige konfiguratie, gebruik te maken van
een R.P.D. (retarding potential difference) methode.

L.Kerwin e.a., in Case Studies in Atomic Collisision Physics I, p. 529-530,
N.Holland Publ. Cy,Amsterdam (1969).

9

De bewering van DAVIES e.a. dat in een niet-zelfstandige Townsend-ontla-
ding een monochromatische ultra violet bron bij kleine veranderingen van
de uittree-energie zorg zou kunnen dragen voor een konstante initiële
foto-elektronenstroom, is onjuist.

D.E.Davies e.a., Proc.4th Int.Conf.Ionization Phenomena in Gases, p. 161, Uppsala (1959).

De meting van de totale doorsnede van meeratomige molekulen bij botsingen
met atomen levert geen uitsluitsel over de anisotropie van de wissel-
werkingspotentiaal van deze molekulen.

Het verdient aanbeveling om ter bescherming van jonge kinderen in het
verkeer de voorrangsituatie tussen overstekende voetgangers en rijdend
verkeer te wijzigen in die straten van de bebouwde kom, die voor het
doorgaande verkeer van weinig of geen belang zijn.

De bestaande direkte en indirekte subsidiëringen als premieregelingen en
aftrekbaarheid van de renten van hypotheekleningen bij de inkomstenbelas-
ting, welke bestaan voor huur- en koophuizen, staan een evenwichtig sub-
sidiebeleid gebaseerd op de inkomensverdeling in de weg.

Ieder programma in het kader van ontwikkelingshulp dient vergezeld te
gaan van een programma ter stimulering van de geboortebeperking.

De op de T.H.E. gevolgde verkiezingsprocedure voor Hogeschoolraad en
afdelingsraden dient aangemerkt te worden als nodeloos ingewikkeld; een
systeem waarbij elke kiezer evenveel stemmen uitbrengt als voor zijn
geleding zetels ter beschikking zijn en degenen met de meeste stemmen
verkozen worden verklaard, verdient de voorkeur.

Een goede diskussie over de toelaatbaarheid van de aanleg van de start-
en landingsbaan 04-22 op het vliegveld Welschap bij Eindhoven uit het
oogpunt van lawaai-overlast, wordt niet bevorderd door aanvechtbare prog-
noses omtrent het aantal en de soort vliegtuigbewegingen van de "Stichting
Vliegveld Welschap" enerzijds, en een aantal diskutabele beweringen in de
rapporten van de "Werkgroep tegen Geluidshinder door Vliegtuigen" anderzijds.

Rapport Technisch Physische Dienst TNO-TH nr. 018-213.
Enige rapporten van de "Werkgroep geluidshinder door Vliegtuigen", januari-juli 1971.